Fall 2013

Light Hadron Properties From Lattice QCD

Parikshit M. Junnarkar

Light Hadron Properties From Lattice QCD

BY

PARIKSHIT M. JUNNARKAR

B.E. in Electrical Engg, University of Pune (2002)

DISSERTATION

Submitted to the University of New Hampshire

in Partial Fulfillment of

the Requirements for the Degree of

Doctor of Philosophy

in

Physics

September, 2013

UMI Number: 3575985

UMI

Dissertation Publishing

UMI 3575985

ProQuest®
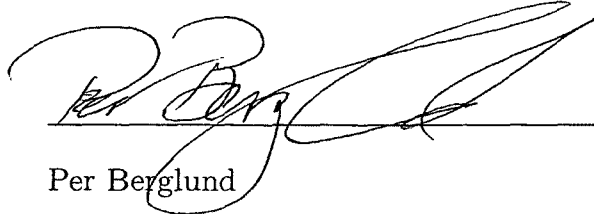
This dissertation has been examined and approved.

_____

Thesis Director, Silas Beane
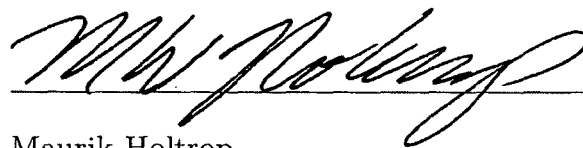
Associate Professor, Department of Physics

_____

Per Berglund
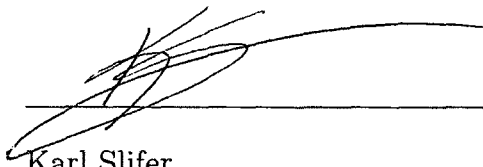
Associate Professor, Department of Physics

_____

Maurik Holtrop

Associate Professor, Department of Physics

_____

Karl Slifer

Associate Professor, Department of Physics

_____

Ben Chandran

Associate Professor, Department of Physics

_____ 7/9/2013

Date

DEDICATION

I dedicate this thesis to my family for their unconditional love and encouragement.

ACKNOWLEDGMENTS

TABLE OF CONTENTS

LIST OF TABLES

LIST OF FIGURES

ABSTRACT

Light Hadron Properties From Lattice QCD

by

PARIKSHIT M. JUNNARKAR
University of New Hampshire, September, 2013

The subject of this thesis is mainly concerned with dynamics of light quarks. The question that will be attempted to answer is, What is the quark mass dependence of low lying hadrons ? In particular, this work will focus on the quark mass dependence of mesons and baryons with the tools of lattice calculations and effective field theories.

The two and three flavor effective field theories are applied to pions and kaons respectively to study the quark mass dependence of their masses and decay constants. In addition, the phenomenologically interesting f_K/f_π is analysed in three flavor theory. It is found that the results of extrapolation agree with experimental results indicating that the effective field theory correctly accounts for effects of lattice calculations.

In the baryon sector, a calculation for the scalar strange content of the nucleon is performed. This quantity and the heavy quark matrix elements of the nucleon are of great phenomenological importance as they provide an estimate for the scattering cross-section of a dark matter candidate with nucleon. Within the limitation of this work, it is found the result is in agreement with the lattice average.

INTRODUCTION

Quantum Chromodynamics (QCD), the theory of interactions of quarks and gluons, constitutes the strong nuclear force and together with quantum electrodynamics (QED) and weak interactions presents a complete description of all the phenomena associated with hadrons. Conceived nearly four decades ago and standing on a strong foundation of experimentally verified predictions, QCD is a very well defined theory at all length scales (and hence all energies), describing nature with different degrees of freedom at different scales. At short distances (and hence at high energies), quarks and gluons are the dominant degrees of freedom and the quark-gluon coupling is small enough to allow the use of perturbation theory, a property known as asymptotic freedom[2, 3, 4]. It is due to this property that QCD can be used to make predictions which have been in tested in the deep inelastic scattering experiments [5]. At long distances (and hence at low energies), the quark-gluon coupling grows large enough that the perturbative description breaks down changing the dominant degrees of freedom by confining quarks and gluons to form hadrons (mesons and baryons). In addition to the confinement of quarks and gluons, QCD is also endowed with flavor symmetry of quarks and together with their chirality forms the chiral flavor symmetry. At low energies, chiral symmetry is broken spontaneously, generating pseudo-goldstone bosons and contributing to hadron masses. The presence of such rich and dynamical phenomena at low energies combined with the fact of lack of applicability of perturbation theory in the QCD coupling constant, low energy QCD has stood as a hard problem in order to generate an understanding of hadrons from its fundamental theory QCD.

Decades of experimental investigations has helped generating a very precise phenomenological understanding of the hadrons. However, a lot of fundamental questions about hadrons remain unanswered. For example, How does the spin of quarks and gluons combine to give rise to the observed spin of the nucleon ? How does the observed hadronic properties such as masses, depend on the fundamental parameters such as quark masses and gauge coupling ? Traditionally, these questions were attacked by constructing an effective description of quarks and gluons in terms of mesons and baryons in the form of an effective field theory known as *chiral perturbation theory*. Chiral perturbation theory (χPT) by construction encodes the spontaneous breaking of chiral symmetry and provides a quark mass and momentum expansion of the low energy hadronic observables [6, 7, 8] . At each order in the chiral expansion, the theory contains a finite number of renormalised constants known as low energy constants (LEC) which are determined from experiments. In most cases, the required number of LEC's beyond the first two orders become large enough that cannot be determined alone from experimental data. Hence the predictions made by χPT based purely on experimental results is very limited and leaves a lot of questions unanswered. One needs a framework and methodology where the low energy QCD issues could be tackled head-on.

The framework required to study QCD especially in the non-perturbative regime is that of Lattice QCD. It was originally realised by K. Wilson [9] for the very purpose of introducing a framework to explore issues in non-perturbative QCD such as confinement. In this formulation, one discretises space-time into a four dimensional euclidean lattice. Due to the discretisation, the path integral for QCD becomes well defined, and lends itself to numerical evaluation. Computing correlation functions directly from the QCD path integral, without any approximations on the gauge coupling, one can obtain a result which is truly non-perturbative. Thus the lattice framework serves

2

as a first principle evaluation of QCD and allows us to attempt to answer difficult questions as described above.

Lattice techinques provide with a powerful tool to explore hadronic physics from QCD. This however introduces constraints of its own on the size of the lattices used. Any given lattice calculation, by its definition is performed in a finite box and the size of the box has to be greater than the compton wavelength of the pions. The discretised lattice spacing serves as an ultraviolet cut-off and is always chosen such that it is much smaller than the chiral symmetry breaking scale for its effects to be small. The computational resources required to perform lattice calculation depend on the masses of quarks utilised. As such in this work, lattice calculations are performed at unphysical quark masses due to finite computational resources.

Due to the said effects, the computed masses from lattice calculations are different from those observed in nature and one needs a method to systematically account for all these effects in order to compare results with experiments. Chiral perturbation theory is now reincarnated as that sytematic method to include all the above mentioned effects. The results of lattice calculations are fitted to χPT to determine the LEC's and hence remove the limitation on χPT to be dependent on experimental data.

In this work, we have employed the methods of lattice QCD and χPT to gain an insight on the quark mass dependence of low lying hadrons. In chapter 3 and 4, we employ these methods to understand quark mass dependence of the pion and kaon mass and decay constants in two and three flavor χPT. We then extend our studies to explore quantities which cannot measured experimentally, viz the scalar strange content of the proton and finally study the χPT for baryons in last chapter.

3

Chapter 1

QCD on the Lattice

1.1 Quantum Chromodynamics

Quantum Chromodynamics (QCD) is the theory of strong interactions. It is a non-abelian gauge theory with gauge group SU(3), representing color charge, and describing the interactions of quarks and gluons. The QCD lagrangian is given as

$$\mathcal{L}_{QCD} = -\frac{1}{4}G_a^{\mu\nu}G_{\mu\nu}^a + \sum_f \bar{\psi}_f^a(\gamma^\mu D_\mu - m_f)\psi_f^a \tag{1.1}$$

where, the $G_a^{\mu\nu}$ is the gluon field strength and the covariant derviatives D_μ are,

$$D^\mu = \partial^\mu + gT_aG_a^\mu, \quad igT_aG_a^{\mu\nu} = [D^\mu, D^\nu], \quad G_a^{\mu\nu} = \partial^\mu G_a^\nu - \partial^\nu G_a^\mu - gf_{abc}G_b^\mu G_c^\nu \tag{1.2}$$

where g is the gauge coupling. ψ_f^a are the quark fields with f as internal flavor degree of freedom and $a = 1, 2, 3$ as color degree of freedom which is also gauge degree of freedom. The T_a's are 3×3 hermitian Gell-Mann matrices and are the generators of the color gauge group. The f_{abc} are the structure constants of the lie algebra of SU(3) given as,

$$\left[\frac{T_a}{2}, \frac{T_b}{2}\right] = f_{abc}\frac{T_c}{2} \tag{1.3}$$

Under color SU(3), the quarks are realised in the fundamental representation **3**, the antiquarks are realised in the complex representation **3*** and the gauge fields in the

Table 1.1: *Quark Properties*

Flavor	Symbol	Charge	Mass
up	u	$\frac{2}{3}$ e	0.0023 GeV
down	d	$-\frac{1}{3}$ e	0.0048 GeV
strange	s	$-\frac{1}{3}$ e	0.095 GeV
charm	c	$\frac{2}{3}$ e	1.27 GeV
bottom	b	$-\frac{1}{3}$ e	4.18 GeV
top	t	$\frac{2}{3}$ e	173 GeV

adjoint representation **8**. In the "low energy regime" (I explain, in chapter 2, what I mean by "low energy"), the interactions of quark and gluons form bound color neutral objects such as,

$$\bar{q}q \longrightarrow \text{Mesons} \quad \text{and} \quad \epsilon_{ijk}q_i q_j q_k \longrightarrow \text{Baryons}$$

In nature, we have observed only the aforementioned color neutral combinations. The existence of higher order color-neutral operators is conjectured to exist in hadronization of quark-gluon plasma but yet to be observed.

Although QCD allows arbitary number of quark flavors, only six of such flavors have been observed. Their properties such as flavor, mass and charge are given as in Table 1.1. With the different flavors of quarks, QCD forms bound states of flavor neutral objects constituting a flavor symmetry. The dynamics of this flavor symmetry with the so called light quarks (up, down and strange quarks) is the subject of this thesis and will be discussed in detail in the next chapter. Together with the color and flavor neutral objects, QCD predicts the spectrum of observed hadrons and as well as states which are yet unobserved.

QCD is a celebrated theory of nature due to its dynamical properties such as asymptotic freedom and confinement which arise in its renormalisation group be-

haviour. In perturbation theory, the QCD beta function upto one loop is given as,

$$\beta(g) = \mu\frac{\partial g}{\partial \mu} = \frac{-g^3}{16\pi^2}\left[\frac{11}{3}N_c - \frac{2}{3}N_f\right] \tag{1.4}$$

where N_c is the number of colors and N_f is the number of flavors. The scale dependent coupling constant is a solution to the Callan-Symanzik equation which is given as,

$$g(\mu) = \frac{1}{\beta_0\,\log\!\left(\mu^2/\Lambda_{QCD}^2\right)} \tag{1.5}$$

This equation shows that for $\mu \gg \Lambda_{QCD}$, the coupling $g(\mu)$ is small enough so that quark-gluon interaction is very weak and QCD lagrangian behaves likes a free field theory, which is understood to be Asymptotic freedom. This is a well tested [10] in experimental fact as shown in Figure 1-1, where Eq.[1.5] is fitted to the experimental data. As is evident in Fig 1-1, the experimental result is in good agreement with QCD predictions. An interesting aspect of Eq 1.5 is the appearance of the scale Λ_{QCD} which is a scale independent (but scheme dependent) quantity and hence is a renormalisation group invariant. Eq 1.5 also predicts the failure of perturbation theory, when $\mu \sim \Lambda_{QCD}$. For scales $\mu < \Lambda_{QCD}$, one has to use non-perturbative methods such as lattice regularisation to explore physics in the non-perturbative regime.

1.2   QCD on the Lattice

QCD in the strong coupling limit can be studied by doing a lattice calculation. A lattice calculation is a non-perturbative way of implementing a field theory via the path integral method. Such an attempt was first made by Kenneth Wilson in 1974 [9] with the motivation to study quark confinement. The basic idea is to evaluate,

$$\langle \mathcal{O}_1\mathcal{O}_2 \rangle = \frac{1}{Z}\int \mathcal{D}A_\mu\,\mathcal{D}\bar{\psi}\,\mathcal{D}\psi\,\mathcal{O}_1\mathcal{O}_2\,e^{-S_{QCD}} \tag{1.6}$$

directly without making an expansion in any parameters of the theory. Operators $\mathcal{O}_1$ & $\mathcal{O}_2$ in Eq 1.6 are any observables of interest and S_{QCD} is the QCD action in
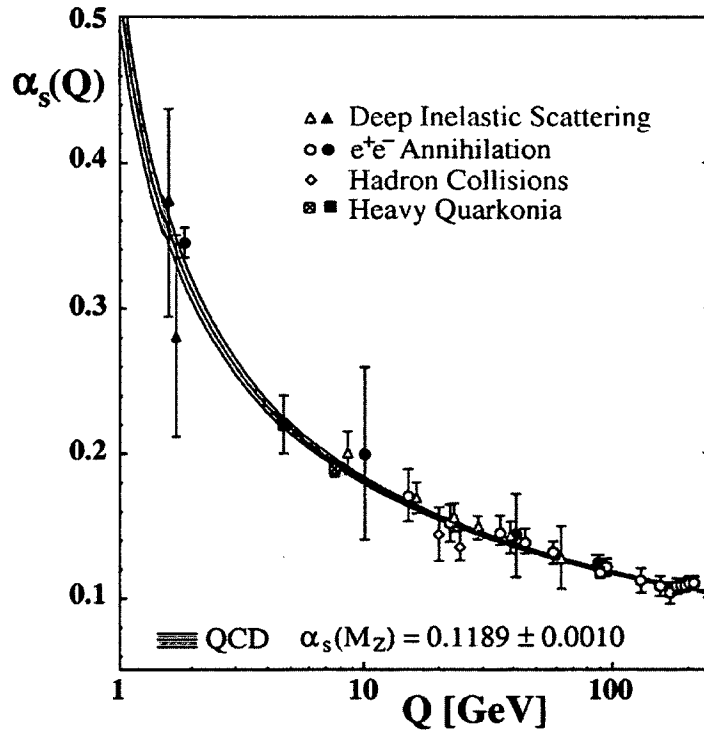
Figure 1-1: *Asymptotic Freedom*

euclidean space. Lattice methods are applicable only to field theories formulated in euclidean space for computational reasons :

- The integrand in Eq 1.6 is absoutely convergent and real in euclidean space.

- Numerical methods are suited better for calculations in real space than complex.

The non-perturbative calculation of $\langle \mathcal{O}_1 \mathcal{O}_2 \rangle$ is done in several steps viz;

- Introducing an ultraviolet cutoff by discretization of space-time into a lattice.

- Construction of gauge fields on the lattice.

- Construction of fermions on the lattice.

In the following sections, I discuss the construction of above steps in detail.

7

1.3 Gauge Fields on the Lattice

A lattice transcription of any continuum field theory begins by replacing the continuum space x_μ by discrete space-time points as bn_μ where, n_μ is a set of four dimensional integers and b is the lattice spacing. One also replaces continuous derivatives by finite differences,

$$x_\mu \longrightarrow bn_\mu \qquad \partial_\mu \psi(x_\mu) \longrightarrow \Delta_\mu \psi_{n_\mu} \equiv \frac{1}{2b}\left(\psi_{n_\mu + \hat{x}_\mu} - \psi_{n_\mu - \hat{x}_\mu}\right) \tag{1.7}$$

In the continuum theory, gauge invariance is preserved by a covariant derivative, which exactly cancels the terms generated by the local transformation. The naive implementation of such a covariant derivative on the lattice fails to preserve gauge invariance. It was shown by K. Wilson [9] that the gauge field can be thought of as a connection which parallel transports fermion fields from one site to other. Such an operator would simply be a series of infinitesimal parallel transports from say x_0 to x as,

$$U(x_0, x_n, C) = \exp\left(i \int_C A_\mu^a dx^\mu T^a\right) \tag{1.8}$$

The operator $U(x_0, x_n, C)$ is appropriately called a *Wilson line* from points x_0 to x_c along the curve C. Hence, on a space-time lattice such an operator is given by,

$$U_\mu(n) = \exp\left(i \int_{x_\mu}^{x_\mu + b\hat{\mu}} A_\mu^a(x + dl)dl T^a\right) = \exp\left(ibT^a A_\mu^a\right) \tag{1.9}$$

The problem of constructing gauge invariant object is now reduced to parallel transporting U_μ around a loop, which also will be non-trivial if there is presence of a curvature which is this case will be the field strength $F_{\mu\nu}$. The simplest such object is given by,

$$\text{Tr}\Box_{\mu\nu}(x) \equiv \text{Tr } U_\nu(x)U_\mu(x + \hat{\nu})U_\nu^\dagger(x + \hat{\mu})U_\mu^\dagger(x) \tag{1.10}$$

8

This is used to construct the action for the lattice gauge fields known as *Wilson gauge action* given as,

$$S_G = \frac{\beta}{3} \sum_{x,\mu>\nu} \left(3 - \text{Tr}\square_{\mu\nu}(x)\right), \qquad \beta \equiv \frac{6}{g_0^2} \tag{1.11}$$

In th continuum limit, this action reduces to the standard Yang-Mills action upto $\mathcal{O}(b^2)$ lattice corrections,

$$S_G = \frac{1}{4} \int d^4x \left(F_{\mu\nu}^a\right)^2 + \mathcal{O}(b^2) \tag{1.12}$$

1.4 Fermions on the lattice

The implementation of gauge fields on the lattice can be done elegantly as discussed in the previous section. Introducing fermions on the lattice turns out to be complicated due to the so called "doubling problem" which will be discussed now. Consider a continuum gauge invariant fermion lagrangian, which can be transcribed on to the lattice as follows,

$$\bar{\psi}\gamma^\mu D_\mu \psi \longrightarrow \sum_{x,\mu} \bar{\psi}(x)\gamma^\mu \left(\frac{U_\mu(x)\psi(x+\hat{\mu}) - U_\mu^\dagger(x-\hat{\mu})\psi(x-\hat{\mu})}{2b}\right) \tag{1.13}$$

The partial derivative of the continuum theory has been replaced with an average of forward and backward difference of the fermion fields. Such a definition of finite difference preserves invariance under the hypercubic symmetry and reflection hermiticity. The above expression can also be represented in the kernel form to include all the degrees of freedom such color, flavor and spinor at all points on the lattice as,

$$\sum_{\alpha,\beta} \bar{\psi}_\alpha K_{\alpha\beta}\psi_\beta \tag{1.14}$$

The inverse propagator to the above action is given by,

$$S^{-1}(p) = m + i\sum_\mu \gamma_\mu \frac{1}{a}\sin(p_\mu a) \equiv m + i\sum_\mu \gamma_\mu \hat{p}_\mu \tag{1.15}$$

9

Now for the massless case, this has a zero at $p_\mu = 0$. The periodic function appearing in the expression above causes a lot of trouble namely for every value of $p_\mu = (0, \pi/a, 0, 0)$, $p_\mu = (\pi/a, \pi/a, 0, 0)$,..., one finds additional 16 zeros. Taking the continuum limit, these zeros survive giving 16 fermions instead of one. This issue is the infamous *"Fermion doubling problem"*. There has been a non-trivial amount effort put into understanding and eliminating this issue in the lattice community over a number of years. Naively it may appear to be an engineering problem to eliminate such species in the continuum. The issue is however deeper as the naive fermion action above fails to reproduce the chiral anomaly and the restoration of such an anomaly turned out to be less than straightforward.

There are very many different fermion discretisation used in the lattice calculations and I will be discussing only those relevant to the work done in this thesis. In my research, we have used the so called staggered fermions and domain wall fermions which will be discussed in the subsections below.

1.4.1   Staggered Fermions

Staggered fermion formulation also known as Kogut-Susskind fermions [11] was one of the initial attempts at the doubling problem. The essence of their formulation is realising the kernel $K_{\alpha\beta}$ can be block diagonalised. This is done by diagonalisation in the spinor space by transforming the fermion field as,

$$\psi(x) = \Gamma_x \chi(x) \qquad \bar\psi(x) = \bar\chi(x)\Gamma_x^\dagger \qquad \Gamma_x = \gamma_1^{x_1}\gamma_2^{x_2}\gamma_3^{x_3}\gamma_4^{x_4} \tag{1.16}$$

$$\alpha_\mu \equiv \Gamma_x^\dagger \gamma_\mu \Gamma_{x+\hat\mu} = \left(-1\right)^{x_1 + \ldots x_{\mu-1}}$$

Hence the transformed gauge invariant fermion action 1.13 is given by,

$$\begin{aligned}
S_{KS} &= \frac{1}{2b}\sum_{x,\mu}\bar\chi(x)\alpha_\mu\big(U_\mu(x)\chi(x+\hat\mu) - U_\mu(x-\hat\mu)\chi(x-\hat\mu)\big) + m\sum_x \bar\chi(x)\chi(x) \tag{1.17}\\
&= \frac{1}{b}\bar\chi M(U)\chi
\end{aligned}$$

The block diagonal kernel $M(U)$ now has 4 degenerate single component Dirac fermions at four lattice sites instead of 16. They are called as "tastes" to distinguish them from flavor as different tastes have same mass. The single component taste fermion, staggered fermion, has an exact chiral symmetry however they occur in species of four. This property is crucial as it suppresses additive mass renormalisation. The strongest feature of staggered fermion is its computational efficiency as it is four times faster than any other fermion discretisation. In order to get a single fermion in the continuum, one takes a fourth root of the determinant which eliminates the taste quantum number in the continuum.

1.4.2 Domain Wall Fermions

The implementation of chiral fermions, fermions with exact chiral symmetry at finite lattice spacing and with only single species of them in the continuum, is very non-trivial was shown by D. Kaplan [12]. It was shown that in terms of a five dimensional theory, one can find a local chiral fermion on a four dimensional submanifold. Consider a free Dirac operator in a five dimensional continuum Euclidean space,

$$D_5 = D_4 + \gamma_5 \partial_5 - M(s) \tag{1.18}$$

where, $D_4 = \gamma^\mu \partial_\mu$, $\partial_5 = \partial/\partial s$ and M is the mass parameter assumed to vary with s. Now a solution to the five dimensional dirac equation $D_5 \chi = 0$, where $\chi(x,s) = \exp(ip.x)u(s)$ gives us the following for the fifth dimension,

$$\left(\gamma_5 \partial_5 - M(s)\right)u = -i\gamma^\mu p_\mu u \tag{1.19}$$

Now, it was shown by Kaplan that the massless modes of the equation above have exact chirality even at finite lattice spacing.

The lattice construction of Domain wall fermions is done discretising the four dimensions while having a finite length L_s for the fifth dimension. The gauge fields

are assumed to have no variation in the fifth dimension, so that the action can be given as a sum over four dimensional piece. The domain wall fermion is constructed as done by Shamir where are the chiral modes are explicity summed over and given as,

$$
\begin{aligned}
S_{DW} \quad = \quad & \sum_{x,x'} \sum_{s=0}^{L_s-1} \left(\bar{\psi}(x,s)(D_w(x,x')+1) \right) - \\
& - \left[\bar{\psi}(x,s) \frac{1-\gamma_5}{2} \psi(x',s+1) + \bar{\psi}(x,s) \frac{1+\gamma_5}{2} \psi(x',s-1) \right] + \\
& + \; m \left[\bar{\psi}(x,0) \frac{1+\gamma_5}{2} \psi(x',L_s-1) + \bar{\psi}(x,L_s-1) \frac{1-\gamma_5}{2} \psi(x',0) \right]
\end{aligned}
\tag{1.20}
$$

The four dimensional quark fields are located on the boundary, the domain wall, are given as the sum of the chiral modes as,

$$
\begin{aligned}
q(x) &= \frac{1-\gamma_5}{2} \psi(x,0) + \frac{1+\gamma_5}{2} \psi(x,L_s-1) \\
\bar{q}(x) &= \bar{\psi}(x,L_s-1) \frac{1-\gamma_5}{2} + \bar{\psi}(x,0) \frac{1+\gamma_5}{2}
\end{aligned}
\tag{1.21}
$$

Domain wall fermions are very desirable to use in lattice calculations especially in low energy hadronic physics where the physics due to chiral symmetry and its breaking dominates. The price one has to pay for is considerably increased computational cost. In the work done for this thesis, staggered fermions have been used for the non-valence which is computationally more intensive. In the valence sector, we have used domain wall fermions due to its exact chiral symmetry.

Chapter 2

Chiral Perturbation Theory

2.1 Chiral Symmetry and It's Breaking

Consider the classical QCD lagrangian with massless quarks for simplicity (It will be made clear later why this is a good demonstrative idea). The massless quarks that we consider are only the quarks with lightest flavors as up, down and strange. (u,d and s). The lagrangian reads as follows,

$$\mathcal{L}_{QCD} = \sum_{l=u,d,s} \bar{q}_{l,R} i\gamma^\mu D_\mu q_{l,R} + \bar{q}_{l,L} i\gamma^\mu D_\mu q_{l,L} - \frac{1}{4} F^{\mu\nu} F_{\mu\nu} \tag{2.1}$$

where the color indices on the quark fields are supressed. Since the covariant derivative arises from the gauging of the color degree of freedom, the quark fields can decoupled into left handed and right handed fields as,

$$q_{i,L} = \frac{1 - \gamma_5}{2} q_i \qquad q_{i,R} = \frac{1 + \gamma_5}{2} q_i \tag{2.2}$$

This decoupling combined with the flavor symmetry of QCD forms a global $U(N_f)_L \times U(N_f)_R$ symmetry of classical QCD.

In the quantum theory, the axial $U(1)_A$ part of $U(1)_L \times U(1)_R$ has an anomaly and thus the non-anomalous part of the original symmetry of the QCD lagrangian is given as,

$$U(N_f)_L \times U(N_f)_R \longrightarrow SU(N_f)_L \times SU(N_f)_R \times U(1)_V \tag{2.3}$$

The $U(1)_V$ is a global symmetry of quark fields and the associated conserved charge is the quark number. $SU(N_f)_L \times SU(N_f)_R$ now represents the flavor symmetry implying

that QCD lagrangian is invariant under independent L and R chiral transformations and hence is known the chiral symmetry of QCD.

If the chiral symmetry was realised exactly in nature, the hadrons would then be observed as multiplets of $SU(N_f)_L \times SU(N_f)_R$ and any given hadronic state would be accompanied by degenerate opposite parity state. However such behaviour is not observed in nature and we postulate that the chiral symmetry must be spontaenously broken in nature to its vector subgroup [13]

$$SU(N_f)_L \times SU(N_f)_R \longrightarrow SU(N_f)_V \qquad (2.4)$$

Now from the Goldstone's theorem, we expect $N_f^2 - 1$ number of massless bosons. In QCD with two flavors, we do see three such bosons namely, pions π^+, π^- and π^0 which are much lighter than all other hadrons and we interpret them as pseudo-goldstone bosons due to the fact that in nature the light quarks are massive although really small.

In the presence of quark masses, the chiral symmetry is explicitly broken to its vector subgroup. However the three light flavors of quarks are small enough compared to the scale of QCD, Λ_{QCD} that they could be treated perturbatively.

2.2 Chiral Perturbation Theory

2.2.1 Two Flavor χPT - SU(2) χPT

Chiral perturbation theory (χPT) is an effective field theory of QCD which is built on the fact above that of spontaneous breaking of chiral symmetry to its vector subgroup. It is a theory constructed from the pseudo-goldstone bosons such that the χPT lagrangian is invariant under the global chiral symmetry $SU(N_f)_L \times SU(N_f)_R$ and the ground state of the theory is invariant under the vector subgroup.

This can be done by means of a non-linear realisation of chiral symmetry as [14, 15]

$$\Sigma = \exp\left(\frac{i\phi}{f}\right) \qquad \phi = \begin{pmatrix} \frac{\pi^0}{\sqrt{2}} & \pi^+ \\ \pi^- & -\frac{\pi^0}{\sqrt{2}} \end{pmatrix} \tag{2.5}$$

where the field Σ represents the pseudo-goldstone bosons, the pions, non-linearly. The non-linear field Σ transforms under chiral symmetry as,

$$\Sigma \longrightarrow \Sigma' = L\Sigma R^\dagger \tag{2.6}$$

where $L \in SU(N_f)_L$ and $R \in SU(N_f)_R$. Now to construct the most general lagrangian invariant under the chiral symmetry and CPT, we need to include the quark masses which break chiral symmetry explicitly. Since the quark masses itself don't transform under chiral symmetry, they are included as spurion fields which transform as,

$$M \longrightarrow RML^\dagger \tag{2.7}$$

The most general lagrangian invariant under chiral symmetry at leading order is given by,

$$\mathcal{L} = \frac{f^2}{4}\mathrm{Tr}\left(\partial_\mu\Sigma\partial^\mu\Sigma^\dagger\right) + \frac{f^2 B_0}{2}\mathrm{Tr}\left(\Sigma M^\dagger + M\Sigma^\dagger\right) \tag{2.8}$$

The leading order lagrangian is characterised by unknown parameters viz f, the decay constant which is an artifact of spontaneous symmetry breaking and B_0 which represents the chiral condensate and is artifact of structure of QCD vacuum. These are known as the low energy constants (LEC's) at the leading order and they are a priori undetermined and have to obtained either from experimental data or in our case fitting lattice data of mesons.

The pion mass can be obtained at leading order by expanding Eq. 2.8 upto $\mathcal{O}(\phi^2)$ as,

$$m_\pi^2 = B_0(m_u + m_d) \tag{2.9}$$

The pion mass receives systematic chiral corrections from higher orders of chiral operators. At next to leading order, we have to include the following lagrangian which provides the one loop corrections masses and decay constants.

$$\mathcal{L} = \frac{l_1}{4}\left[\text{Tr}(\partial_\mu \Sigma \partial^\mu \Sigma^\dagger)\right]^2 + \frac{l_2}{4}\text{Tr}(\partial_\mu \Sigma \partial_\nu \Sigma^\dagger)\text{Tr}(\partial^\mu \Sigma \partial^\nu \Sigma^\dagger) + \tag{2.10}$$

$$\frac{l_3 B_0^2}{4}\left[\text{Tr}(\Sigma M^\dagger + M\Sigma^\dagger)\right]^2 + \frac{l_4 B_0}{4}\text{Tr}(\partial_\mu \Sigma \partial^\mu \Sigma^\dagger)\text{Tr}(\Sigma M^\dagger + M\Sigma^\dagger)$$

At this order, the lagrangian has four more LEC's which are undetermined. In this thesis, we have performed lattice calculations to determine l_3 and l_4. For details, the reader is referred to Chapter 3.

The Chiral perturbation theory for baryons is more complicated compared to mesons due to its transformation properties as well as renormalisation issues which we will only gloss over. In two flavor, the nucleon fields form doublets under $SU(2)_V$ as,

$$N = \begin{pmatrix} p \\ n \end{pmatrix} \tag{2.11}$$

and they transform as,

$$N_i \longrightarrow U_{ij}N_j \tag{2.12}$$

where U is an element of the chiral group. As it was shown by Georgi, (cite Georgi), there are infinitely many choices of nucleon fields which transform identically as above. It is usually the method suggested in [14, 15] that is adopted to construct the nucleon lagrangian. The chiral pertubation theory for baryons can systematically described with the heavy baryon approximation [16] as in the heavy baryon approximation which provides a velocity expansion for the baryons, the chiral expansion for baryons is well defined. The complete description of the heavy baryon approximation is out of scope for this thesis and the interested reader should look in Ref. [16]

The chiral lagrangian for baryons in the isospin limit of light quarks is given as,

$$\mathcal{L} = \bar{N}\ iv \cdot D\ N + 2\sigma_M\ \bar{N}N\text{Tr}(\mathcal{M}) \tag{2.13}$$

16

where the nucleon covariant derivative D is constructed as [14, 15] as,

$$(D_\mu N)_i = \partial_\mu N_i + \mathcal{V}_i^j N_j \qquad \mathcal{V} = \frac{1}{2}\left(\xi\partial_\mu\xi^\dagger + \xi^\dagger\partial_\mu\xi\right) \qquad (2.14)$$

and the associated "gauge field" $\mathcal{V}$ is chiral vector field constructed from $\xi^2 = \Sigma$, the goldstone boson fields. In this work we have also included the Delta degrees of freedom and their the interactions with the nucleon through the nucleon axial coupling constant g_A and the Nucleon-Delta coupling constant $g_{\Delta N}$. The corresponding interaction lagrangian is given by,

$$\mathcal{L} = 2g_A \bar{N}\, S \cdot \mathcal{A}\, N + g_{\Delta N}\left(\bar{T}^\mu \mathcal{A}_\mu N + \bar{N}\mathcal{A}^\mu T_\mu\right) + 2g_{\Delta\Delta}\bar{T}^\mu S \cdot \mathcal{A}T_\mu \qquad (2.15)$$

The baryonic coupling constants σ_M, g_A and $g_{N\Delta}$ are determined from the fitting of lattice data and is the topic for the Chapter 6.

2.2.2 Three Flavor χPT - SU(3) χPT

The three flavor chiral perturbation is the one includes the strange quark in addition to light quarks. The three flavor is more complicated than the two flavor in the sense that there exist more states. The lagrangian for three flavor case looks identical to the two flavor case except there are more goldstone bosons. The field ϕ for the three flavor case is now given as,

$$\phi = \begin{pmatrix} \frac{\pi^0}{\sqrt{2}} + \frac{\eta}{\sqrt{6}} & \pi^+ & K^+ \\ \pi^- & -\frac{\pi^0}{\sqrt{2}} + \frac{\eta}{\sqrt{6}} & K^0 \\ K^- & \overline{K}^0 & -\frac{2\eta}{\sqrt{6}} \end{pmatrix} \qquad (2.16)$$

and the leading order goldstone boson masses are given as,

$$m_\pi^2 = B_0(m_u + m_d) \qquad (2.17)$$

$$m_K^2 = B_0(m_{u,d} + m_s)$$

$$m_\eta^2 = \frac{B_0}{3}(m_u + m_d + 4m_s)$$

The NLO lagrangian for the three flavor case is also analysed in this thesis and is given as [8],

$$
\begin{aligned}
\mathcal{L} = \quad & L_1 \Big[\mathrm{Tr}\big(\partial_\mu \Sigma \partial^\mu \Sigma^\dagger\big) \Big]^2 + L_2 \mathrm{Tr}\big(\partial_\mu \Sigma \partial_\nu \Sigma^\dagger\big) \mathrm{Tr}\big(\partial^\mu \Sigma \partial^\nu \Sigma^\dagger\big) \qquad (2.18) \\
& + L_3 \mathrm{Tr}\big(\partial_\mu \Sigma \partial_\nu \Sigma^\dagger \partial^\mu \Sigma \partial^\nu \Sigma^\dagger\big) + 2B_0 \, L_4 \mathrm{Tr}\big(\partial_\mu \Sigma \partial^\mu \Sigma^\dagger\big) \mathrm{Tr}\big(\Sigma M^\dagger + M \Sigma^\dagger\big) \\
& + 2B_0 \, L_5 \mathrm{Tr}\Big(\big(\partial_\mu \Sigma \partial^\mu \Sigma^\dagger (\Sigma M^\dagger + M \Sigma^\dagger)\big) \Big) + 4L_6 B_0^2 \Big[\mathrm{Tr}\big(\Sigma M^\dagger + M \Sigma^\dagger\big) \Big]^2 \\
& + 4L_6 B_0^2 \Big[\mathrm{Tr}\big(\Sigma M^\dagger - M \Sigma^\dagger\big) \Big]^2 + 4L_8 B_0^2 \mathrm{Tr}\big(\Sigma M^\dagger \Sigma M^\dagger + M \Sigma^\dagger M \Sigma^\dagger\big)
\end{aligned}
$$

As it is evident ther are more LEC's in SU(3) χPT compared to SU(2) due to more complex group representation of SU(3). The contribution of the above lagrangian to the meson masses and decay constants is the subject of the Chapter 4 and the reader is directed to Chapter 4 for more details.

The baryons in SU(3) χPT belong to the adjoint representation of $SU(3)_V$ and are given as,

$$
B = \begin{pmatrix} \frac{1}{\sqrt{6}}\Lambda + \frac{1}{\sqrt{2}}\Sigma^0 & \Sigma^+ & p \\ \Sigma^- & \frac{1}{\sqrt{6}}\Lambda - \frac{1}{\sqrt{2}}\Sigma^0 & n \\ \Xi^- & \Xi^0 & -\frac{2}{\sqrt{6}}\Lambda \end{pmatrix} \qquad (2.19)
$$

The baryons transform as,

$$
B \longrightarrow B' = U B U^\dagger \qquad (2.20)
$$

Now, the most general chirally symmetric lagrangian constructed from baryon fields B is given as,

$$
\begin{aligned}
\mathcal{L} = \quad & \mathrm{Tr}\big(\bar{B} \, iv \cdot D \, B\big) + 2b_D \mathrm{Tr}\big(\bar{B}\{\mathcal{M}, B\}\big) + 2b_F \mathrm{Tr}\big(\bar{B}[\mathcal{M}, B]\big) \qquad (2.21) \\
& + 2\sigma_M \mathrm{Tr}\big(\bar{B}B\big) \mathrm{Tr}\big(\mathcal{M}\big)
\end{aligned}
$$

where the chiral covariant derivative is defined as,

$$
D_\mu = \partial_\mu B + [\mathcal{V}_\mu, B] \qquad (2.22)
$$

The coupling constants in SU(3) between mesons and baryons are given by,

$$\mathcal{L} = \quad 2D \, \text{Tr}\big(\bar{B}S^{\mu}\{\mathcal{A}_{\mu}, B\}\big) + 2F \, \text{Tr}\big(\bar{B}S^{\mu}[\mathcal{A}_{\mu}, B]\big) + 2\mathcal{H}\big(\bar{T}^{\mu}S \cdot \mathcal{A}T_{\mu}\big) \quad (2.23)$$
$$+ \, \mathcal{C} \, \big(\bar{T}^{\mu}\mathcal{A}_{\mu}B + \bar{B}\mathcal{A}_{\mu}T^{\mu}\big)$$

The axial coupling constants can be matched to the two flavor theory and are given as,

$$g_A = D + F, \qquad g_{\Delta\Delta} = \mathcal{H}, \qquad g_{\Delta N} = \mathcal{C} \qquad (2.24)$$

As is evident, there more operators in the SU(3) theory for baryons than the SU(2) counterpart. The contributions of the above LEC's to baryon masses is the subject of Chapter 6 and will be discussed in detail there.

2.3 Chiral Perturbation Theory and Lattice QCD

Chiral perturbation theory (χPT) and lattice calculations are complementary to each other. To be able to make precise predictions from χPT , the LEC's from upto two orders (NLO and NNLO) have to be determined. As explained before, this cannot be done alone from just experimental data. This is where lattice calculations become important as they provide much more access in determining these LEC's. Lattice calculations, on the other hand, are performed with several unphysical effects and inherently demand a systematic method to include all such effects. χPT being an EFT can be modified systematically to account for all such effects. We now describe these effects and the associated χPT modifications.

2.3.1 Unphysical quark masses and Finite Volume

The computation time of a given lattice calculation directly depends the size of lattice due to finite computer memory and inversely on the quark masses as the algorithmic time for smaller quark masses is exorbitantly high. As such, in this work, we have

19

used lattices of finite size with the box length of 2-3 fm and the light quark masses higher than those in nature. Hence the hadron masses computed from this calculation is significantly different than those seen in nature. Since χPT provides a natural expansion of hadron masses in terms of quark masses, the problem of unphysical quark masses is taken care of, by fitting the lattice data of masses to determine the LEC's of χPT and then extrapolating the results to the physical quark masses. The issue of finite volume is also taken care of by changing the regularisation of the loop integrals in χPT [17, 18, 19] to that of the box regularisation. In this manner, these effects are systematically accounted for. The details of these is described later in Chapters 3 and 4.

2.3.2   Partial Quenching

A given lattice calculation is usually performed in two steps viz, generation of gauge configurations by means of markov chain monte-carlo processes and then the calculations of quark propagators in the presence of the gauge configurations. The gauge configuration part is the most computationally intensive part and requires a large scale computer resources. The propagator calculation part is comparatively less expensive and could be done on smaller clusters. As mentioned before, due to the cost of a calculation for lower quark masses being quite high, in practise the quark masses for the gauge field generation are usually higher than those for propagator calculations. By doing this, we have different quark masses in the sea and valence sector and this is known as partial quenching. The effects due to partial quenching introduces complications which can be systematically included by constructing an effective field theory known as PQχPT . In addition to partial quenching, we have also changed the discretisation scheme for both valence and sea sector. The effects of those are included in the mixed action χPT (MAχPT) described in the next section.

20

2.3.3 Lattice spacing effects

The fact that we are using a finite lattice is an additional source of chiral symmetry breaking and can taken into account by a construction following symanzik which organises the lagrangian systematically in lattice spacing. For fermions with exact chiral symmetry, ginsparg-wilson fermions, we only have dimension 6 operators and the new lagrangian is given by,

$$\mathcal{L}_{SET} = \mathcal{L}_{QCD}^{(4)} + a^2 L_S^{(6)} + \dots \tag{2.25}$$

These effects can be included in χPT by treating them as an additional source of explicit chiral symmetry breaking just like the quark masses.

2.4 Mixed Action χPT

Mixed-action χPT description systematically includes all unphysical effects relevant to lattice calculations performed in this work. It takes into account the effect of partial quenching and different discretisation of sea and valence quarks and also the effects of lattice spacing. Hence the structure of the MAχPT is considerably complicated with the presence of mesons from the sea, valence and mixed sectors. The power counting is now set up in terms of expansion parameters of MAχPT as,

$$\epsilon_M^2 = \frac{m_\pi^2}{\Lambda_\chi^2} \qquad \epsilon_a^2 = a^2 \Lambda_{QCD}^2 \tag{2.26}$$

The lagrangian for MAχPT is set up as non-linear realisation of meson fields. Upto leading order the lagrangian is given as,

$$\mathcal{L}_{MA} = \frac{f^2}{8} \, \text{str}\left(\partial_\mu \Sigma \partial^\mu \Sigma^\dagger\right) + \frac{f^2 B_0}{4} \text{str}\left(m_q \Sigma^\dagger + \Sigma m_q^\dagger\right) + a^2 \left(\mathcal{U}_{sea} - \mathcal{U}_{VS}\right) \tag{2.27}$$

where,

$$\Sigma = \exp\left(\frac{2i\Phi}{f}\right), \qquad \Phi = \begin{pmatrix} M & \chi^\dagger \\ \chi & \tilde{M} \end{pmatrix} \tag{2.28}$$

21

The matrices M and $\tilde{M}$ contain bosonic mesons while χ and $\chi^\dagger$ contain fermionic mesons. The lattice spacing corrections are $\mathcal{O}(a^2)$ both from the sea sector and valence sector. In this work we include mixed action χPT corrections upto NLO in two and three flavor to our lattice data which have been done in Chapters 3 and 4.

Chapter 3

SU(2) Low Energy Constants from Lattice QCD

In this work we focus on determining the $\bar{l}_3$ and $\bar{l}_4$ from the lattice computed pion mass and decay constant. We perform a rigorous analysis on the lattice data incorporating finite volume corrections and lattice spacing effects using Mixed Action χPT appropriately suited to this work i.e. the one which describes staggered sea-quarks and domain wall valence quarks. In section II, we describe the details of the lattices used in this work. Section III describes the details of χPT used for analysis. In section IV, we perform the chiral and continuum extrapolation of the lattice data.

3.1 Details of the Lattice Calculation

The lattice calculation performed in this work is referred to as so called mixed action calculation and is a part of an extensive research program of the NPLQCD collaboration [20, 21, 22, 23, 24, 25, 26, 27, 28, 29, 30, 31, 32] to study the properties of hadrons in the low energy regime. The mixed action program was initiated by the LHP collaboration [33, 34, 35, 36, 37, 38]. In a mixed action lattice calculation, one uses a different lattice discretisation of dirac operator for the sea sector and valence sector. The primary reason to adopt this strategy is as follows, in a lattice calculation the sea quarks are included while generating the field configurations which is

a computationally expensive endeavour. Hence it makes sense to use a fermion discretisation which is numerically cheap. The staggered fermion formulation [39] is four times faster than any other fermion formulations and has been used extensively by the MILC collaboration [40, 1] in generating the gauge configurations. The calculation for valence fermions comprise of inversions of dirac operator and is less numerically intensive than the generation of field configurations. One can therefore use discretisation which have improved properties such minimally doubled and chirally symmetric fermions such as domain wall fermions [12, 41, 42, 43, 44]. Domain wall fermions preserve exact chiral symmetry at finite lattice spacing and are desirable in studying low energy QCD which is dominated by the chiral symmetry breaking effects.

3.1.1 Lattice Input Parameters

In this work, we have used the publicly available MILC gauge configurations [40, 1] generated with SU(3) gauge links and staggered quarks. These configurations denoted as $N_f = 2 + 1$ were generated with two flavors of degenerate light quarks bm_l^{sea} and one flavor of strange quark bm_s^{sea}. The input parameters for these configurations are tabulated in Table 5.1. We have performed calculations on two lattice spacings as coarse $b \sim 0.12$ fm and as fine $b \sim 0.09$ fm with a spatial extent ranging from $L \sim 2 - 3.5$ fm on all the lattices. This has allowed us to study the finite volume dependence of various hadronic observables. On the configurations we have used, the strange quark mass was fixed to its physical value while the degenerate light quarks were varied over a range of masses as can be seen in Table 5.1. Further, due to limited number of gauge configurations, we improved the statistics by performing the propagator inversions on a number of sources placed randomly within the lattice.

In the valence sector, we have used the domain wall fermion action due to its exact chiral properties. The masses of valence should be such that they are the same as the

Table 3.1: *Input parameters of the Lattice calculation*

$b \approx 0.125$ fm ensembles

β	bm_l^{sea}	bm_s^{sea}	L×T	bm_l^{dwf}	$bm_l^{res} \times 10^3$	bm_s^{dwf}	$bm_s^{res} \times 10^4$	N_{cfg}
6.76	0.007	0.050	20×32	0.0081	1.581(14)	0.081	8.95(3)	468
6.76	0.007	0.050	24×64	0.0081	1.64(3)	0.081	9.1(2)	1081
6.75	0.010	0.030	20×64	0.0138	1.564(3)	0.081	8.92(2)	328
6.76	0.010	0.050	20×32	0.0138	1.566(11)	0.081	9.13(2)	656
6.76	0.010	0.050	28×64	0.0138	1.566(11)	0.081	9.13(2)	274
6.79	0.020	0.050	20×64	0.0313	1.227(11)	0.081	8.36(3)	486
6.79	0.030	0.030	20×64	0.0478	1.052(4)	0.081	8.09(4)	367
6.81	0.030	0.050	20×32	0.0478	1.013(6)	0.081	8.62(7)	486

$b \approx 0.09$ fm ensembles

β	bm_l^{sea}	bm_s^{sea}	L×T	bm_l^{dwf}	$bm_l^{res} \times 10^4$	bm_s^{dwf}	$bm_s^{res} \times 10^4$	N_{cfg}
7.06	0.0031	0.0186	40×96	0.0035	4.73(7)	0.0252	3.16(5)	355
7.06	0.0031	0.0186	40×96	0.0035	4.73(7)	0.0423	2.45(4)	356
7.08	0.0031	0.031	40×96	0.0038	1.56(3)	0.0423	0.73(2)	170
7.08	0.0031	0.031	40×96	0.0035	4.28(3)	0.0423	2.33(2)	422
7.09	0.0062	0.031	28×96	0.0080	3.75(4)	0.0423	2.30(3)	1001
7.11	0.0124	0.031	28×96	0.0164	2.90(3)	0.0423	2.04(2)	513

sea quark masses as in QCD there is no difference between the sea quarks and valence quarks. The use of staggered action for sea quarks however introduces an ambiguity due to the non- degeneracy of the 16 staggered bosons associated with each pion. In practise, the valence masses are chosen such that the valence pion is tuned to one of the taste-singlet pions. The mismatch in the tuning is then removed while doing the analysis using the mixed action χPT .

3.1.2 Correlators and Fitting methods

In order to perform our calculations of the correlation functions we have used the software suite *Chroma*[34] developed at the Jefferson Lab. In order to compute the correlation functions, one has to construct interpolating operators from quark fields with appropriate quantum numbers. For example, the pion correlator constructed in terms of the interpolating operator is given as,

$$C_{\pi^+}(t) = \sum_x \langle \pi^+(t,\mathbf{x}) \; \pi^-(0,\mathbf{0}) \rangle \tag{3.1}$$

where $\pi^+(t,\mathbf{x}) = \bar{u}(t,\mathbf{x})\gamma_5 d(t,\mathbf{x})$ where u and d are the quark fields and the correlator is constructed from the propagators of quark fields. The long time behaviour of the correlator above is given as,

$$C_{\pi^+}(t) \sim A_{\pi^+}\cosh(m_{\pi^+}t) \tag{3.2}$$

Now, to improve the overlap with the ground state of the pion, one can use different techniques with interpolating fields such as smearing of the quark fields. In this work, we have used gauge invariant gaussian smearing of the sources and sinks of the quark fields and we make a linear combination of the two types of interpolating fields to facilitate a better extraction of ground state masses as follows,

$$C_{lin} = C_{(SS)} - \alpha \; C_{(SP)} \tag{3.3}$$

where, α is an arbitary parameter used in such a way that it minimizes the correlated χ^2 of the particular correlator. The ground state masses are obtained from correlators by a suitable redefinition in the form of an "effective mass" as follows,

$$m_\pi^{eff} = \frac{1}{J}\cosh^{-1}\left[\frac{C(t+J) + C(t-J)}{2C(t)}\right] \tag{3.4}$$

The results of such effective masses are shown in Fig 3-1 for coarse ensembles. The plots of other ensembles can be found in the Appendix for plots.

$m_\pi = 0.18175 \pm 0.00039 \pm 0.00013$ $\chi^2/dof = 1.1$ — Ensemble m007m050

$m_\pi = 0.22287 \pm 0.00028 \pm 2e\text{-}05$ $\chi^2/dof = 1.7$ — Ensemble m010m050

$m_\pi = 0.31091 \pm 0.00028 \pm 5e\text{-}05$ $\chi^2/dof = 1.3$ — Ensemble m020m050

$m_\pi = 0.37472 \pm 0.00024 \pm 0.00012$ $\chi^2/dof = 3.2$ — Ensemble m030m050
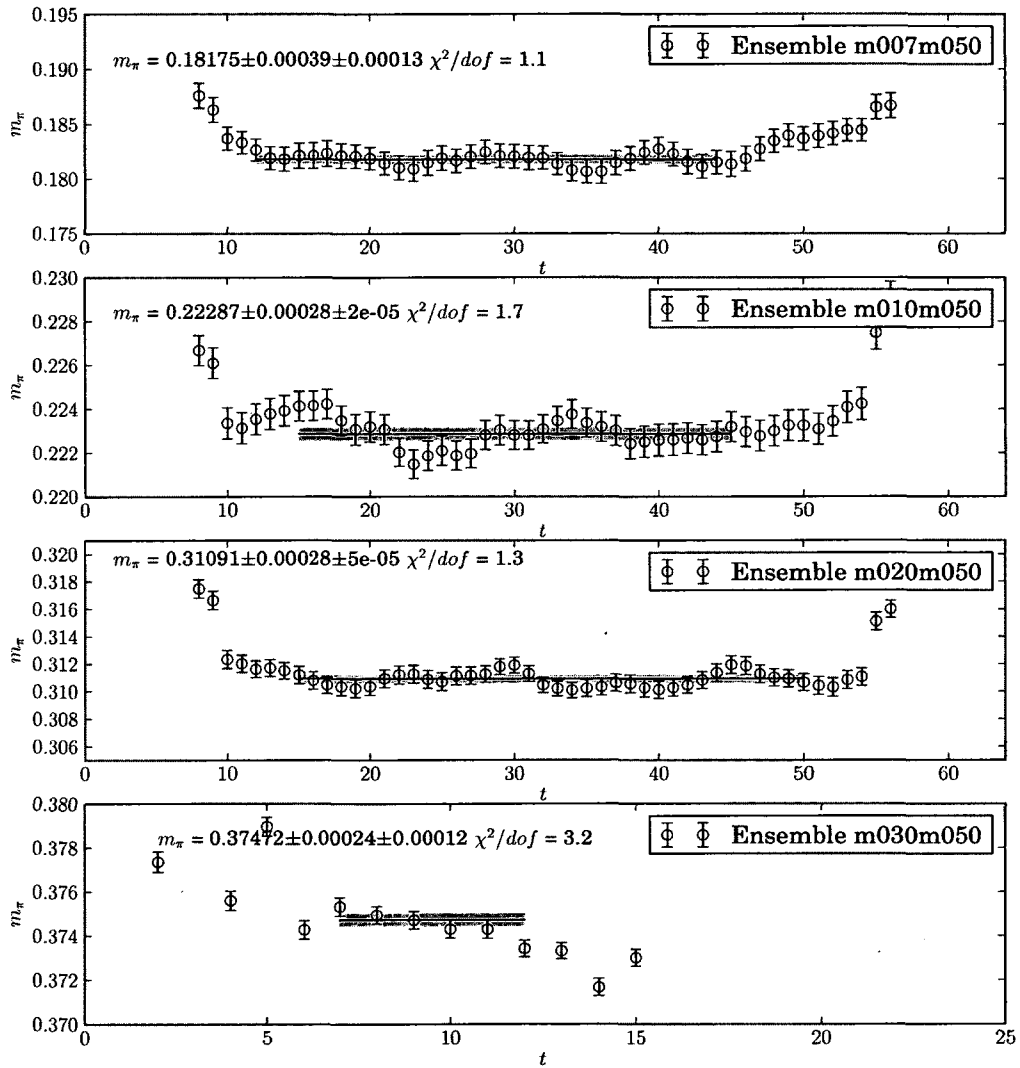
Figure 3-1: *Effective masses of Pions on coarse ensembles*
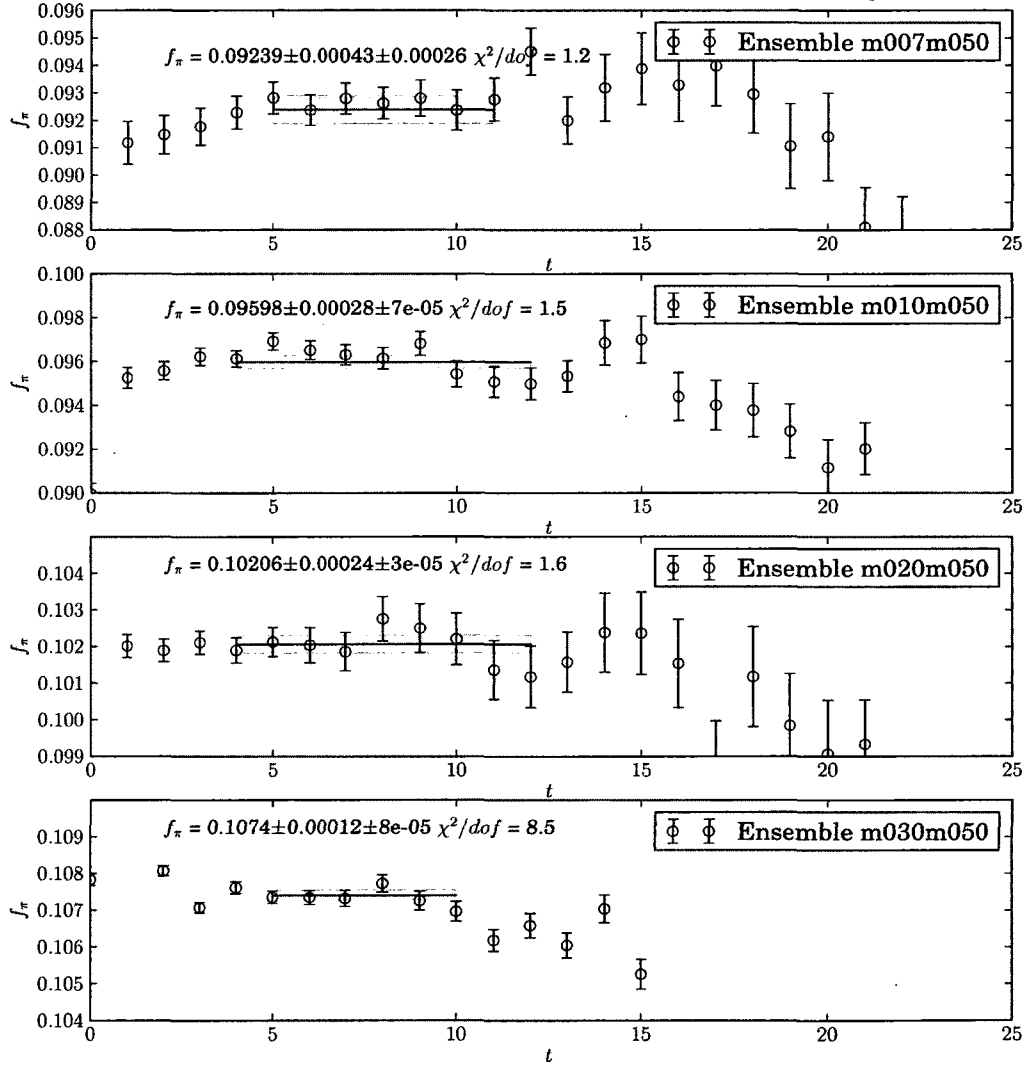
Figure 3-2: *Effective Pion Decay constant on coarse ensembles*

Table 3.2: *Pion masses and decay constants by Fitting the correlators*

$b \approx 0.125$ fm ensembles

m_{sea}	$L \times T \times L_5$	bm_π	bf_π	$bm_{\pi\text{mix}}$	$m_\pi L$
m007m050	$20 \times 32 \times 16$	0.18175(39)(13)	0.09239(43)(26)	0.2553(15)	3.78
m007m050	$24 \times 64 \times 16$	0.18202(45)(22)	0.09235(27)(13)	0.2553(15)	4.36
m010m030	$20 \times 64 \times 16$	0.22146(35)(10)	0.09402(17)(02)	0.28040(73)	4.48
m010m050	$20 \times 32 \times 16$	0.22287(28)(05)	0.09598(28)(07)	0.2842(15)	4.48
m010m050	$28 \times 64 \times 16$	0.22279(47)(22)	0.09650(45)(17)	0.2901(25)	6.27
m020m050	$20 \times 32 \times 16$	0.31091(28)(14)	0.10206(24)(03)	0.35159(93)	6.22
m030m030	$20 \times 64 \times 16$	0.37323(28)(05)	0.10641(17)(06)	0.40740(51)	7.56
m030m050	$20 \times 32 \times 16$	0.37465(26)(12)	0.10740(12)(08)	0.412(8)	7.56

$b \approx 0.09$ fm ensembles

m_{sea}	$L \times T \times L_5$	bm_π	bf_π	$bm_{\pi\text{mix}}$	$m_\pi L$
m0031m0186	$40 \times 96 \times 12$	0.10189(58)(12)	0.06182(79)(21)	0.13061(78)	4.08
m0031m0186	$40 \times 96 \times 12$	0.10189(58)(12)	0.06182(79)(21)	0.13064(78)	4.08
m0031m031	$40 \times 96 \times 40$	0.10397(89)(37)	0.06135(86)(33)	0.1344(14)	4.07
m0031m031	$40 \times 96 \times 12$	0.10205(54)(32)	0.06154(51)(12)	0.12934(82)	4.07
m0062m031	$28 \times 96 \times 12$	0.14548(21)(09)	0.06554(14)(05)	0.16320(98)	4.07
m0124m031	$28 \times 96 \times 12$	0.20045(33)(06)	0.07052(23)(03)	0.21530(25)	5.78

The computation pion decay constant f_π is done by computing the amplitudes of the correlation functions of smeared-smeared (SS) and smeared-point (SP) correlators as was done in [45]. The f_π from the lattice is computed as,

$$f_\pi = \frac{A_{SP}}{\sqrt{A_{SS}}} \left(\frac{2\sqrt{2}(m_l^{dwf} + m_l^{res})}{m_\pi^{3/2}} \right) \qquad (3.5)$$

With the redefinitions of correlators, one can also construct effective decay constant given as,

$$f_\pi^{eff} = \frac{C_\pi^{SP}(t)^{t+1}C_\pi^{SS}(t+1)^{t/2}}{C_\pi^{SS}(t)^{(t+1)/2}C_\pi^{SP}(t+1)^t} \left(\frac{2\sqrt{2}(m_l^{dwf} + m_l^{res})}{[\log(C_\pi^{SP}(t)C_\pi^{SP}(t+1)^{-1})]^{3/2}} \right) \qquad (3.6)$$

Table 3.3: r_1/b from MILC [1]. We use the values extrapolated to the physical light quark masses (right most column) to convert our lattice results to r_1 units.

m_{sea}	$L \times T \times L_5$	β	$\frac{r_1}{b}(bm_l, bm_s, \beta)$	$\frac{r_1}{b}(bm_l^{phy}, bm_s^{phy}, \beta)$
m007m050	$20 \times 64 \times 16$	6.76	2.635(3)	2.739(3)
m010m030	$20 \times 64 \times 16$	6.75	2.658(3)	2.711(3)
m010m050	$20 \times 64 \times 16$	6.76	2.618(3)	2.738(3)
m010m050	$28 \times 64 \times 16$	6.76	2.635(3)	2.738(3)
m020m050	$20 \times 64 \times 16$	6.79	2.644(3)	2.821(3)
m030m030	$20 \times 64 \times 16$	6.79	2.650(7)	2.821(7)
m030m050	$20 \times 64 \times 16$	6.81	2.650(4)	2.876(4)
m0031m0186	$40 \times 96 \times 12$	7.06	3.607(4)	3.687(4)
m0031m031	$40 \times 96 \times 40$	7.04	3.742(3)	3.755(3)
m0031m031	$40 \times 96 \times 12$	7.04	3.742(3)	3.755(3)
m0062m031	$28 \times 96 \times 12$	7.08	3.699(3)	3.788(3)
m0124m031	$28 \times 96 \times 12$	7.11	3.712(3)	3.858(3)

The pion effective decay constant plots are shown in Fig 3-2 on the coarse ensembles. The results on all the other ensembles are tabulated in Table

3.1.3 Scale Setting

To perform the chiral extrapolations of our computed pion masses and decay constants, we must address the issue of scale setting. As we are interested in determining the LECs of the two-flavor chiral Lagrangian, it is important to adopt a quark mass independent scale setting procedure. The MILC Collaboration has performed extensive scale setting analysis on their various ensembles. In this work we adopt their scale setting method and convert our pion mass and decay constant data into r_1 units extrapolated to the physical values of the light quark masses.[1] In Table 3.3 we

---

[1]The distance r_1 is defined using the heavy-quark potential as the sepparation $r_1^2 F(r_1) \equiv -1$.

list these values for the ensembles used in this work, which can be found in Ref. [1]. In this reference, the MILC Collaboration has determined $r_1 = 0.318(7)$ fm using the static quark potential and $r_1 = 0.312(2)\binom{3}{8}$ fm using f_π to set the scale. For this work, we take

$$r_1 = 0.312(2)\binom{3}{8} \text{ fm}, \tag{3.7}$$

as our central value for the scale setting.

3.2 Lattice Systematics

In order to make contact with experiment, numerical results computed with lattice QCD must be extrapolated to the continuum and infinite volume limits as well as the physical values of the light quark masses. Chiral perturbation theory is the natural tool to perform these extrapolations. Additionally, by performing this analysis, one determines the values of the low-energy constants, the *a priori* unknown coefficients of the operators in the chiral Lagrangian.

3.2.1 Light quark mass dependence

In two flavor chiral perturbation the quark mass dependence of the pion mass and decay constant upto NLO is given by,

$$m_\pi^2 = 2Bm_q\left\{1 + \frac{\xi}{2}\ln\left(\frac{\xi}{\xi^{phy}}\right) - \frac{1}{2}\xi\bar{l}_3\right\} \qquad f_\pi = f\left\{1 - \xi\ln\left(\frac{\xi}{\xi^{phy}}\right) + \xi\bar{l}_4\right\} \tag{3.8}$$

where,

$$\xi = \frac{m_\pi^2}{8\pi^2 f_\pi^2} \quad \text{and} \quad \bar{l}_i = \frac{\Lambda_i^2}{(m_\pi^{phy})^2} \tag{3.9}$$

and Λ_i is an intrinsic scale not determined by chiral symmetry. The finite volume corrections are also computed to the above quantities,

$$\Delta^{FV}\frac{m_\pi^2}{2Bm_q} = 8\pi^2\Delta\mathcal{I}(\xi, m_\pi L) \qquad \Delta^{FV}\frac{f_\pi}{f} = -16\pi^2\Delta\mathcal{I}(\xi, m_\pi L) \tag{3.10}$$

31

where,

$$8\pi^2 \Delta\mathcal{I} = \frac{2\xi}{m_\pi L} \sum_{n=1}^{\infty} \frac{k(n)}{\sqrt{n}} K_1(\sqrt{n} m_\pi L) \tag{3.11}$$

where, k(n) is the number of ways a given number n can be written as sum of squares of three integers, $n = \sum_{i=1}^{3} n_i^2$ with $n_i \in \mathbb{Z}$.

With available we are also able to perform an NNLO analysis of chiral expansion of m_π and f_π. In the continuum, they read as,

$$
\begin{aligned}
\frac{m_\pi^2}{2Bm_q} &= 1 + \frac{1}{2}\xi\left\{\ln\left(\frac{\xi}{\xi^{phy}}\right) - \bar{l}_3\right\} + \\
&\quad \frac{7}{8}\xi^2\ln^2(\xi) - \xi^2\ln(\xi)\left[\frac{16}{3} + \frac{1}{3}\bar{l}_{12} - \frac{9}{4}\bar{l}_3 - \bar{l}_4 - \frac{7}{4}\ln(\xi^{phy})\right] - \bar{l}_4\xi\xi^{phy} + \xi^2 k_M
\end{aligned}
\tag{3.12}
$$

and

$$
\begin{aligned}
\frac{f_\pi}{f} &= 1 + \xi\left\{\bar{l}_4 - \ln\left(\frac{\xi}{\xi^{phy}}\right)\right\} + \frac{5}{4}\xi^2\ln^2(\xi) + \\
&\quad \xi^2\ln(\xi)\left[\frac{53}{12} + \frac{1}{6}\bar{l}_{12} - 5\bar{l}_4 - \frac{5}{2}\ln(\xi^{phy})\right] + 2\bar{l}_4\xi\xi^{phy} + \xi^2 k_F
\end{aligned}
\tag{3.13}
$$

3.2.2 Mixed Action χPT

The low-energy EFT for mixed-action lattice calculations is well understood [46, 47, 48, 49, 50, 51, 52, 53, 54, 55, 56, 57, 58, 59]. At NLO in the MA expansion, including finite volume effects, the pion mass and decay constant are given by

$$
\begin{aligned}
\frac{m_\pi^2}{2Bm_q} &= 1 + \frac{1}{2}\xi\ln\left(\frac{\xi}{\xi^{phy}}\right) - \frac{1}{2}\xi\,\bar{l}_3 \\
&\quad -\frac{1}{2}(\tilde{\xi}_{\text{sea}} - \xi)\left[1 + \ln(\xi)\right] - l_{PQ}^m (\tilde{\xi}_{\text{sea}} - \xi) + l_b^m \left(\frac{b}{r_1}\right)^2 \\
&\quad +8\pi^2\Delta\mathcal{I}(\xi, m_\pi L) - \frac{\tilde{\xi}_{\text{sea}} - \xi}{2}\Delta\partial\mathcal{I}(\xi, m_\pi L)
\end{aligned}
\tag{3.14}
$$

$$
\begin{aligned}
\frac{f_\pi}{f} &= 1 - \tilde{\xi}_{\text{Mix}}\ln\left(\frac{\tilde{\xi}_{\text{Mix}}}{\xi^{phy}}\right) + \xi\bar{l}_4 - \left(\tilde{\xi}_{\text{Mix}} - \xi\right)\ln\left(\xi^{phy}\right) \\
&\quad -l_{PQ}^f (\tilde{\xi}_{\text{sea}} - \xi) + l_b^f \left(\frac{b}{r_1}\right)^2 - 16\pi^2\Delta\mathcal{I}(\tilde{\xi}_{\text{Mix}}, m_{\pi\text{Mix}} L),
\end{aligned}
\tag{3.15}
$$

Table 3.4: *Expansion parameters ξ, $\tilde{\xi}_{\text{Mix}}$, $\tilde{\xi}_{\text{sea}} - \xi$, $\xi_{\text{sea}} - \xi$ and $\frac{m^{res}}{m_q}$.*

m_{sea}	V	ξ	$\tilde{\xi}_{\text{Mix}}$	$\tilde{\xi}_{\text{sea}} - \xi$	$\xi_{\text{sea}} - \xi$	$\frac{m^{res}}{m_q}$
m007m050	$20^3 \times 64 \times 16$	0.04901	0.097	0.114	0.003	0.163
m007m050	$24^3 \times 64 \times 16$	0.04920	0.097	0.114	0.003	0.168
m010m030	$20^3 \times 64 \times 16$	0.07026	0.112	0.108	0.0015	0.101
m010m050	$20^3 \times 64 \times 16$	0.06828	0.111	0.103	0.0009	0.102
m010m050	$28^3 \times 64 \times 16$	0.06750	0.114	0.103	0.0014	0.102
m020m050	$20^3 \times 64 \times 16$	0.11753	0.150	0.091	0.0004	0.038
m030m030	$20^3 \times 64 \times 16$	0.15581	0.185	0.088	0.0043	0.021
m030m050	$20^3 \times 32 \times 16$	0.15411	0.186	0.087	0.0052	0.020
m0031m0186	$40 \times 96 \times 12$	0.0344	0.0565	0.0488	0.0024	0.119
m0031m0186	$40 \times 96 \times 12$	0.0344	0.0565	0.0488	0.0024	0.119
m0031m031	$40^3 \times 96 \times 40$	0.03601	0.060	0.0480	0.0008	0.039
m0031m031	$40^3 \times 96 \times 12$	0.03652	0.055	0.049	0.0023	0.109
m0062m031	$28^3 \times 96 \times 12$	0.06290	0.079	0.043	0.0019	0.045
m0124m031	$28^3 \times 96 \times 12$	0.10367	0.120	0.041	0.0063	0.017

where

$$\Delta \partial \mathcal{I}(\tilde{\xi}, mL) = \frac{1}{(4\pi)^2} \sum_{n=1}^{\infty} k(n) \left(\frac{2K_1(\sqrt{n}mL)}{\sqrt{n}mL} - K_0(\sqrt{n}mL) - K_2(\sqrt{n}mL) \right) \quad (3.16)$$

For our calculation, the extra expansion parameters of the theory are defined as

$$\tilde{\xi}_{\text{Mix}} = \frac{m_{\pi_{\text{Mix}}}^2 + b^2 \Delta'_{\text{Mix}}}{8\pi^2 f_\pi^2} \quad (3.17)$$

$$\tilde{\xi}_{\text{sea}} = \frac{m_{\pi_{\text{sea},5}}^2 + b^2 \Delta_{\text{I}}}{8\pi^2 f_\pi^2}$$

$$\xi_{\text{sea}} = \frac{m_{\pi_{\text{sea},5}}^2}{8\pi^2 f_\pi^2}$$

where $m_{\pi_{\text{sea},5}}$ is the taste-5 staggered pion mass, $b^2 \Delta_{\text{I}}$ is the mass splitting of the taste identity staggered pion and $b^2 \Delta'_{\text{Mix}}$ is the mass splitting of the mixed valence-

sea pion [56, 59]. In Table 3.4, we list the values of these parameters relevant for our calculation.

3.2.3 Residual chiral symmetry breaking effects

At finite L_5 extent, the domain-wall action has residual chiral symmetry breaking due to the overlap of the modes bound to opposite walls of the fifth-dimension. The m^{res} parameter is a symptom of this residual chiral symmetry breaking. It is customary to then define the quark mass as

$$m_l = m_l^{dwf} + m_l^{res} \tag{3.18}$$

This definition captures the dominant effects of the residual chiral symmetry breaking appearing at LO in the chiral Lagrangian. However, it is known that there are sub-leading effects. If one defines the quark mass through Eq. (3.18) and takes the standard definition of m^{res} [45]

$$m^{res} \equiv \frac{\langle 0 | J_{5q}^b | \pi \rangle}{\langle 0 | J_5^b | \pi \rangle} \tag{3.19}$$

there are two important consequences; the quantity $m^{res} = m^{res}(m_l)$ depends upon the input quark mass and lattice spacing; see Ref. [60] or a discussion of these effects. Therefore, the chiral Lagrangian receives a simple modification at NLO [61, 62, 63]. Following the method of Ref. [64], we can define the modifications to the Lagrangian at NLO as follows,

$$
\begin{aligned}
\delta\mathcal{L}_{res} &= \frac{l_3^{res} + l_4^{res}}{16} \mathrm{tr}\left(2Bm_q\Sigma + 2Bm_q\Sigma^\dagger\right)\mathrm{tr}\left(2Bm^{res}\Sigma + 2Bm^{res}\Sigma^\dagger\right) \quad (3.20) \\
&\quad + \frac{l_4^{res}}{8}\mathrm{tr}\left(\partial_\mu\Sigma\partial^\mu\Sigma^\dagger\right)\mathrm{tr}\left(2Bm^{res}S + 2Bm^{res}\Sigma^\dagger\right)
\end{aligned}
$$

This choice becomes clear when one computes the corrections to m_π and f_π arising from these new terms;

$$
\begin{aligned}
\frac{\delta m_\pi^2}{2 B m_q} &= -\frac{m^{res}}{m_q} \frac{\xi}{2} \bar{l}_3^{res} \\
\frac{\delta f_\pi}{f} &= \frac{m^{res}}{m_q} \xi \bar{l}_4^{res}
\end{aligned}
\tag{3.21}
$$

with $\bar{l}_i^{res} = \frac{l_i^{res}}{\gamma_i}$.

3.3 Chiral and Continuum Extrapolations

In this section, we perform chiral and continuum extrapolation of the lattice calculation of pion mass and decay constant. The lattice calculations are performed at unphysical quark masses and χPT provides a systematic expansion in quark mass and momentum of observables such as m_π and f_π. Hence, the lattice data can be used to determine the low energy constants of χPT and we shall attempt to do that here. The strategy we adopt is, first we fit the LEC's of both m_π and f_π to vanilla χPT , i.e, the one which does not include the effects of lattice artifacts. We fit the LEC's differently at $b \sim 0.125$ fm and $b \sim 0.09$ fm and perform the continuum extrapolation at NLO and NNLO in χPT . We use a fit ansatz for continuum extrapolation motivated by MAχPT as follows,

$$
\lambda(b) = \lambda_0 + \lambda_1 \left(\frac{b}{r_1}\right)^2
\tag{3.22}
$$

We then use MAχPT which systematically includes the effects of finite lattice spacing, different sea and valence discretisation and make comparison with the results of vanilla χPT extrapolations.

35

Table 3.5: *Results from continuum NLO χPT analysis of m_π.*

Max	Coarse Ensembles		
m_l/m_s	$\bar{l}_3$	χ^2	dof
0.4	4.908(29)(07)	18	2
0.4	5.061(36)(05)	37	3
0.6	5.008(13)(04)	38	4
Max	Fine Ensembles		
m_l/m_s	$\bar{l}_3$	χ^2	dof
0.2	4.132(95)(26)	9	2
0.2	3.658(56)(17)	10	3
0.4	4.004(25)(05)	12	4

3.3.1 Vanilla χPT Extrapolations

NLO SU(2) Fit

We fit the NLO expressions Eq.[3.8] to lattice computed m_π and f_π and determine the SU(2) LEC's $\bar{l}_3$ and $\bar{l}_4$. This is done independently for $b \sim 0.125$ fm and $b \sim 0.09$ fm including the finite volume corrections Eqs.[3.10]. The results for the fits are shown in Tables 3.5 and3.6]. The uncertainty in ξ is used to determine the uncertainty in $\bar{l}_3$ and $\bar{l}_4$ by performing a Monte-carlo. The fits are performed in such a way that we include the degrees of freedom by including data with higher quark masses. This is denoted in the data included by the ratio of m_l/m_s.

The results presented in Tables 3.5 and 3.6 should be looked at cautiously. From the results of m_π, the NLO χPT fails to describe the lattice data at either lattice spacing. The results of f_π, NLO χPT seems to describe the data well at both lattice spacings. Taking the results of the fits with $m_l/m_s \leq 0.4$ and performing continuum

36

Table 3.6: *Results from continuum NLO χPT analysis of f_π.*

Max	Coarse Ensembles $b \sim 0.125$ fm			
m_l/m_s	$r_1 f$	$\bar{l}_4$	χ^2	dof
0.4	0.2114(4)(1)	5.164(34)(11)	2.3	2
0.4	0.2116(5)(2)	5.158(38)(10)	2.3	3
0.6	0.2136(2)(1)	4.990(15)(06)	9.3	4
Max	Fine Ensembles $b \sim 0.09$ fm			
m_l/m_s	$r_1 f$	$\bar{l}_4$	χ^2/dof	
0.2	0.1980(10)(04)	5.52(12)(04)	0.9	2
0.2	0.1974(08)(04)	5.59(9)(4)	1.3	3
0.4	0.1959(08)(01)	5.74(8)(1)	1.7	4

extrapolation described the Eq. 6.12, we find,

$$\bar{l}_3 = 3.13(12)(03) \quad \text{and} \quad \bar{l}_4 = 5.97(3)(1) \tag{3.23}$$

NLO + NNLO SU(2) Fit

At NNLO at in two flavor χPT , more LEC's appear in addition to $\bar{l}_3$ & $\bar{l}_4$, namely k_M & k_F and $\bar{l}_1$ & $\bar{l}_2$ and their linear combination such $\bar{l}_{12} = 7\bar{l}_1 + 8\bar{l}_2$. Both $\bar{l}_1$ and $\bar{l}_2$ are reasonably well determined from $\pi\pi$ scattering [65];

$$\bar{l}_1 = -0.4(6), \quad\quad\quad \bar{l}_2 = 4.3(1). \tag{3.24}$$

To perform these analyses, we input the values of $\bar{l}_1$ and $\bar{l}_2$. For each of these LECs, we generate a list of normally distributed values with mean and width given by Eq. (3.24), and then use the spread of the results to propagate this systematic uncertainty through the analysis.

The results of the fits are presented in Table 3.7. The NNLO formula can describe both m_π and f_π excluding the heaviest mass point. If we take the the $b \approx 0.125$ fm

Table 3.7: *Results from continuum NNLO χPT analysis of m_π and f_π.*

$b \approx 0.125$ fm						
Fit	$r_1 f$	$\bar{l}_3$	$\bar{l}_4$	k_M	k_F	χ^2/dof
0.4	0.212(6)(3)	7.53(67)(1.1)	4.68(90)(39)	-5(4)(10)	-13(16)(6)	2.68/3
0.6	0.211(7)(7)	5.50(82)(1.2)	4.47(68)(73)	-11(5)(8)	-6(10)(10)	37/3

$b \approx 0.09$ fm						
Fit	$r_1 f$	$\bar{l}_3$	$\bar{l}_4$	k_M	k_F	χ^2/dof
0.4	0.202(2)(2)	5.96(49)(43)	4.07(22)(25)	-8(3)(3)	3(3)(3)(4)	6/3

and $b \approx 0.09$ fm fit and use them to perform a continuum extrapolation, we obtain

$$\bar{l}_3 = 3.90(84)(1.0), \qquad \bar{l}_4 = 3.54(39)(59). \qquad (3.25)$$

The value of $\bar{l}_3$ is a bit unstable in going from NLO to NNLO. However, one can not conclude much from this since the NLO fit to m_π was poorly behaved. For $\bar{l}_4$, we find nice stability of the result, with the value going towards the lattice average value with the inclusion of the NNLO analysis.

3.3.2 Mixed Action χPT Extrapolations

The Mixed action χPT includes the lattice spacing effects and other unphysical effects such partial quenching. At NLO, the analysis for m_π and f_π can be separately and since the lattice spacing effects are already included, one can fit the data on $b \approx 0.09$ fm and $b \approx 0.125$ fm . This provides an enlarged data set for analysis.

MAχPT Fit at NLO

The MAχPT fits are presented in Tables 3.8 and 3.9 for various sets of quark masses indicating various degrees of freedom. There are a few observations to make. First, the NLO MAPT formula is capable of describing the results of the Lattice QCD

Table 3.8: *Results from NLO MA χPT analysis of m_π*

Fit	$\bar{l}_3$	$\bar{l}_3^b$	$\bar{l}_3^{res}$	$\bar{l}_3^{PQ}$	χ^2/dof
A	3.66(53)(38)	-1.3(1.0)(0.9)	13(27)(25)	0.25(9)(8)	7/1
B	3.75(48)(21)	-1.34(59)(51)	12(16)(14)	0.86(7)(6)	10/2
C	3.56(50)(32)	-1.37(43)(28)	12(11)(7)	0.42(1.4)(1.0)	11/3
D	3.58(49)(28)	-1.60(47)(27)	6(12)(7)	0.02(1.6)(0.89)	14/4

Table 3.9: *Results from NLO MA χPT analysis of f_π*

Fit	$r_1 f$	$\bar{l}_4$	$\bar{l}_4^b$	$\bar{l}_4^{res}$	$\bar{l}_4^{PQ}$	χ^2/dof
A	0.1787(34)(56)	6.82(33)(31)	0.39(49)(73)	1(6)(11)	-0.54(6)(14)	1.2/1
B	0.1797(30)(33)	6.78(23)(18)	0.14(42)(44)	3(5)(5)	-2(4)(4)	1.8/2
C	0.1799(21)(25)	6.75(18)(19)	0.14(27)(34)	3(3)(4)	-2(2)(3)	2/3
D	0.1840(13)(08)	6.36(20)(12)	0.16(36)(24)	2(4)(3)	0.9(1)(0.9)	4.9/4

calculations of m, unlike the NLO PT formula. Second, the MAPT provides a slightly better description of the pion decay constant than of the pion mass. In both cases, the NLO formula is capable of describing the results of the Lattice QCD calculations over the full range of quark-masses. To quote our final results for MA analysis, we perform a weighted average of our results using the $1/\chi^2$ as the weights such that the results with lower χ^2 will have a higher a weight. The result for $\bar{l}_3$ and $\bar{l}_4$ from the weighted average is given as,

$$\bar{l}_3 = 3.70(22)(11)\,, \qquad\qquad \bar{l}_4 = 6.72(38)(12)\,. \qquad\qquad (3.26)$$

The result for $\bar{l}_3$ is consistent with the lattice average. The results for $\bar{l}_4$ is noticeably higher than the average.

Results for f_π from NNLO MAχPT plus NNLO SU(2) χPT.

Fit	$r_1 f$	$\bar{l}_4$	k_F	l_b^f	$\bar{l}_4^{res}$	$\chi^2/\,dof$
A	0.1772(38)(12)	5.56(58)(17)	$-17(9)(4)$	0.5(4)(3)	1(6)(4)	1.60/ 3
B	0.1784(35)(09)	5.27(40)(10)	$-13(6)(5)$	0.68(30)(12)	$-2(4)(3)$	2.00/4
C	0.1867(20)(14)	4.28(14)(09)	3(10)(4)	0.3(3)(3)	$-1(4)(2)$	11.3/5

Hybrid Fit - NLO MAχPT + NNLO SU(2) χPT

In this section, we consider a hybrid MA χPT fit due to lack of availability of NNLO MAχPT expressions. It will be an interesting study look at the change in LEC's at NLO by considering NNLO effects. The LEC's at NLO will still include the lattice spacing and discretisation effects, although the NNLO LEC's will not be free of those. The NNLO contribution to f_π contains only the LEC $\bar{l}_4$ and can be fit separately. The results of the fits with several degrees of freedom is presented in Table 3.10. We have also performed a weighted average with the weights as $1/\chi^2$ and the result of this averaging is given as,

$$\bar{l}_4 = 5.32(38)(14) \tag{3.27}$$

The NNLO contribution to m_π has contributions depends on both $\bar{l}_3$ and $\bar{l}_4$ and hence we need to perform a combined analysis on m_π and f_π . We therefore fit the total $\chi^2 = \chi^2_{m_\pi} + \chi^2_{f_\pi}$. The results are given as,

$$\bar{l}_3 = 4.08(28)(19), \qquad \bar{l}_4 = 5.42(47)(12) \tag{3.28}$$

3.3.3 Convergence of SU(2) chiral expansion

The analysis of the above LEC's enables us to explore the convergence of the chiral expansion from the orders LO, NLO and NNLO. The quantities we have used for the

expansion are,

$$\frac{m_\pi^2}{2Bm_q} - 1 \qquad \frac{f_\pi}{f} - 1 \tag{3.29}$$
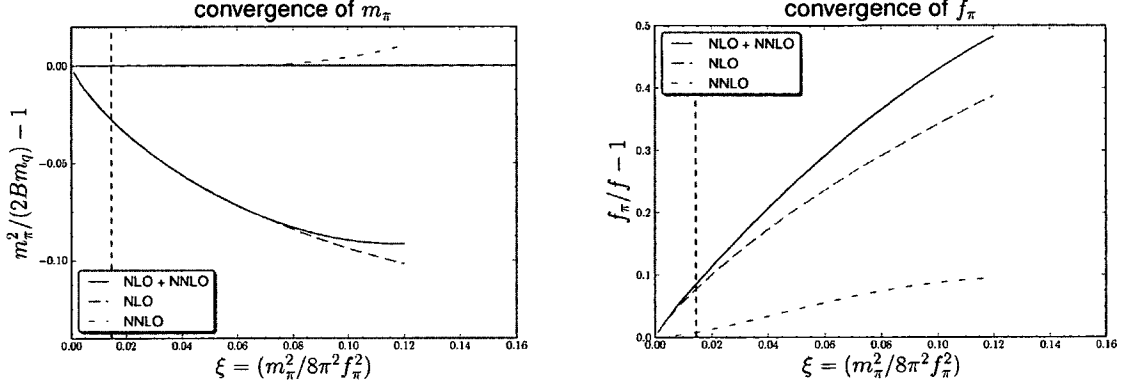
The results for the LEC's that we have used, have been extrapolated to continuum and infinite volume limits. As seen in the figures, the red dashed line is the NLO contribution and blue dashed line is NNLO contribution. The solid line is the combined contribution of NLO and NNLO. For the case of m_π, the NNLO contribution is negligible over most of the range of ξ used in this work. Hence we conclude that the chiral expansion for m_π has a good perturbative behaviour. The case of f_π does not seem to appear so perturbative. The NNLO contributions to the f_π at higher quark masses is substanstial on the order of 40 % signalling the breakdown of chiral expansion.

3.4 Results and Conclusions

The mixed action program has been widely used in the lattice community to compute observables. In this work, we have explored the effects of discretisation in two flavor χPT for m_π and f_π. We did this with a detailed analysis on continuum χPT at NLO and NNLO orders at two lattice spacings independently, and then performed a continuum extrapolation of the LECs. Our analysis revealed that the continuum χPT did not provide a good description for m_π while the continuum χPT formula for

f_π is able to describe the data well.

We then performed a mixed action analysis and the resulting values of $\bar{l}_3$ and $\bar{l}_4$ from our analysis are,

$$\bar{l}_3 = 4.08(28)(19), \qquad \bar{l}_4 = 5.42(47)(12) \tag{3.30}$$

Our analysis for the mixed-action χPT showed that the mixed-action χPT provides a good fit to the lattice data. With this analysis, we also explored the convergence of the two flavor chiral expansion for m_π and f_π. The expansion for m_π is convergent over the range of quark masses used in this work while the expansion for f_π broke down for higher quark masses.

Chapter 4

SU(3) Low Energy Constants from Lattice QCD

The SU(3) χPT is a low energy effective field theory of QCD with three light flavors of quarks (u,d and s). The π, K and η are the pseudo-Goldstone bosons in this theory and we intend to explore the quark mass dependence of the masses and decay constants of these goldstone bosons. Due to limited computaional ability, we are not able to study the η meson and in this work, we will focus only on pions and kaons.

In this chapter we will present our results on SU(3) low energy constants from our lattice calculations. In Sec 4.1, we discuss the details of the lattices used, scale setting procedure and the analysis of lattice data . In Sec 4.2, we discuss the systemactics of the SU(3) χPT along with finite volume corrections and MAχPT used in this work. In Sec 4.3, we perform analysis of the lattice data and finally in Sec 4.4, we dwell on the results of our analysis and draw conclusions thereof.

4.1   Details of Lattice Calculation

We have used the mixed action scheme [33, 34, 35, 36, 37, 38] of lattice calculations in our work. For the purpose of this chapter, the lattices used are the same as detailed in Sec 3.1. We briefly summarize that content for the purpose of completeness.

4.1.1 Lattice input parameters

According to the mixed action scheme, we have employed the domain-wall valence quarks (as described in Sec 1.4.2) [12, 41, 42, 43, 44] on $N_f = 2+1$ (two flavors of light degenerate quarks and one flavor of heavy/strange quark) MILC gauge configurations [40, 1, 66] with staggered sea quarks as described in Sec 1.4.1. In the generation of configurations, the strange quark mass was fixed near its physical value, determined from mass of hadrons containing strange quarks. We have used configurations with a variety of quark masses at two lattice spacings namely $b \approx 0.125$ fm and $b \approx 0.09$ fm with box size ranging from $L \sim 2 - 3.5$fm. The parameters used in this calculation are tabulated as in Table 3.1 of chapter 2

4.1.2 Correlators, Fitting and Scale Setting

In order to study SU(3) χPT from lattice data, one has to perform a lattice calculation with three flavors of sea and valence quarks. The mesons generated from such a calculation will include the effects of all three flavors. In this work, we have used lattices with three flavors of quarks as described above. Hence the pion correlators calculated in 3.2 already include the effects of all three flavors and are amenable to a SU(3) analysis. For kaons, we have computed kaon correlators from the interpolating operators with appropriate quantum numbers as follows,

$$C_{K^+}(t) = \sum_x \langle K^+(\mathbf{x}, t) K^+(0, 0) \rangle \tag{4.1}$$

where, $K^+(\mathbf{x}, t) = \bar{s}(\mathbf{x}, t)\gamma_5 u(\mathbf{x}, t)$ and the sum over all spacial points makes a projection onto a zero momentum state. The long time behaviour of a mesonic correlator on the lattice has a hyperbolic cosine behaviour as discussed in Sec 3.1.2. The ground state masses and decay constants are extracted by constructing their respective ef-

Table 4.1: *Kaon masses and decay constants from Fitting the correlators*

m_{sea}	$L \times T \times L_5$	bm_K	bf_K	$\frac{m_K^2}{m_\pi^2}$
		$b \approx 0.125$ fm ensembles		
m007m050	$20 \times 64 \times 16$	0.36782(41)(11)	0.10650(30)(10)	4.0880(136)(37)
m007m050	$24 \times 64 \times 16$	0.36761(32)(08)	0.10585(23)(04)	4.0942(70)(08)
m010m030	$20 \times 64 \times 16$	0.37612(32)(08)	0.10545(15)(06)	2.8786(57)(21)
m010m050	$20 \times 64 \times 16$	0.37841(29)(05)	0.10760(27)(01)	2.8843(54)(13)
m010m050	$28 \times 64 \times 16$	0.37896(50)(22)	0.10802(39)(12)	2.8921(46)(03)
m020m050	$20 \times 64 \times 16$	0.40505(28)(06)	0.10947(26)(01)	1.6975(16)(02)
m030m030	$20 \times 64 \times 16$	0.42941(30)(16)	0.11107(18)(09)	1.3206(04)(01)
m030m050	$20 \times 32 \times 16$	0.43043(24)(18)	0.11212(13)(02)	1.3203(03)(03)
		$b \approx 0.09$ fm ensembles		
m0031m0186	$40 \times 96 \times 12$	0.18814(57)(11)	0.06768(54)(04)	3.4430(186)(030)
m0031m0186	$40 \times 96 \times 12$	0.23486(62)(11)	0.07142(52)(12)	5.3571(331)(054)
m0031m031	$40 \times 96 \times 40$	0.23582(91)(31)	0.07233(70)(11)	5.2146(321)(074)
m0031m031	$40 \times 96 \times 12$	0.23568(56)(41)	0.07176(42)(06)	5.4039(242)(039)
m0062m031	$28 \times 96 \times 12$	0.24685(19)(06)	0.07328(17)(08)	2.8754(34)(08)
m0124m031	$28 \times 96 \times 12$	0.26428(32)(11)	0.07574(30)(10)	1.7408(11)(0)

fective quantities are as follows,

$$m_K^{eff} = \frac{1}{J}\cosh^{-1}\left[\frac{C_K(t+J)+C_K(t-J)}{2C_K(t)}\right] \tag{4.2}$$

$$f_K^{eff} = \frac{C_K^{SP}(t)^{t+1}C_K^{SS}(t+1)^{t/2}}{C_K^{SS}(t)^{(t+1)/2}C_K^{SP}(t+1)^t}\left(\frac{\sqrt{2}(m_l^{dwf}+m_l^{res}+m_s^{dwf}+m_s^{mres})}{[\log(C_K^{SP}(t)C_K^{SP}(t+1)^{-1})]^{3/2}}\right)$$

The results for the masses and decay constants on a subset of $b \approx 0.125$ fm ensembles is presented in Figures 4-1 and 4-2. The results on all the other ensembles can be found in the Appendix for plots.

In addition to pion and kaon masses and decay constants, it is also desirable to
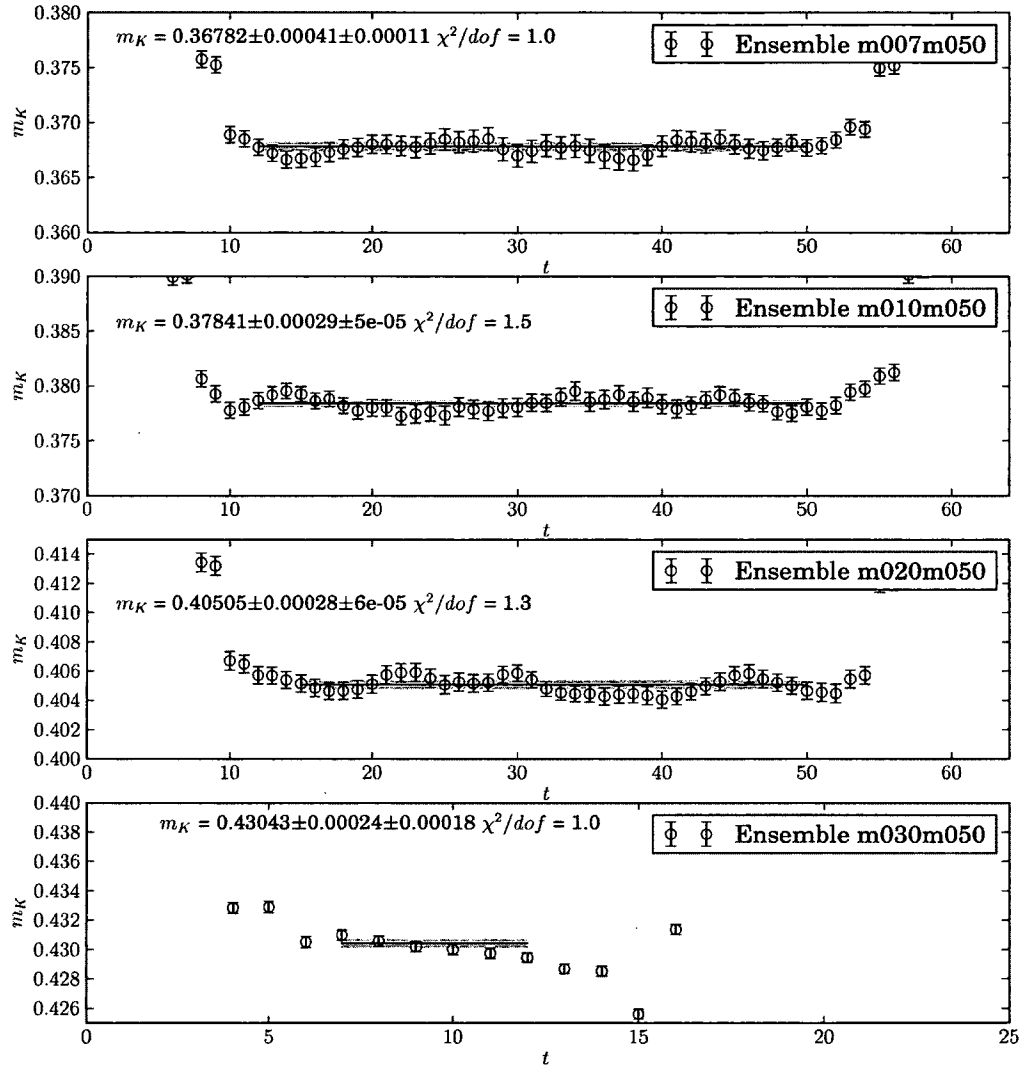
Figure 4-1: *Effective Kaon masses b ≈ 0.125 fm ensembles*
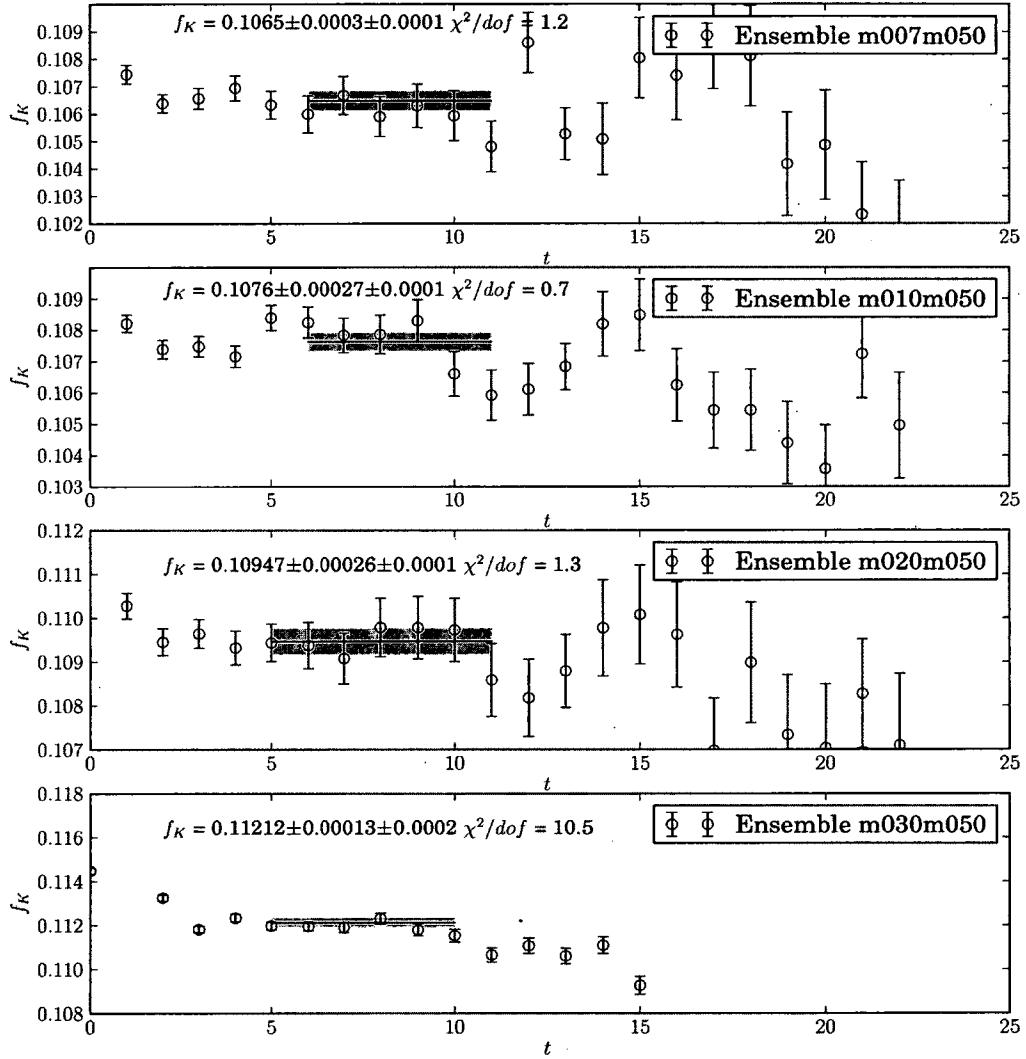
Figure 4-2: *Effective Kaon Decay constant b ≈ 0.125 fm ensembles*

construct their ratios as $\frac{m_K^2}{m_\pi^2}$ and $\frac{f_K}{f_\pi}$ since analysing the ratios simplifies the analysis and also provides a consistency check. We have used the lattice data to construct such ratios and the results are presented in Table 4.1.

In order to determine quantities in physical units from lattice calculations, the scale at which lattice calculations are performed must be determined. The procedure for scale setting for this work is already discussed in Sec 3.1.3, and will not be repeated here.

4.2   Systematics of SU(3) χPT

The SU(3) χPT is a three flavor expansion of u,d and s quark around the chiral limit of low energy QCD [8]. In comparision with the SU(2), there two LEC's at the leading order $\mathcal{O}(p^2)$ and ten LEC's at NLO $\mathcal{O}(p^4)$. The masses and decay constants of the pseudo Nambu-Goldstone bosons in the isospin limit have been evaluated by Gasser and Leutwyler [8] as,

$$
\begin{aligned}
\frac{m_\pi^2}{2\bar{m}} &= B_0\Big\{1 + \mu_\pi - \frac{1}{3}\mu_\eta + 16\xi^2(2L_8 - L_5) + 16(\xi^2 + 2\eta^2)(2L_6 - L_4)\Big\} \quad (4.3) \\
\frac{m_K^2}{(\bar{m} + m_s)} &= B_0\Big\{1 + \frac{2}{3}\mu_\eta + 16\eta^2(2L_8 - L_5) + 16(\xi^2 + 2\eta^2)(2L_6 - L_4)\Big\} \\
f_\pi &= f_0\Big\{1 - 2\mu_\pi - \mu_K + 8\xi^2 L_5 + 8(\xi^2 + 2\eta^2)L_4\Big\} \\
f_K &= f_0\Big\{1 - \frac{3}{4}\mu_\pi - \frac{3}{2}\mu_K - \frac{3}{4}\mu_\eta + 8\eta^2 L_5 + 8(\xi^2 + 2\eta^2)L_4\Big\}
\end{aligned}
$$

In our lattice calculation, we have not computed the η correlators as evaluating them involves computing disconnected diagrams and as such is computationally expensive. From χPT point of view, the order at which we are working allows us to use the leading order GMO (Gell-Mann Okubo) mass relations among mesons as follows,

$$
m_\eta = \frac{1}{3}\big(4m_K^2 - m_\pi^2\big) \tag{4.4}
$$

Table 4.2: *The ratio $\frac{f_K}{f_\pi}$ computed on the Lattice and Chiral Expansion parameters*

		$b \approx 0.125$ fm ensembles		
m_{sea}	$L \times T \times L_5$	$\frac{f_K}{f_\pi}$	ξ^2	η^2
m007m050	$20 \times 64 \times 16$	1.1449(47)(34)	3.977(28)(15)	15.93(90)(44)
m007m050	$24 \times 64 \times 16$	1.1443(30)(06)	3.885(42)(02)	15.84(12)(05)
m010m030	$20 \times 64 \times 16$	1.1242(13)(09)	5.548(38)(07)	16.003(85)(14)
m010m050	$20 \times 64 \times 16$	1.1198(22)(10)	5.380(29)(16)	15.488(70)(49)
m010m050	$28 \times 64 \times 16$	1.1155(31)(19)	5.330(72)(29)	15.42(18)(07)
m020m050	$20 \times 64 \times 16$	1.0722(11)(04)	9.315(43)(27)	15.807(66)(39)
m030m030	$20 \times 64 \times 16$	1.0443(05)(03)	12.302(58)(17)	16.285(75)(03)
m030m050	$20 \times 64 \times 16$	1.0430(03)(02)	12.242(67)(31)	16.173(87)(45)

		$b \approx 0.09$ fm ensembles		
m_{sea}	$L \times T \times L_5$	$\frac{f_K(L)}{f_\pi(L)}$	ξ^2	η^2
m0031m0186	$40 \times 96 \times 12$	1.0865(57)(32)	2.71(10)(02)	9.26(29)(07)
m0031m0186	$40 \times 96 \times 12$	1.1454(77)(32)	2.71(10)(02)	14.43(44)(11)
m0031m031	$40 \times 96 \times 40$	1.1594(103)(27)	2.87(13)(05)	14.77(52)(19)
m0031m031	$40 \times 96 \times 12$	1.1509(79)(35)	2.750(75)(28)	14.66(31)(10)
m0062m031	$28 \times 96 \times 12$	1.1224(14)(03)	4.927(35)(14)	14.186(82)(29)
m0124m031	$28 \times 96 \times 12$	1.0764(13)(03)	8.080(79)(12)	14.04(12)(02)

The functions μ_P in Eq 4.3 are redefined as follows,

$$\mu_\pi \equiv \frac{1}{16\pi^2}\xi^2\log(\xi^2), \quad \mu_K \equiv \frac{1}{16\pi^2}\eta^2\log(\eta^2), \quad \mu_\eta \equiv \frac{1}{16\pi^2}\frac{(4\eta^2 - \xi^2)}{3}\log\left(\frac{4\eta^2 - \xi^2}{3}\right)$$
$$(4.5)$$

In the redefinitions of μ_P, the renormalisation scale is set to $\mu = bf_\pi$ and the variables ξ and η are set to $\xi = m_\pi/f_\pi$ and $\eta = m_K/f_\pi$. The results of chiral expansion parameters ξ and η computed from the ground state meson masses and decay constants is presented in Table 4.2. The lattice data of masses and decay

constants is corrected for finite volume corrections as computed [67, 17, 18],

$$\Delta_{FV}\left(\frac{m_\pi^2}{2\bar{m}B_0}\right) = \frac{1}{2}\mathcal{I}(\xi, m_\pi L) - \frac{1}{6}\mathcal{I}(\xi_\eta, m_\eta L) \tag{4.6}$$

$$\Delta_{FV}\left(\frac{m_K^2}{(\bar{m}+m_s)B_0}\right) = \frac{1}{3}\mathcal{I}(\xi_\eta, m_\eta L)$$

$$\Delta_{FV}\left(\frac{f_\pi}{f_0}\right) = -2\mathcal{I}(\xi, m_\pi L) - \mathcal{I}(\eta, m_K L)$$

$$\Delta_{FV}\left(\frac{f_K}{f_0}\right) = -\frac{3}{4}\mathcal{I}(\xi, m_\pi L) - \frac{3}{2}\mathcal{I}(\eta, m_K L) - \frac{3}{4}\mathcal{I}(\xi_\eta, m_\eta L)$$

where the definition of ξ_η is the straightforward extension. The finite volume sums $\mathcal{I}(\xi)$ are evaluated as [18],

$$\mathcal{I}(\xi, mL) \equiv \frac{\xi^2}{4\pi^2}\sum_{n=1}^{\infty}\frac{k(n)}{\sqrt{n}mL}K_1(\sqrt{n}mL) \tag{4.7}$$

where, $k(n)$ is the multiplicity of the number ways a given number in the sum can represented as sum of squares three integers. Such sums arise as a part of summing over three dimension after replacing the regularising integral by sums.

4.2.1 Fitting Strategy

Our aim is to determine to all the LEC's appearing in the Eq.[4.3]. A direct way to obtain these is to perform a simultaneous χ^2 minimization of Eq.[4.3] which is what we will be doing. However the fits can be performed consistently if we make certain observations of Eq.[4.3]. The strategy that we will be adopting is to fit ratios of masses and decay constants and compare the fits to global fit to Eq.[4.3].

Determination of L_5

The ratio of f_K/f_π is described by only one constant that of L_5 and can be obtained by fitting lattice computed results. At NLO in SU(3) χPT , it is evaluated including

finite volume corrections as,

$$\frac{f_K}{f_\pi} = 1 + \frac{5}{4}\mu_\pi - \frac{1}{2}\mu_K - \frac{3}{4}\mu_\eta + 8(\eta^2 - \xi^2)L_5 + \frac{5}{4}\mathcal{I}(\xi, m_\pi L) - \frac{1}{2}\mathcal{I}(\eta, m_K L) - \frac{3}{4}\mathcal{I}(\xi_\eta, m_\eta L)$$

(4.8)

The determination of L_5 is significant by itself as the ratio $\frac{f_K}{f_\pi}$ is important in accurately determining the CKM matrix elements . In particular, the CKM matrix element $|V_{us}|$ can be determined accurately from $|V_{ud}|$ with the lattice determinations of $\frac{f_K}{f_\pi}$ as shown in [68]. We will present a separate and detailed analysis of f_K/f_π with finite volume effects and mixed action corrections.

Determination of $2L_8 - L_5$

The ratio of mesons m_K^2/m_π^2 in SU(3) χPT has two constants L_8 and L_5 at NLO. We perform a simulteneous χ^2 minimization with f_K/f_π to obtain L_8.

$$\frac{m_K^2}{m_\pi^2} = \frac{\bar{m} + m_s}{\bar{m}}\left\{1 + \mu_\eta - \mu_\pi + 16(\eta^2 - \xi^2)(2L_8 - L_5) + \frac{1}{2}\mathcal{I}(\xi_\eta, m_\eta L) - \frac{1}{2}\mathcal{I}(\xi, m_\pi L)\right\}$$

(4.9)

The results for the fits will include finite volume and mixed action corrrections and will be presented in Sec 4.3.

4.2.2 Three flavor Mixed Action χPT

The mixed action χPT has been studied extensively [46, 47, 48, 49, 50, 51, 52, 53, 54, 55, 56, 57, 58, 59] describes the results of lattice calculation very closely as it includes the knowledge of discretisation of sea and valence sector including the effects of different sea and valence quark masses and the effects of finite lattice spacing. The three flavor MA χPT [54] includes the valence and sea strange quarks effects and is considerably complicated compared to its two flavor cousin. In the three flavor theory, the unitarity violating effects are taken into account via the light and strange

Table 4.3: *Expansion parameters for MA χPT*

m_{sea}	$L \times T \times L_5$	Δ_{ju}^2	Δ_{rs}^2	$\tilde{m}_X$
$b \approx 0.125$ fm ensembles				
m007m050	$20 \times 64 \times 16$	0.23197(50)	0.526(11)	0.9389(78)
m007m050	$24 \times 64 \times 16$	0.23197(50)	0.526(11)	0.9389(78)
m010m030	$20 \times 64 \times 16$	0.22400(51)	0.1904(60)	0.8225(43)
m010m050	$20 \times 64 \times 16$	0.22825(59)	0.479(16)	0.9405(43)
m010m050	$28 \times 64 \times 16$	0.22853(102)	0.515(25)	0.953(10)
m020m050	$20 \times 64 \times 16$	0.24135(79)	0.488(10)	0.989(16)
m030m030	$20 \times 64 \times 16$	0.25251(91)	0.1330(63)	0.8968(64)
m030m050	$20 \times 64 \times 16$	0.2653(53)	0.434(12)	1.0225(45)
$b \approx 0.09$ fm ensembles				
m_{sea}	$L \times T \times L_5$	Δ_{ju}^2	Δ_{rs}^2	$\tilde{m}_X$
m0031m0186	$40 \times 96 \times 12$	0.0807(4)	0.1804(74)	0.6134(70)
m0031m0186	$40 \times 96 \times 12$	0.0807(4)	-0.0300(83)	0.6134(70)
m0031m031	$40 \times 96 \times 40$	0.0819(5)	0.210(17)	0.744(14)
m0031m031	$40 \times 96 \times 12$	0.0839(3)	0.205(11)	0.7409(98)
m0062m031	$28 \times 96 \times 12$	0.0853(7)	0.204(14)	0.757(11)
m0124m031	$28 \times 96 \times 12$	0.0982(5)	0.1961(44)	0.7955(32)

partially quenched parameters as,

$$\Delta_{ju}^2 \equiv \tilde{m}_{jj}^2 - m_{uu}^2 = 2B_0(m_j - m_u) + b^2 \Delta_I + ... \qquad (4.10)$$

$$\Delta_{rs}^2 \equiv \tilde{m}_{rr}^2 - m_{ss}^2 = 2B_0(m_r - m_s) + b^2 \Delta_I + ...$$

where the subscript j and r correspond to the light and strange sea quarks and u and s correspond to the light and sea valence degree of freedom. These parameters quantify the departure of the mixed action theory from QCD and to have the most QCD like situation have to be tuned to zero by the appropriate choice of valence

quarks. The mixed mesons (mesons comprised of one sea and one valence quarks) and sea mesons also receive corrections due to the finite lattice spacing and the effect of discretisation (in case of mixed mesons) and are given as follows [54],

$$\tilde{m}_{vs}^2 = B_0(m_v + m_s) + b^2 \Delta_{mix} \tag{4.11}$$

$$\tilde{m}_{ss}^2 = 2B_0 m_s + b^2 \Delta_I$$

where the subscript vs indicate a mixed meson with valence-sea degree of freedom and ss indicate sea-sea degree of freedom. The quantities $b^2 \Delta_{mix}$ and $b^2 \Delta_I$ were computed for our lattice calculations in Ref [56, 59] and are given as,

$$b^2 \Delta_{mix} = \begin{cases} (280 \text{ MeV})^2 & b \sim 0.125 \text{ fm} \\ (190 \text{ MeV})^2 & b \sim 0.09 \text{ fm} \end{cases} \qquad b^2 \Delta_I = \begin{cases} (450 \text{ MeV})^2 & b \sim 0.125 \text{ fm} \\ (280 \text{ MeV})^2 & b \sim 0.09 \text{ fm} \end{cases} \tag{4.12}$$

The results for the mixed mesons and partially quenched parameters are presented in Table. Finally, the expressions for the pion and kaon masses and decay constants are derived in [54] and are presented here in the appendix as they are considerably long expressions. We will discuss the fitting of these expressions in Sec 4.3.

4.3 SU(3) Chiral Extrapolation of the Lattice Data

In this section, we present the results of chiral, continuum extrapolations of SU(3) χPT . As shown in Tables [4.1,3.2,4.2], we have results at several light quark masses and two lattice spacings $b \approx 0.09$ fm and $b \approx 0.125$ fm . To perform chiral extrapolation, we need to determine the LEC's from the lattice data which will be performed as a simultaenous χ^2 minimization of Eq 4.3 as follows,

$$\chi^2 = \sum_{SU(3)} \sum_{m_q} \left(\frac{m_{Latt}(m_q) - m_{SU(3)}[m_\pi^g(m_q), m_K^g(m_q), f_\pi^g(m_q), f_K^g(m_q)]}{\sigma(m_q)} \right)^2 \tag{4.13}$$

where, $m_{Latt} = \{m_\pi, f_\pi, m_K, f_K\}$ is the set of SU(3) quantities computed on the lattice at the given quark mass. $m_{SU(3)}$ is the relevant chiral expression in Eq [4.3].

53

To determine the uncertainties in the extracted LEC's, we have generated gaussian distributed samples $\{m_\pi^g, m_K^g, f_\pi^g, f_K^g\}$ at the relevant quark mass m_q and use them in the χ^2 minimization Eq. [6.18].

The continuum extrapolation is done from the results of χ^2 minimization Eq 6.18 at lattice spacings $b \approx 0.09$ fm and $b \approx 0.125$ fm by simplistic fit motivated from MAχPT as,

$$\lambda(b) = \lambda_0 + \lambda_1 \left(\frac{b}{r_1}\right)^2 \tag{4.14}$$

The effects of finite volume are presented by considering the change in the corresponding LEC with and without the corrections. They are characterised as,

$$\delta(\lambda)|_{FV} = \frac{\lambda^\infty - \lambda^{FV}}{\lambda^{FV}} \tag{4.15}$$

where, λ^∞ is the LEC obtained from fiting the finite volume corrected data and λ^{FV} is the LEC obtainted from fitting the lattice computed results. *The results presented in the following sections are by default results to finite volume corrected data.*

We now proceed to analysis of the lattice data. As described previously, we will perform analysis on f_K/f_π, m_K^2/m_π^2 and the all the expressions in Eq. 4.3 including the finite volume and mixed action effects.

4.3.1 SU(3) NLO fits

Determination of L_5

The LEC L_5 is obtained from a χ^2 minimization of lattice data of $\frac{f_K}{f_\pi}$ as in Table 4.2. The results are present in Table 4.4 at coarse and fine lattice spacings.

We have performed various fits as {A,B,C..} on the lattice results indicating various degrees of freedom. These degrees of freedom are chosen in such a way that Fit A corresponds to the fit to all available degrees of freedom and the subsequent fits {B,C...} are chosen by eliminating the heavier quark masses. The fit presented in the

Table 4.4: *Extrapolation results for $\frac{f_K}{f_\pi}$*

		Fit to Coarse ensembles			
Fit	$L_5 \times 10^3$	$\frac{f_K}{f_\pi}$(extrapolated)	% $\delta(L_5)\|_{FV}$	χ^2/dof	dof
A	5.5791(61)(27)	1.2100(6)(3)	0.0 %	38	7
B	5.5123(52)(22)	1.2030(6)(2)	0.35 %	9	4
C	5.5459(59)(22)	1.2065(6)(2)	0.40 %	4.4	2
		Fit to Fine ensembles			
Fit	$L_5 \times 10^3$	$\frac{f_K}{f_\pi}$(extrapolated)	%$\delta(L_5)\|_{FV}$	χ^2/dof	dof
A	5.583(12)(03)	1.2115(12)(03)	0.0 %	12	5
B	5.539(10)(03)	1.2074(12)(04)	0.44 %	9.7	4

Table 4.4 includes the finite volume corrections and the effects of such corrections is presented in Column 4. After performing the continuum extrapolation, we have

$$L_5(\mu = f_\pi^{phys}) = 5.733(10)(03) \times 10^{-3} \qquad (4.16)$$

$$\left(\frac{f_K}{f_\pi}\right)_{phy} = 1.2257(10)(03)$$

In our fitting procedure the scale we have chosen is that $\mu = bf_\pi$ and we could trade the scale to $\mu = f_\pi^{phys}$ as the effects of difference in the scale will be at the next order in chiral expansion. The scale dependence of L_5 as computed in [8] is given by,

$$L_5(f_\pi^{phys}) = L_5(\mu) - \frac{3}{8}\frac{1}{16\pi^2}\log\left(\frac{f_\pi^{phys}}{\mu}\right) \qquad (4.17)$$

As a matter of convention, the scale often used to quote results for LEC's is the mass of rho meson $m_\rho = 770$ MeV. We quote our results at $\mu = m_\rho$ as follows,

$$L_5(m_\rho) = 1.521(10)(03) \times 10^{-3} \qquad (4.18)$$

The results presented here although in agreement with the experimental contain discretisation effects and should be considered with caution. A mixed action analysis

Table 4.5: *Extrapolation results for* $\frac{m_K^2}{m_\pi^2}$

		Fit to Coarse ensembles			
Fit	$L_8 \times 10^3$	$\delta(L_8)|_{FV}$	$(2L_8 - L_5) \times 10^3$	χ^2/dof	dof
A	1.7403(13)(08)	0.11%	-2.1776(10)(04)	70	6
B	1.6167(8)(2)	0.23%	-2.3020(9)(2)	22	4
C	1.5533(8)(2)	0.30 %	-2.4022(8)(2)	6.9	2
		Fit to Fine ensembles			
Fit	$L_8 \times 10^3$	$\delta(L_8)|_{FV}$	$(2L_8 - L_5) \times 10^3$	χ^2/dof	dof
A	1.7635(21)(06)	0.35%	-2.0461(20)(03)	36	4
B	1.5547(32)(09)	0.30%	-2.2030(22)(06)	4.5	2

will be more complete where the effects of different discretisation schemes for the sea and valence sector will be accounted for properly.

4.3.2 Determintation of $(2L_8 - L_5)$

In this section, we have performed a simultaneous χ^2 minimization of the ratio of $\frac{m_K^2}{m_\pi^2}$ in Eq 4.9 with that of $\frac{f_K}{f_\pi}$ to obtain LEC's L_8 and $(2L_8 - L_5)$. The results of this are presented in Table. As before the results presented include the finite volume corrections at both lattice spacings $b \approx 0.09$ fm and $b \approx 0.125$ fm . The Fits {A,B,C} describe the fits with varying degrees of freedom by eliminating the heavier quark masses. The continuum extrapolated results are given as,

$$\left(L_8(f_\pi^{phys})\right)_{phys} = 1.5517(43)(11) \times 10^{-3} \tag{4.19}$$

$$\left(2L_8 - L_5\right)(f_\pi^{phys})_{phys} = -2.6413(33)(08) \times 10^{-3}$$

The scale dependence of L_8 is given by the solution of the RG equation [8],

$$L_8(f_\pi^{phys}) = L_8(\mu) - \frac{5}{48}\frac{1}{16\pi^2}\log\left(\frac{f_\pi^{phys}}{\mu}\right) \tag{4.20}$$

Table 4.6: *Extrapolation results for SU(3) Low Energy Constants-I*

	Fit to Coarse ensembles				
Fit	$L_5 \times 10^3$	$L_8 \times 10^3$	$L_6 \times 10^3$	$L_4 \times 10^3$	χ^2/dof
A	5.2381(87)(47)	1.5044(86)(48)	0.000(10)(00)	0.048(23)(10)	135/10
B	5.252(17)(06)	1.505(15)(06)	0.000(12)(00)	0.098(41)(17)	53/6
	Fit to Fine ensembles				
Fit	$L_5 \times 10^3$	$L_8 \times 10^3$	$L_6 \times 10^3$	$L_4 \times 10^3$	χ^2/dof
A	5.815(41)(07)	1.764(17)(03)	0.995(40)(06)	1.471(64)(11)	26/10
B	5.790(47)(06)	1.754(19)(03)	0.924(33)(05)	1.368(55)(09)	16/6

The above results computed at scale $\mu = m_\rho$ are given as,

$$\left(L_8(m_\rho)\right)_{phys} = 0.3819(43)(11) \times 10^{-3} \tag{4.21}$$

$$\left(2L_8 - L_5\right)(m_\rho)_{phys} = -0.7696(33)(08) \times 10^{-3}$$

As can be seen in Table 4.5, even with two degrees of freedom the χ^2 for the results presented in relatively high, due to inclusion of discretisation and partial quenching effects. Hence one should consider these results with caution and motivates a mixed action analysis which is done in the next section.

4.3.3 Determintation of L_8, L_5, L_6, L_4

In this section, we will present the results of simulateneous χ^2 minimization of SU(3) pion and kaon masses and decay constants. This is done at both lattice spacings and several fits with varying degrees of freedom are performed. The uncertainties in the extracted LEC's are determined by generating a gaussian distributed input errors of the pion and kaon masses and decay constants. The results are presented in the Table 4.6 and Table 4.7 for the sake of convenience. Looking at the results of Tables 4.6 and 4.7, several remarks are in order,

Table 4.7: *Extrapolation results for SU(3) Low Energy Constants-II*

Fit	f_0 [MeV]	$(2L_8 - L_5) \times 10^3$	$(2L_6 - L_4) \times 10^3$	χ^2/dof
		Fit to Coarse ensembles		
A	190(3)(2)	-2.2308(60)(49)	-0.048(23)(10)	135/10
B	187(5)(3)	-2.241(14)(06)	-0.098(41)(17)	53/6
		Fit to Fine ensembles		
A	116(2)(1)	-2.285(10)(02)	0.518(22)(04)	26/10
B	115(2)(1)	-2.282(10)(02)	0.480(18)(04)	16/6

1. The extracted LEC's have a relatively higher χ^2 at coarser lattice spacings and the results should be considered with care.

2. Although we have enough data to describe SU(3) χPT , we have perfomed fits with only limited degrees of freedom as these fits become unstable for higher quark masses. This is an indication of failure of SU(3) χPT at higher quark masses which is attributed to lack of lighter quark masses at coarse lattice spacings.

3. The fits to the finer ensemble have a better χ^2 as there are more light quark masses than those on the coarse ensembles.

The results after performing the continuum extrapolation at the scale $\mu = f_\pi$ are as follows

$$L_5 = 6.170(67)(15) \times 10^{-3} \qquad L_8 = 1.930(20)(06) \times 10^{-3} \qquad (4.22)$$

$$L_4 = 2.244(87)(30) \times 10^{-3} \qquad L_6 = 1.561(82)(08) \times 10^{-3}$$

$$(2L_8 - L_5) = -2.310(12)(04) \times 10^{-3} \qquad (2L_6 - L_4) = 0.900(40)(10) \times 10^{-3}$$

As is in the convention, we also present our results at the scale $\mu = m_\rho$ as follows,

$$L_5 = 1.959(67)(15) \times 10^{-3} \qquad L_8 = 0.760(20)(06) \times 10^{-3} \qquad (4.23)$$

$$L_4 = 0.840(87)(30) \times 10^{-3} \qquad L_6 = 0.704(82)(08) \times 10^{-3}$$

$$(2L_8 - L_5) = -0.439(12)(04) \times 10^{-3} \qquad (2L_6 - L_4) = 0.588(40)(10) \times 10^{-3}$$

4.3.4 NLO Mixed Action Analysis

Three flavor MAχPT describes the lattice data closely as it takes into account the effects of partial quenching and different discretisation of sea and valence sectors. Since the lattice spacing corrections are included in MAχPT , we do not have to perform continuum extrapolation and this provides a relatively large data set for analysis.

At NLO, there are additional two low energy constants describing the lattice spacing effects namely L_{fa^2} and L_{ma^2}. These will be have to determined from the lattice data. The unphysical effects of partial quenching are included as Δ_{ju}^2 for the light sea and valence quarks and Δ_{rs}^2 for the strange sea and valence quark masses. These are computed from mixed mesons and the results are provided in Table 4.3.

We now proceed to the analysis results of mixed action χPT . The results are presented Table 4.8 and 4.9. and as before the results table is split in two for convenience. The various fits {A,B,C,D} are fits with varying (increasing) quark masses. We have several remarks about the fits

1. The Fit D with MAχPT has a low χ^2 and describes the data well.

2. The overall quality fits is better than the SU(3) analysis, as with the variation of quark masses, especially with the inclusion higher quark masses, all the fits are stable.

Table 4.8: *Extrapolation results for MAχPT -I*

Fit	$L_5 \times 10^3$	$L_8 \times 10^3$	$L_6 \times 10^3$	$L_4 \times 10^3$	χ^2/dof
A	5.220(08)(02)	1.86(1)(0)	1.216(5)(2)	1.864(5)(2)	510/16
B	5.30(02)(00)	1.89(03)(01)	1.39(06)(01)	1.74(02)(01)	90/12
C	5.82(17)(02)	1.65(21)(05)	1.75(18)(03)	1.92(10)(01)	23/8
D	5.75(18)(01)	1.71(25)(13)	1.74(32)(12)	2.04(13)(03)	6/4

Table 4.9: *Extrapolation results for MAχPT -II*

Fit	f_0 [MeV]	$(2L_8 - L_5) \times 10^3$	$(2L_6 - L_4) \times 10^3$	L_{fa^2}	L_{ma^2}
A	123.9(2)(0)	-1.49(1)(0)	0.56(1)(0)	-0.441(1)(2)	-1.3(1)(1)
B	129(2)(1)	-1.52(06)(01)	1.03(12)(03)	-0.51(01)(0)	-0.5(2)(0)
C	102(7)(2)	-2.52(39)(09)	1.59(34)(05)	0.17(21)(01)	2(1)(0)
D	102(3)(2)	-2.31(54)(24)	1.44(55)(24)	0.09(24)(04)	0.7(2.0)(1.2)

3. This can be understood as the mixed action χPT accounts for the unphysical effects of partial quenching and discretisation correctly.

4. We use the Fit D to present as the final result of this analysis as below.

The results of Fit D at scale $\mu = f_\pi$ are as below,

$$L_5 = 5.77(13)(05) \times 10^{-3} \qquad L_8 = 1.71(25)(13) \times 10^{-3} \qquad (4.24)$$

$$L_4 = 2.04(13)(03) \times 10^{-3} \qquad L_6 = 1.74(32)(12) \times 10^{-3}$$

$$(2L_8 - L_5) = -2.31(54)(24) \times 10^{-3} \qquad (2L_6 - L_4) = 1.44(55)(24) \times 10^{-3}$$

We also present the results of Mixed action χPT analysis at scale $\mu = m_\rho$ are

given as follows,

$$L_5 = 1.48(13)(05) \times 10^{-3} \quad L_8 = 0.44(25)(13) \times 10^{-3} \quad (4.25)$$

$$L_4 = 0.63(13)(03) \times 10^{-3} \quad L_6 = 0.93(32)(12) \times 10^{-3}$$

$$(2L_8 - L_5) = -0.59(54)(24) \times 10^{-3} \quad (2L_6 - L_4) = 1.23(55)(24) \times 10^{-3}$$

4.4 Results and Conclusions

In this work, we have studied the SU(3) χPT for the pions and kaons through the determination of the corresponding LEC's from our lattice data. The lattice calculation that we have performed is a mixed action calculation and it is important to quantify the effects of discretisation for pions and kaons. The approach we have taken is similar to the SU(2) analysis, in that, we have determined the SU(3) LEC's by fitting the lattice data to continuum SU(3) expression. We found that they suffer from discretisation effects which makes the fits unstable. Consequently, the fits could be performed over a very limited range of quark masses.

We then made fits with the mixed-action expressions and found that these expression fit the data very well and that we were able to perform fits with consistent determinations of LEC's over a larger range of quark masses. This gives us confidence that the mixed action expressions correctly account for discretisation effects.

Chapter 5

Scalar Strange Content of Proton from Lattice QCD

The observed quantum numbers of proton can be explained in terms of three light quarks, two up quarks and one down quark. The constituent quark model was formulated based on this belief and it enjoyed much success before the advent of QCD. Later as the EMC experiment demonstrated, the proton has much more complicated structure than painted by the naive constituent quark model. This experiment showed that quarks carry only a fraction of proton's spin and also a nonzero value for $\langle N | \bar{s} \gamma_\mu \gamma_5 s | N \rangle$. There must be a significant contribution from the virtual $q\bar{q}$ pairs, also known as sea quarks or non-valence quarks, to all the properties of the proton.

The puzzle between the current quarks of QCD and constituent quarks of the quark model was later resolved Kaplan & Manohar who proposed that the effect of sea quarks is to renormalize the current quarks of QCD into the constituent quarks of the quark model. Thus the "new" redefined constituent quarks were made up of gluons and virtual $s\bar{s}$ pairs. This resolved the inaccuracies in axial and vector form factors of the proton as the inclusion of strange matrix elements described the data more accurately compared to the prediction made by the constituent quark model. They also proposed how elastic neutral current scattering experiments can be used to extract strangeness content of the proton. This was later utilized successfully by the HAPPEX and G0 series experiments at Jefferson lab which has now shown the

strangeness contribution to the charge and magnetization of proton to be 10 % of the total. In our work, we are mainly concerned only with the scalar strange matrix element $\langle N|\bar{s}s|N\rangle$.

The strange matrix element $\langle N|\bar{s}s|N\rangle$ appears as a non-valence contribution i.e, from sea quarks to the mass of nucleon. The non-valence strange matrix element has its importance for dark matter searches as the cross-section for scattering of a neutralino off a nucleon couples to these matrix elements [69]. Experimentally this quantity is not accessible as there doesn't exist a scalar probe to measure this quantity. $\langle N|\bar{s}s|N\rangle$ being inherently non-perturbative, one has to resort to lattice QCD for computations.

Recently, there has been a lot of interest in computing $\langle N|\bar{s}s|N\rangle$. The lattice computation of $\langle N|\bar{s}s|N\rangle$ is not a straight forward computation as strange quarks appear in loops and one has to compute the insertion of the loop to the nucleon propagator. The computation of loop diagrams on the lattice is expensive as one has to use all-to-all propagator techniques. The method used by most groups in computing $\langle N|\bar{s}s|N\rangle$ employs computing the loop diagram via a 3-point correlator and the strangeness content is given as follows,

$$R(\Delta t, \Delta t_s) \equiv \frac{C_{3pt}(\Delta t, \Delta t_s)}{C_{2pt}(\Delta t)} \xrightarrow{t \to \infty} \langle N|\bar{s}s|N\rangle \qquad (5.1)$$

where Δt is the temporal interval between nucleon source and sink, C_{3pt} is the three point correlator with a loop vertex, C_{2pt} is the nucleon two point correlator. The collaboration MILC has also performed computation of $\langle N|\bar{s}s|N\rangle$. They are able to compute the $\langle N|\bar{s}s|N\rangle$ from prior measurements of $\int d^4x \bar{s}s$ during lattice generations on all of their configurations . They then relate $\langle N|\bar{s}s|N\rangle$ to $\frac{\partial M_n}{\partial m_s}$ and compute the partial derivative by product expansion.

The present work utilizes the Feynman-Hellmann Theorem which has some distinct advantages over the direct method: it is numerically less expensive and the

ground state contributions to the two-point correlation functions can be significantly more reliably determined than plateaus in direct matrix element calculations.

We begin by presenting an overview of our method in Sec. 5.1 and then details of our lattice calculation in and thereafter present the determination of $m_s\langle N|\bar{s}s|N\rangle$ in Sec. 5.3. We also present results for heavy matrix elements and finally present our conclusions to this work.

5.1 Computational Methodology

The scalar matrix elements can be calculated from H_{QCD} by invoking the Feynman-Hellman theorem as [70],

$$\langle N|m_q\bar{q}q|N\rangle = m_q\frac{\partial}{\partial m_q}\langle N|H_{QCD}|N\rangle = m_q\frac{\partial M_N}{\partial m_q} \tag{5.2}$$

where M_N is the mass of the nucleon and H_{QCD} is the QCD hamiltonian. The behavior of nucleon to the N^{3}LO in HBχPT is given by[70],

$$M_N = M_0(\mu) - M_N^{(1)}(\mu) - M_N^{(3/2)}(\mu) - M_N^{(2)}(\mu) + ... \tag{5.3}$$

where the $M_N^{(n)}$ term denotes the contribution to the order m_q^n. For example to the NLO in χPT, the nucleon mass is given explicitly by [70],

$$M_N = M_0 + (m_u + m_d)\sigma_{\pi N} + m_s\beta + \mathcal{O}(m_q^{3/2}) \tag{5.4}$$

where M_0 is the nucleon mass in the chiral limit, $\sigma_{\pi N}$ is the nucleon sigma-term and $\beta = \langle N|\bar{s}s|N\rangle$ is the strange matrix element contribution. Applying Feynman-Hellman theorem, we have to the LO in chiral expansion,

$$\beta = \langle N|\bar{s}s|N\rangle = \frac{\partial M_N}{\partial m_s} = \frac{M_{N1} - M_{N2}}{m_{s1} - m_{s2}} + \mathcal{O}(m_q^{3/2}) \tag{5.5}$$

Hence one can compute the strange matrix element by comparing the nucleon mass on two sets of lattice ensembles varying only by the strange sea mass.

While the matrix element $\langle N|\bar{s}s|N\rangle$ is a renormalisation dependent quantity, it is more desirable to study strange quark contribution $m_s\langle N|\bar{s}s|N\rangle$ to the nucleon mass, as it is a RG invariant quantity. The strangeness contribution is defined by,

$$
\begin{aligned}
m_s\langle N|\bar{s}s|N\rangle &= m_s\frac{\partial M_N}{\partial m_s} = m_{ss}^2\frac{\partial M_N}{\partial m_{ss}^2} \\
&= (2m_K^2 - m_\pi^2)\left[\frac{1}{2}\frac{\partial}{\partial m_K^2} + \frac{2}{3}\frac{\partial}{\partial m_\eta^2}\right]M_N + \mathcal{O}(m_q)
\end{aligned}
\tag{5.6}
$$

5.2 Lattice Calculation and Data Analysis

5.2.1 Lattice Details

The computation for $\langle N|\bar{s}s|N\rangle$ was performed on gauge configurations generated by MILC namely on coarse ensembles MILC_2064f21b675m010m030 & MILC_2064f3b679m030 and fine ensemble MILC_4096f21b711m0031m0186. These employ $N_f = 2+1$ (2 degenerate light and 1 heavy) & $N_f = 3$ (3 degenerate) flavors of improved rooted-staggered quarks known as the Asqtad action[66]. The lattices are of size $20^3 \times 64$ and $40^3 \times 96$ respectively with the spacing determined from the Sommer scale, which inturn is determined from heavy baryon spectroscopy, as $b \approx 0.123$ and $b \approx 0.095$. The validity of our calculation depends on the assumption that the rooting procedure yields the correct continuum limit of QCD. We assume that the rooting procedure gives the correct continuum QCD.

For the valence quarks, we used the domain wall fermion (DWF) action with hypercubic smearing (HYP-smearing) to improve the chiral symmetry. We employed anti-periodic boundary conditions in our computation as done by NPLQCD. Since we are interested in finding the effects due to sea quarks, we had to set all the valence parameters on our ensembles to what was used by the NPLQCD collaboration. Hence the valence parameters on set MILC_2064f21b675m010m030
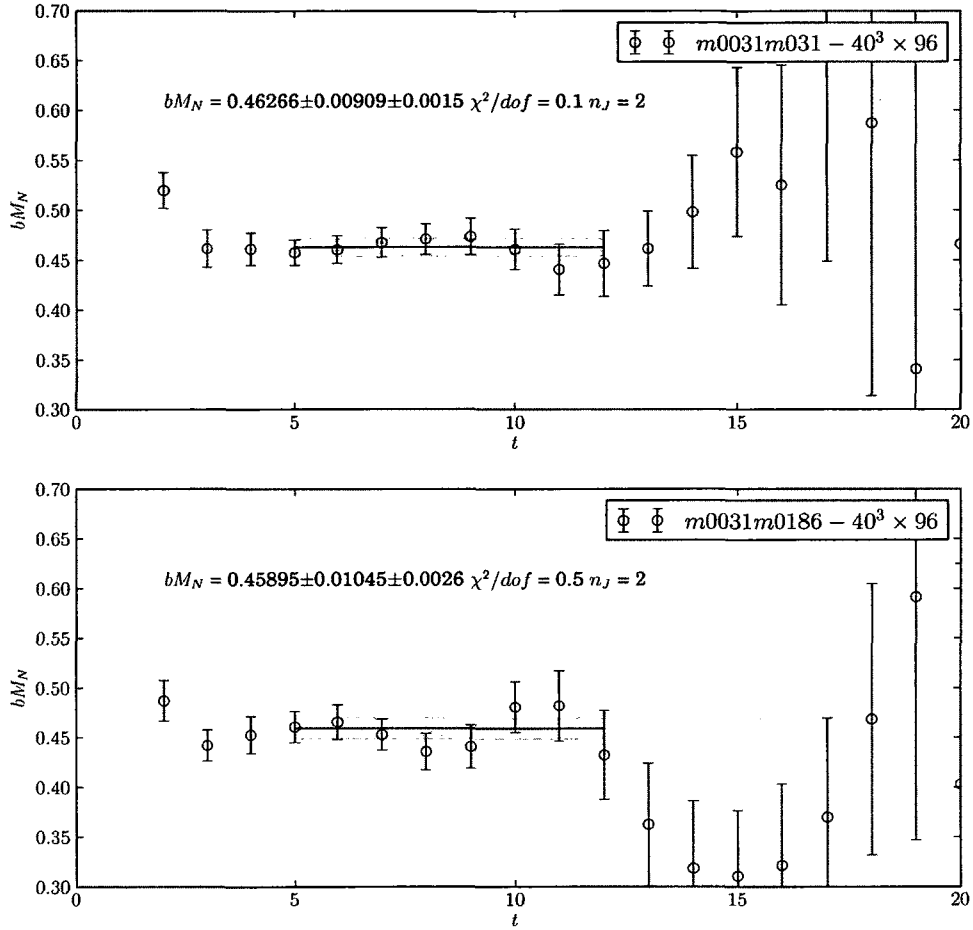
Figure 5-1: *Effective Mass Plots on Ensemble* MILC_4096f21b708m0031m031 *and Ensemble* MILC_4096f21b706m0031m0186

were the same as valence parameters on set MILC_2064f21b676m010m050 and the same follows for ensembles MILC_2064f3b679m030 & MILC_2064f21b681m030m050 and MILC_4096f21b706m0031m0186 & MILC_4096f21b708m0031m031 . This enabled us to have $\langle N|\bar{s}s|N\rangle$ at different light quark masses which is essential for chiral extrapolation. The parameters are tabulated in Table 5.1 for convenience.
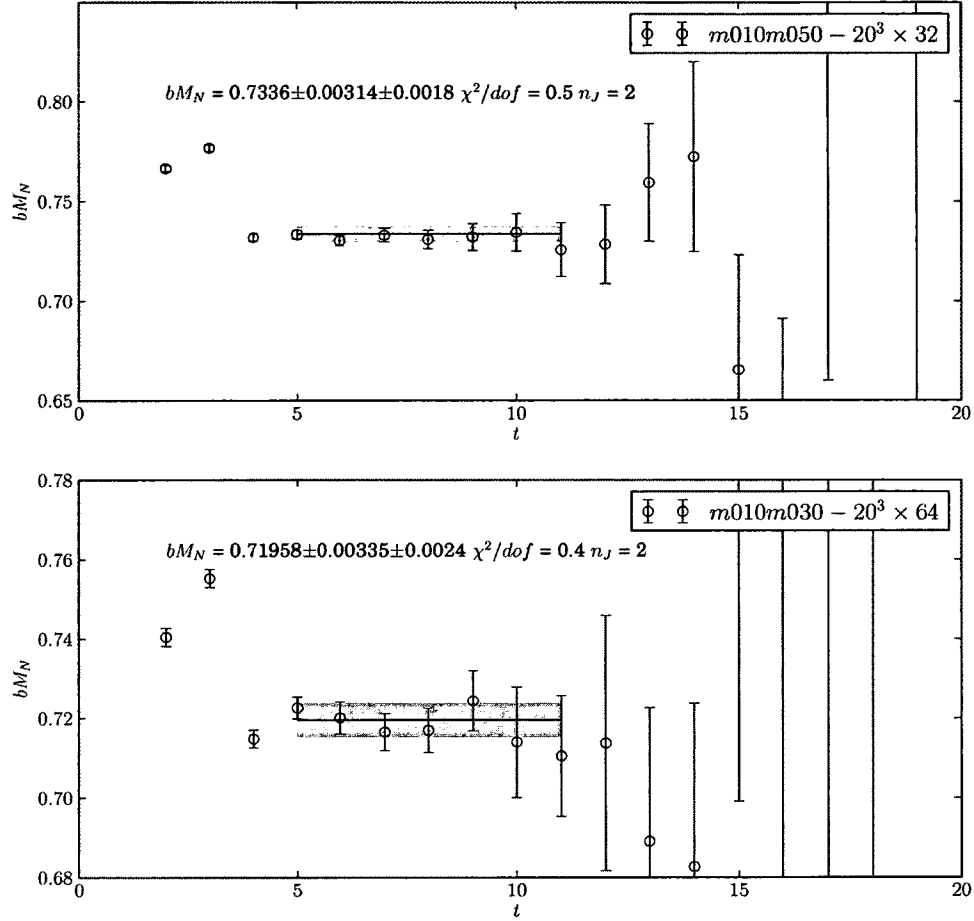
Figure 5-2: *Effective Mass Plots on Ensemble* MILC_2064f21b676m010m050 *and Ensemble* MILC_2064f21b675m010m030

5.2.2 Data Analysis

We computed meson and baryon masses on sets MILC_2064f21b675m010m030,

MILC_2064f3b679m030 and MILC_4096f21b706m0031m0186 from approximately 18,000

correlators on each set. This was done by placing a source at a random space-time

point within the lattice throughout all the configurations. To account for the auto-

correlation between the configurations, all the correlators were averaged using the

single elimination jackknife. The masses of mesons and baryons are extracted from

67
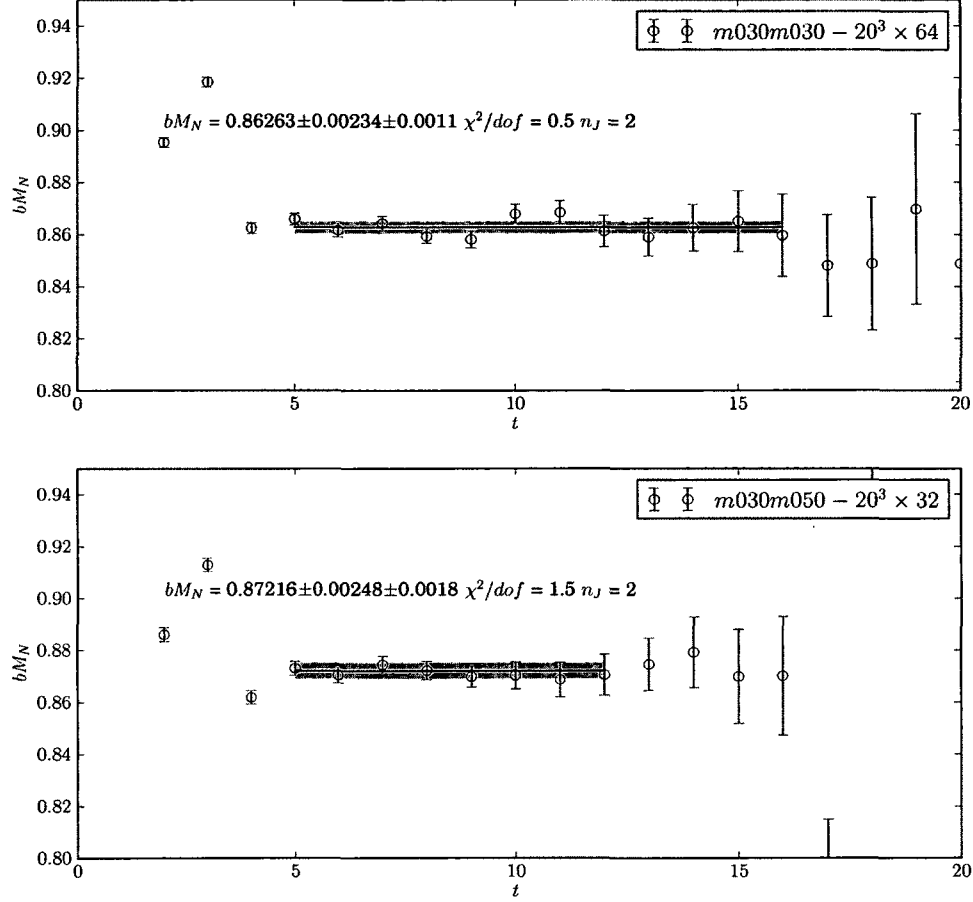
Figure 5-3: *Effective Mass Plots on Ensemble* MILC_2064f21b681m030m050 *and Ensemble* MILC_2064f3b679m030

asymptotic behavior of the respective correlator given by,

$$C_X(t) \longrightarrow A_X\ e^{-M_X t} \qquad M_X = \frac{1}{n}\ \log\left(\frac{C_X(t)}{C_X(t+n)}\right) \tag{5.7}$$

We also employed smeared interpolating operator for the quark fields at the source and two types of interpolating operators at the sink viz. local and smeared quark field operators. This gave us two types of correlators for each physical state viz. $C_X^{SS}(t)$ & $C_X^{SP}(t)$. A linear combination of these,

$$C_X(t) = C_X^{SS}(t) - \alpha\ C_X^{SP}(t)$$

Table 5.1: *Parameters of the Lattice Calculation*

$b \approx 0.125$ fm ensembles

β	bm_l^{sea}	bm_s^{sea}	Vol	bm_l^{dwf}	$bm_l^{res} \times 10^3$	bm_s^{dwf}	$bm_s^{res} \times 10^4$	N_{cfg}
6.75	0.010	0.030	$20^3 \times 64$	0.0138	1.564(3)	0.081	8.92(2)	328
6.76	0.010	0.050	$20^3 \times 64$	0.0138	1.566(11)	0.081	9.13(2)	656
6.79	0.030	0.030	$20^3 \times 64$	0.0478	1.052(4)	0.081	8.09(4)	367
6.81	0.030	0.050	$20^3 \times 32$	0.0478	1.013(6)	0.081	8.62(7)	486

$b \approx 0.09$ fm ensembles

β	bm_l^{sea}	bm_s^{sea}	Vol	bm_l^{dwf}	$bm_l^{res} \times 10^4$	bm_s^{dwf}	$bm_s^{res} \times 10^4$	N_{cfg}
7.06	0.0031	0.0186	$40^3 \times 96$	0.0035	?	0.0423	?	356
7.08	0.0031	0.031	$40^3 \times 96$	0.0035	4.28(3)	0.0423	2.33(2)	422

is used eliminate the first excited state by appropriately fine tuning α such that the correlators form a wider plateau. This gave us more time slices to fit which reduced the systematic error due to fitting. The statistical errors are quoted from single elimination jack-knife. The systematic error due to fitting is computed from a correlated χ^2 fit. We use the scale setting done by MILC collaboration in terms of r_1 units to convert our lattice results to MeV as tabulated in Table 3.3. We use the physical r_1 as $r_1^{phys} = 0.311(2)\binom{3}{8}$ fm which is determined by using f_π to set the scale.

5.3 Scalar Strangeness in Nucleon

As discussed in the introduction, there are two methods for determining the scalar strange quark matrix element in the nucleon: a direct calculation of the matrix element employed by some groups [71, 72, 73, 74, 75, 76, 77] and an indirect determination through the Feynman-Hellmann Theorem [78, 79, 80, 81, 82, 83], Eq. (5.6), and a hybrid approach [84, 85]. This work utilizes the latter method. For each light quark mass ensemble, we have a determination of the nucleon mass at different values
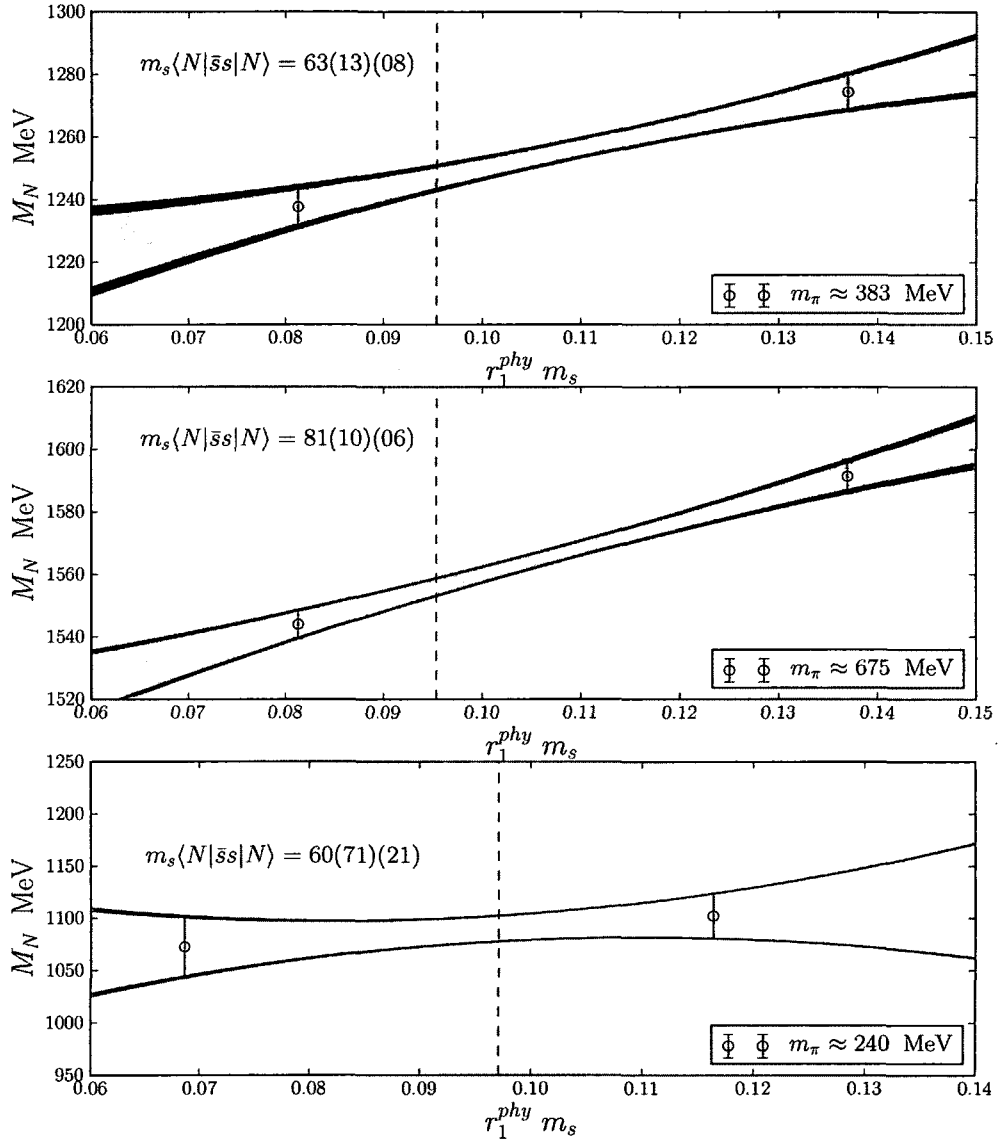
Figure 5-4: *Fits to Nucleon mass on various ensembles*

Table 5.2: *Computed Pion and Nucleon masses*

$b \approx 0.125$ fm Ensembles

bm_{sea}	bm_π	m_π[MeV]	bM_N	M_N[MeV]	$(\frac{r_1}{b})^{phys}$
m010m030	0.22194(31)	381.7(5)	0.7195(33)(24)	1238(6)(4)	2.711(4)
m010m050	0.22298(26)	387.3(5)	0.7336(31)(18)	1274(5)(3)	2.739(3)
m030m030	0.37323(26)	668.0(5)	0.8626(24)(11)	1544(4)(2)	2.821(7)
m030m050	0.37470(24)	683.7(4)	0.8721(24)(18)	1591(4)(3)	2.877(4)

$b \approx 0.09$ fm Ensembles

bm_{sea}	bm_π	m_π[MeV]	bM_N	M_N[MeV]	$(\frac{r_1}{b})^{phys}$
m0031m0186	0.10195(33)	238.4(7)	0.4585(104)(26)	1073(28)(10)	3.687(4)
m0031m031	0.10160(25)	242.0(6)	0.4626(90)(10)	1102(21)(2)	3.755(4)

Table 5.3: *Results for $m_s \langle N|\bar{s}s|N\rangle$ from the fits to Nucleon mass*

m_π [MeV]	$M_N(m_s^{phy})$ [MeV]	$m_s^{phy} \langle N|\bar{s}s|N\rangle$[MeV]
240	1089(12)(8)	60(71)(21)
384	1246(5)(2)	63(13)(8)
676	1556(4)(1)	81(10)(6)

of the strange quark near its physical value. These results, Table 5.2, can be used to interpolate to the physical value of the strange quark mass, Taylor expanding about bm_s^{phy}, and determine the two quantities

$$m_N(m_s^{phy}) , \qquad \frac{\partial m_N(m_s)}{\partial m_s}\bigg|_{m_s^{phy}} . \tag{5.8}$$

The MILC Collaboration has determined values of the strange quark mass to be $bm_s^{phy} = 0.0350(7)$ and $bm_s^{phy} = 0.0261(5)$ on the $b \approx 0.125$ fm and $b \approx 0.09$ fm ensembles respectively [86, 1]. erforming the Taylor expansion about m_s^{phy}, the values of the nucleon mass and $m_s\langle N|\bar{s}s|N\rangle$ are determined on each ensemble. These results are collected in Table 5.3 and the resulting interpolations are displayed in Figure 5-4.
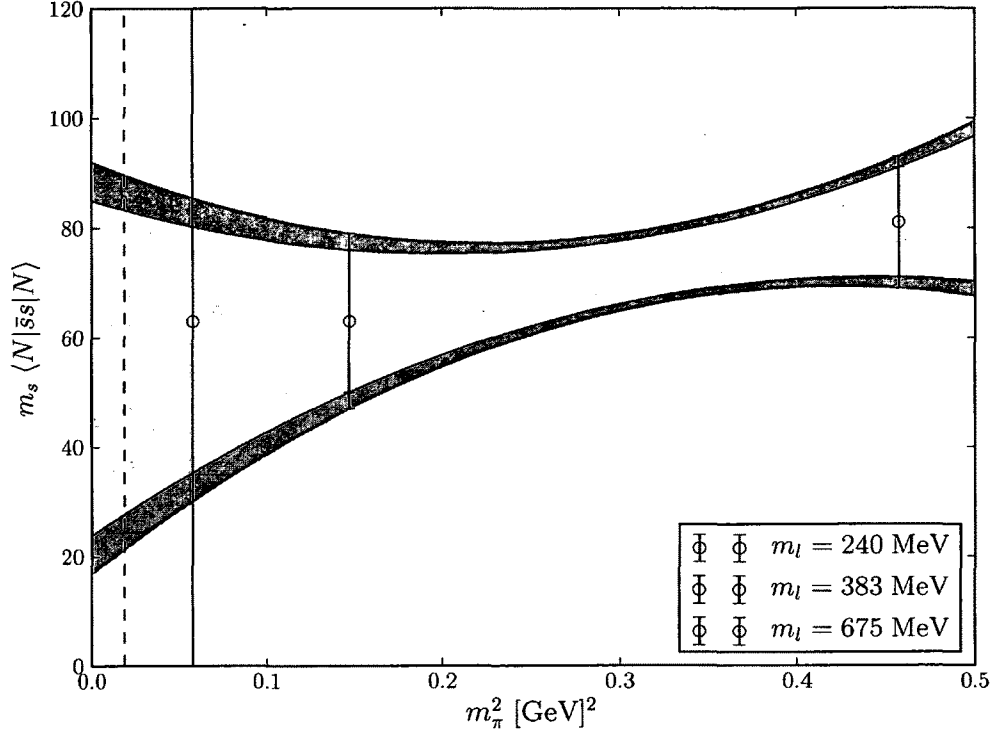
Figure 5-5: *Light quark mass extrapolation of* $m_s \langle N | \bar{s}s | N \rangle$

5.3.1 Chiral Extrapolation of $m_s \langle N | \bar{s}s | N \rangle$

The results for $m_s < N | \bar{s}s | N >$ must be extrapolated to the physical value of the pion mass. In Ref. [87], the two flavor extrapolation formula for this matrix element was determined at next-to-leading order (NLO) in the chiral expansion,

$$\langle N | \bar{s}s | N \rangle = < N | \bar{s}s | N >^0 - \frac{g_{\pi N \Delta}^2}{4\pi^2 f^2} \left(< N | \bar{s}s | N >^0 - < \Delta | \bar{s}s | \Delta >^0 \right) \mathcal{J}_{m_\pi}^\Delta + \tilde{E}_s \frac{m_\pi^2}{8\pi^2 f^2},$$

$$(5.9)$$

where $\langle H | \bar{s}s | H \rangle^0$ represent the leading order (LO) contribution to the scalar strange matrix element in the hadron H, $g_{\pi N \Delta}$ is the axial pion-nucleon-delta coupling appearing in the $SU(2)$ baryon chiral Lagrangian, $\mathcal{J}_{m_\pi}^\Delta$ is a chiral loop function non-analytic in the pion mass and the delta-nucleon mass splitting $(\Delta = m_\Delta - m_N)$ and $\tilde{E}_s$ is a low energy constant appearing at NLO.
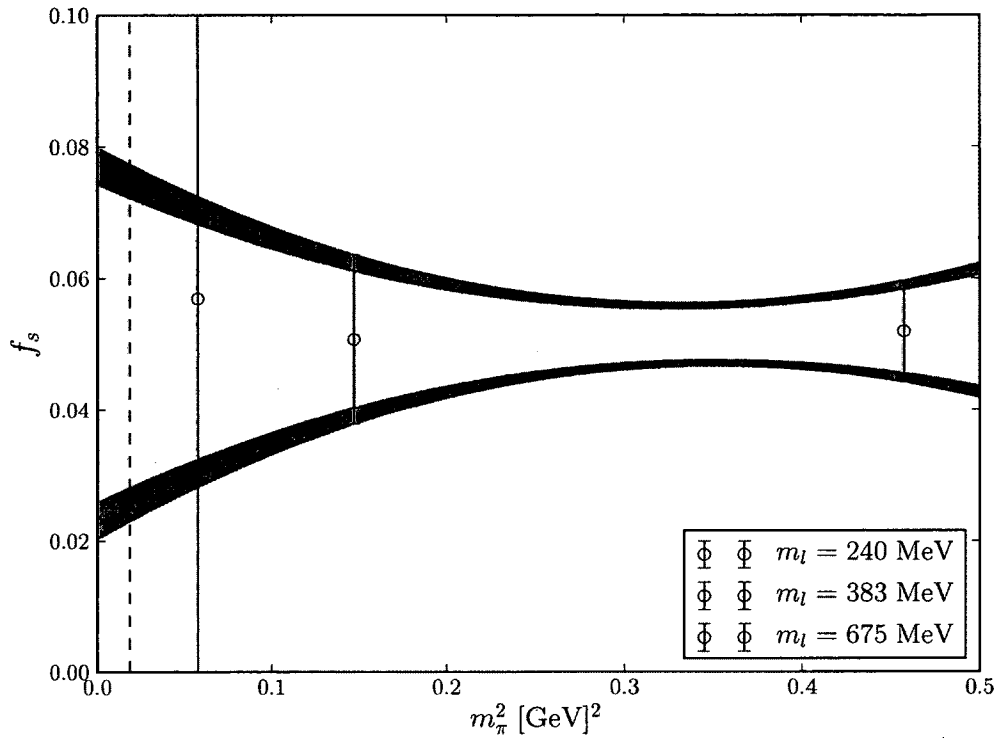
Figure 5-6: *Light quark mass extrapolation of* f_s

In principle, we should be fitting our data to the equation above, but since we are have a very limited data set, we instead make a simple minded fit. The best that can be done with the present results is a simple, effectively zero-degree of freedom extrapolation using the formula

$$m_s \langle N|\bar{s}s|N \rangle = c_0 + c_2 m_\pi^2 . \tag{5.10}$$

While this will not result in a precise and accurate determination of the scalar strange matrix element, it will provide a good guide to the approximate value at the physical point. While not a rigorous expectation, it has been found that matrix elements of the nucleon tend to have very mild pion mass dependence, see for example the recent review [88]. Performing this simplistic pion mass extrapolation, using the isospin

Table 5.4: *Extrapolated values of* $m_s \langle N|\bar{s}s|N \rangle$ *and* f_s. *These results are averaged described in the text.*

Quantity Extrapolated	$m_s^{phy} \langle N|\bar{s}s|N \rangle$ [MeV]	f_s
$m_s^{phy} \langle N|\bar{s}s|N \rangle$	$59 \pm 24 \pm 10$	$0.062 \pm 0.025 \pm 0.001$
f_s	$47 \pm 23 \pm 14$	$0.050 \pm 0.025 \pm 0.002$
Correlated Average	$52 \pm 24 \pm 10$	$0.055 \pm 0.025 \pm 0.002$

averaged $m_\pi^{phy} = 138.0$ MeV,

$$m_s^{phy} \langle N|\bar{s}s|N \rangle \Big|_{m_\pi^{phy}} = 59 \pm 24 \pm 10 \text{ MeV} . \tag{5.11}$$

The extrapolation is displayed in Figure 5-5. Given the limited ability to perform the chiral extrapolation, we also explore the light quark mass dependence of $f_s = m_s \langle N|\bar{s}s|N \rangle / m_N$ to improve the estimate of systematic uncertainties. It has been observed that the nucleon mass displays a remarkably linear dependence on the pion mass [37, 89]. For this reason, two extrapolation functions are used to estimate extrapolation systematics:

$$f_s = f_s^{(0)} + f_s^{(2)} m_\pi^2 , \tag{5.12}$$

yielding the results

$$f_s = 0.050 \pm 0.025 \pm 0.002 \tag{5.13}$$

respectively. These extrapolations are displayed in Figure 5-6. The quantity f_s is observed to have negligible light quark mass dependence.

These results can be compared with the extrapolation of $m_s \langle N|\bar{s}s|N \rangle$ by converting with the isospin averaged nucleon mass $m_N^{phy} = 938.9$ MeV. We perform a weighted average of these results, the weights being the inverse of the uncertainties of the quoted values. Hence, such an average will give more importance to the results

with lower uncertainties. For the result of f_s, to convert to $m_s \langle N|\bar{s}s|N \rangle$, we have used the m_N result as before. The results for weighted average are provided in Table 5.4.

5.3.2 Estimating the heavy quark matrix elements

Knowledge of f_u, f_d and f_s can be used to determine the values of f_c, f_b and f_t [90, 91]. In Ref. [91], these heavy quark matrix elements were computed using perturbative QCD to $\mathcal{O}(\alpha_s^3)$, finding

$$f_c = 0.08896(1 - x_{uds}), \quad f_b = 0.08578(1 - x_{uds}), \quad f_t = 0.08964(1 - x_{uds}), \quad (5.14)$$

where

$$x_{uds} = f_u + f_d + f_s. \quad (5.15)$$

The light quark matrix elements are given by the pion-nucleon sigma term $m_N(f_u + f_d) = \sigma_{\pi N}$, which has also been determined from lattice QCD. As can be seen in Ref. [92], the determination by the BMW Collaboration [79] not only would have the only green-star ranking but also is a good approximation for the average of all lattice QCD calculations of this quantity, with a value $\sigma_{\pi N} = 39(^{+18}_{-8})$ MeV. Combining this with our estimate for f_s yields a value $x_{uds} = 0.085(^{+.022}_{-.014})$, and values of the heavy-quark matrix elements

$$f_c = 0.0814(^{+12}_{-20}), \qquad f_b = 0.0785(^{+12}_{-19}), \qquad f_t = 0.0820(^{+13}_{-20}), \qquad (5.16)$$

or in dimensionful units

$$m_c \langle N|\bar{c}c|N \rangle = 76(^{+11}_{-19}) \text{ MeV},$$

$$m_b \langle N|\bar{b}b|N \rangle = 74(^{+11}_{-18}) \text{ MeV},$$

$$m_t \langle N|\bar{t}t|N \rangle = 77(^{+12}_{-19}) \text{ MeV}. \qquad (5.17)$$

5.4 Results and Discussion

For the present work, the Feynman-Hellmann Theorem was invoked to determine the strange content of the nucleon through a change m_N as the strange quark mass is varied

$$m_s \langle N | \bar{s}s | N \rangle = m_s \frac{\partial m_N}{\partial m_s} \, .$$

By taking care to set the scale using values of r_1/b which were extrapolated to the physical values of the light and strange quark masses, the nucleon mass variation was determined with all other parameters held constant (with precision better than 1%), as is required for a proper determination of this quantity [84, 85]. There are several groups who have used the Feynman-Hellmann Theorem [78, 79, 80, 76, 81, 82, 83] as well as more determinations with a direct calculation of the matrix element [71, 72, 73, 74, 75, 76, 77] and results from a hybrid approach [84, 85]. Before making a detailed comparison with other works, we first highlight advantages and disadvantages of the present work. The distinct advantage of using the Feynman-Hellmann Theorem over direct methods is that the ground state plateau of the nucleon can be significantly more reliably determined than the plateau for the matrix element calculation, see the plots of ratio determinations in any of Refs. [71, 72, 73, 74, 75, 76, 77] (the direct calculation requires a vacuum subtraction, adding substantial statistical noise). The disadvantage of most groups employing the Feynman-Hellmann Theorem is the reliance upon $SU(3)$ baryon χPT [78, 81, 82, 83], which is known to not have a converging expansion for the nucleon mass [37, 93, 32, 94, 95]. Therefore, it is not clear the full extrapolation systematic has been properly addressed in those works. This concern is substantiated by the discrepancy between independent $SU(3)$ baryon χPT analyses and their determination of f_s [78, 82, 81, 83]. The current work does not suffer from this issue.

The most severe limitation of the present work is the small number of light quark

mass points (two) for which there is a non-zero determination of $m_s \langle N | \bar{s}s | N \rangle$. Given the significant numerical cost of the domain-wall propagators on the $b \approx 0.09$ fm ensemble with $m_\pi \simeq 240$ MeV, it is not clear how soon a more precise determination will be obtained at this point. Given the very mild light quark mass dependence observed in this work, and in nucleon matrix elements in general, we believe the present determination offers a reliable estimate of the scalar strange content of the nucleon, but neither a precise nor demonstrably accurate value. Our final result is

$$m_s \langle N | \bar{s}s | N \rangle = 52 \pm 24 \pm 10 \text{ MeV} \,,$$

$$f_s = 0.055 \pm 0.025 \pm 0.002 \,.$$

As was first discussed in Refs. [78, 96], there is now compelling evidence from lattice QCD that the value of the scalar strange content of the nucleon is substantially smaller than previously estimated and does not play as significant a role in dark-matter searches as previously thought [97]. For a recent review of the lattice QCD determinations of the scalar strange content of the nucleon, see Ref. [92].

Chapter 6

Baryons from Lattice QCD

In this chapter, we will study the quark mass dependence of the nucleon mass from our lattice calculations. This will allow us to determine the light quark matrix elements and the strange quark matrix elements of the nucleon from our calculations. This will also facilitate a comparison of results on the scalar strange matrix element of the nucleon by performing a more detailed analysis. Our lattice calculations being performed at unphysical quark masses, we use the chiral perturbation for baryons to obtain results at physical pion masses. The analysis is performed with the two flavor and three flavor χPT .

In section 6.1, we briefly present the overview of our lattice calculation as it has been discussed in previous chapters. In section 6.2, we provide the systematics of the baryon χPT relevant to this work. In section 6.3, we present the results of analysis from baryon χPT and take a look at the issue of convergence. Lastly in section 6.4, we summarise our results and present our calculations.

6.1   Lattice systematics

We only provide a review of the lattice calculation we have used in this work as they have been already talked in Section 3.2, 4.2 and 5.2. The lattice calculation program is that of the mixed-action calculation [33, 34, 35, 36, 37, 38] with chirally symmetric domain wall valence fermions and staggered sea quarks. These have been extensively

Table 6.1: *Nucleon masses on Lattice Ensembles*

m_{sea}	$L \times T \times L_5$	bM_N	bm_π	bm_K
$b \approx 0.125$ fm ensembles				
m007m050	$20 \times 64 \times 16$	0.6931(52)(29)	0.18175(39)(13)	0.36782(41)(11)
m010m030	$20 \times 64 \times 16$	0.7145(50)(42)	0.22146(35)(10)	0.37612(32)(08)
m010m050	$20 \times 64 \times 16$	0.7336(31)(18)	0.22287(28)(05)	0.37841(29)(05)
m010m050	$28 \times 64 \times 16$	0.7224(88)(91)	0.22279(47)(22)	0.37896(50)(22)
m020m050	$20 \times 64 \times 16$	0.8055(22)(16)	0.31091(28)(05)	0.40505(28)(06)
m030m030	$20 \times 64 \times 16$	0.8620(35)(10)	0.37323(28)(05)	0.42941(30)(16)
m030m050	$20 \times 32 \times 16$	0.8721(24)(18)	0.37465(26)(12)	0.43043(24)(18)
$b \approx 0.09$ fm ensembles				
m0031m0186	$40 \times 96 \times 12$	0.442(14)(08)	0.10189(58)(12)	0.18814(57)(11)
m0031m0186	$40 \times 96 \times 12$	0.443(14)(06)	0.10189(58)(12)	0.23486(62)(11)
m0031m031	$40 \times 96 \times 40$	0.446(17)(10)	0.10397(89)(37)	0.23582(91)(31)
m0031m031	$40 \times 96 \times 12$	0.4626(90)(10)	0.10205(54)(32)	0.23568(56)(41)
m0062m031	$28 \times 96 \times 12$	0.4957(25)(18)	0.14548(21)(09)	0.24685(19)(06)
m0124m031	$28 \times 96 \times 12$	0.5509(19)(05)	0.20045(33)(06)	0.26428(32)(11)

used by the NPLQCD collaboration's research program [20, 21, 22, 23, 24, 25, 26, 27, 28, 29, 30, 31, 32]. The sea quark configurations are publicly available as a courtesy of the MILC collaboration. The parameters used in our calculation are tabulated in Table 3.1 and consists of an assortment of quark masses at lattice spacings of $b \approx 0.09$ fm and $b \approx 0.125$ fm . The scale for our calculation has been with the r_1 scale setting procedure as has been described before.

The nucleon mass is determined by computing correlators. This is done by constructing interpolating operator with the appropriate quantum of the nucleon as fol-

lows,

$$C_N(\mathbf{x}, t) = \sum_{x} \langle \bar{N}(\mathbf{x}, t) N(0, 0) \rangle \tag{6.1}$$

where the $N(\mathbf{x}, t)$ is the gaussian smeared nucleon interpolating operator and is given as,

$$N(\mathbf{x}, t) = \epsilon_{abc} u^a(\mathbf{x}, t) \big(u^b(\mathbf{x}, t) C \gamma_5 d^c(\mathbf{x}, t) \big) \tag{6.2}$$

The long time behaviour of correlators computed from such interpolating operators can be shown to be that of a sum of multiexponentials dominated by the ground state as,

$$C_N \longrightarrow A_N e^{-M_N t} + A'_N e^{-M'_N t} + .. \tag{6.3}$$

where M_N is the ground state mass of the nucleon for a given particular ensemble. M'_N represents the excited state of the nucleon. The results for the nucleon masses are presented in Table 6.1 and the plots for nucleon mass on the all ensembles can be found in the appendix for plots.

6.2 Baryon Chiral Perturbation Theory

6.2.1 Nucleons in Two Flavor

In the two flavor, the nucleon is represented as an isospin and transforms in the fundamental representation. At the leading order, the nucleon mass upto $\mathcal{O}(m_\pi^3)$ is given by,

$$M_N = M_0 - 2\alpha_M m_\pi^2 \tag{6.4}$$

where, M_0 represents the nucleon mass in the chiral limit and α_M is the light quark matrix element. At next-to-leading order, the nucleon mass receives corrections from the pion-nucleon axial coupling and the nucleon-delta coupling and is given as,

$$M_N = M_0 - 2\alpha_M m_\pi^2 - \frac{3\pi g_A^2}{(4\pi f_\pi)^2} m_\pi^3 - \frac{8 g_{\Delta N}^2}{3(4\pi f_\pi)^2} \mathcal{F}(m_\pi, \Delta, \mu) \tag{6.5}$$

where the loop function $\mathcal{F}(m_\pi, \Delta, \mu)$ is the non-analytic contribution, for the case of of $m_\pi < \Delta$ is given as,

$$
\begin{aligned}
\mathcal{F}(m_\pi, \Delta, \mu) &= (m_\pi^2 - \Delta^2)\left\{ \sqrt{\Delta^2 - m_\pi^2}\, \ln\left(\frac{\Delta - \sqrt{\Delta^2 - m_\pi^2}}{\Delta + \sqrt{\Delta^2 - m_\pi^2}}\right) - 2\Delta \ln\frac{m_\pi^2}{\mu^2} \right\} \\
&\quad - m_\pi^2 \Delta \ln\frac{m_\pi^2}{\mu^2}
\end{aligned}
\tag{6.6}
$$

In a lattice QCD calculation, the pion masses are a variable and for the case of $m_\pi > \Delta$ and one needs to perform a analytic continuation of the non-analytic above as follows [16],

$$
\ln\left(\frac{\Delta - \sqrt{\Delta^2 - m_\pi^2}}{\Delta + \sqrt{\Delta^2 - m_\pi^2}}\right) \longrightarrow \text{arccot}\left(\frac{\Delta}{\sqrt{m_\pi^2 - \Delta^2}}\right)
\tag{6.7}
$$

where the nucleon delta mass difference $\Delta = 293$ MeV is fixed at its physical value. Since our calculations is done on lattices at different volumes, an attempt is made to include the finite volume corrections to nucleon masses as well. In the SU(2) HBχPT, the nucleon mass in the finite volume is given by,

$$
\delta M_N = M_N(m_\pi, L) - M_N(m_\pi, \infty)
\tag{6.8}
$$

$$
= \frac{9 m_\pi^3 g_A^2}{8\pi f_\pi^2} F_\Delta(m_\pi L, 0) + \frac{m_\pi^3 g_{N\Delta}^2}{\pi f_\pi^2} F_\Delta(m_\pi L, \Delta_\Delta L)
$$

The finite volume functions are given as,

$$
F_\Delta(x, y) = \frac{1}{3\pi} \sum_{\mathbf{n} \neq 0} \int_0^\infty dw\, \bar{\beta}(w, \frac{y}{x}) \left[\bar{\beta}(w, \frac{y}{x}) K_0(|\mathbf{n}| x \bar{\beta}(w, \frac{y}{x})) - \frac{K_1(|\mathbf{n}| x \bar{\beta}(w, \frac{y}{x}))}{|\mathbf{n}| x} \right]
\tag{6.9}
$$

with, $\bar{\beta}(w, \frac{y}{x})) = \sqrt{w^2 + 2wz + 1}$, $\Delta_\Delta = M_\Delta - M_N$ and the $K_n(z)$ are modified Bessel functions. A modified but simple fit is also attempted to explore the finite volume effects as,

$$
M_N(L) = M_N(\infty) + c_V \frac{e^{-m_\pi L}}{m_\pi L}
\tag{6.10}
$$

6.2.2 Baryons in Three Flavor

In the three flavor χPT , the baryons form an octet and transform in the adjoint representation. In order to apply χPT analysis, we would therefore need lattice computations on the baryon octet. We have computed the octet masses on the our lattice ensembles and the results are presented in Table 6.2. At the leading order, the octet baryon masses are given by,

$$M_N = M_0 - m_\pi^2 \, (\alpha_M + \beta_M + \sigma_M) - m_K^2 \, 2\sigma_M \qquad (6.11)$$

$$M_\Lambda = M_0 - m_\pi^2 \, (\beta_M + \sigma_M) - m_K^2 \, (\alpha_M + 2\sigma_M)$$

$$M_\Sigma = M_0 - m_\pi^2 \, (\tfrac{2}{3}\alpha_M - \tfrac{1}{3}\beta_M + \sigma_M) - m_K^2 \, (\tfrac{1}{3}\alpha_M + \tfrac{4}{3}\beta_M + 2\sigma_M)$$

$$M_\Xi = M_0 - m_\pi^2 \, (-\tfrac{2}{3}\alpha_M + \tfrac{1}{3}\beta_M + \sigma_M) - m_K^2 \, (\tfrac{5}{3}\alpha_M + \tfrac{2}{3}\beta_M + 2\sigma_M)$$

In order to describe the meson mass dependence, the sigma terms are redefined as $\alpha'_M = \frac{1}{B_0}(\alpha_M)$. The results for the next-to-leading contributions to the masses are presented in the appendix at the end of the chapter.

6.3   Chiral Analysis of Baryons

In this section, we perform analysis of our lattice data using baryon chiral perturbation theory. The analysis is performed in two flavor and three flavor χPT . In both theories, we fit the low energy constants at leading order (LO) and next-to-leading order (NLO) in the chiral expansion. Once these are known, we use them to make predictions for nucleon mass and masses of other members of the octet. In addition we determine light and strange matrix elements of the nucleon and the octet baryons.

We have lattice calculations at two lattice spacings namely $b \approx 0.09$ fm and $b \approx 0.125$ fm . Hence, we can only perform simplistic continuum extrapolation which

Table 6.2: *Baryon masses from NPLQCD data*

$b \approx 0.125$ fm ensembles					
m_{sea}	$L \times T \times L_5$	M_N	M_Λ	M_Σ	M_Ξ
m007m050	$20 \times 32 \times 16$	0.6978(61)	0.7774(57)	0.8390(22)	0.8872(13)
m010m030	$20 \times 64 \times 16$	0.7210(38)	0.7967(21)	0.8248(20)	0.8919(14)
m010m050	$20 \times 32 \times 16$	0.7311(27)	0.8071(23)	0.8506(19)	0.9013(11)
m010m050	$28 \times 64 \times 16$	0.7214(108)	0.7942(58)	0.8413(83)	0.8931(45)
m020m050	$20 \times 32 \times 16$	0.8069(22)	0.8666(37)	0.8830(18)	0.9233(13)
m030m030	$20 \times 64 \times 16$	0.8626(24)	0.8966(20)	0.9019(30)	0.9374(17)
m030m050	$20 \times 32 \times 16$	0.8741(16)	0.9094(26)	0.9213(13)	0.9461(14)

$b \approx 0.09$ fm ensembles					
m_{sea}	$L \times T \times L_5$	M_N	M_Λ	M_Σ	M_Ξ
m0031m0186	$40 \times 96 \times 12$	0.4423(103)	0.4846(66)	0.5163(71)	0.5347(55)
m0031m0186	$40 \times 96 \times 12$	0.4438(118)	0.5097(70)	0.5497(81)	0.5814(62)
m0031m031	$40 \times 96 \times 40$	0.4823(95)	0.5411(68)	0.5751(70)	0.6174(58)
m0031m031	$40 \times 96 \times 12$	0.4547(85)	0.5213(59)	0.5550(60)	0.5953(47)
m0062m031	$28 \times 96 \times 12$	0.5097(33)	0.5571(27)	0.5813(21)	0.6164(12)
m0124m031	$28 \times 96 \times 12$	0.5598(28)	0.5947(22)	0.6062(23)	0.6366(18)

is done as follows,

$$\lambda(b) = \lambda_0 + \lambda_1 \left(\frac{b}{r_1}\right)^2 \tag{6.12}$$

where, λ is the particular LEC's considered for continuum extrapolation. We now proceed to the analysis which is described in next two subsections.

6.3.1 Two Flavor Analysis

The two flavor theory contains only two light quarks (up and down quarks) and hence describes the pion mass dependence of the nucleon. We perform a χ^2 minimization of the computed nucleon masses as shown in Table 6.1. This is done by constructing

Table 6.3: *Results from LO SU(2) χPT analysis of M_N*

Max	Coarse Ensembles		
m_l/m_s	M_0 [GeV]	α_M [GeV]$^{-1}$	χ^2/dof
0.4	1.0955(7)(1)	-0.5594(21)(03)	0.1/2
0.6	1.1211(5)(1)	-0.4914(11)(01)	0.3/3
Max	Fine Ensembles		
m_l/m_s	M_0 [GeV]	α_M [GeV]$^{-1}$	χ^2/dof
0.2	0.9642(18)(08)	-0.9291(92)(38)	3.6/2
0.4	1.0080(11)(04)	-0.7222(45)(11)	6/4

Table 6.4: *Results from NLO SU(2) χPT analysis of M_N*

Max	Coarse Ensembles				
m_l/m_s	M_0 [GeV]	α_M [GeV]$^{-1}$	g_A	$g_{N\Delta}$	χ^2/dof
0.6	1.0587(22)(3)	-0.862(14)(02)	0.4748(91)(14)	0.0(0)(0)	0.23/2
0.6	0.8243(23)(05)	-4.0240(85)(18)	$g_A = 1.2$	$g_{N\Delta} = 1.5$	0.09/2
Max	Fine Ensembles				
m_l/m_s	M_0 [GeV]	α_M [GeV]$^{-1}$	g_A	$g_{N\Delta}$	χ^2/dof
0.4	0.930(12)(01)	-1.55(13)(01)	0.83(13)(06)	0.0(0.0)(0.0)	3/2
0.4	0.7019(9)(3)	-4.257(3)(1)	$g_A = 1.2$	$g_{N\Delta} = 1.5$	6/2

a χ^2 as follows,

$$\chi^2 = \sum_{m_q} \left(\frac{M_N^{Latt}(m_q) - M_N^{SU(2)}[m_\pi^g(m_q), \alpha_M]}{\sigma(m_q)} \right)^2 \qquad (6.13)$$

where, M_N^{Latt} is the lattice computed nucleon mass and $M_N^{SU(2)}$ is the two flavor chiral expression for the nucleon . To determine the uncertainties in the extracted LEC's, we have generated gaussian distributed samples of m_π^g at the relevant quark mass m_q and use them in the χ^2 minimization. We present the results of our analysis in Tables 6.3 6.4 and 6.5 and perform continuum extrapolation and then make remarks on the

Table 6.5: *Results from Linear Fit* $M_N = M_0 + \alpha_M m_\pi$

Max	Coarse Ensembles		
m_l/m_s	M_0 [GeV]	α_M [GeV]$^{-1}$	χ^2/dof
0.4	0.8519(12)(02)	1.0622(22)(05)	0.2/2
0.6	0.8585(18)(03)	1.0484(39)(06)	0.1/3
Max	Fine Ensembles		
m_l/m_s	M_0 [GeV]	α_M [GeV]$^{-1}$	χ^2/dof
0.2	0.8320(35)(17)	1.027(11)(05)	2.4/2
0.4	0.8123(23)(09)	1.0884(64)(22)	2.6/2

analysis.

At, leading order the finite volume corrections are implicitly included in the LEC's α_M. The results are presented in Table 6.3. At this order, we perform the continuum extrapolation of these LEC's and the results are,

$$M_0[\text{LO}] = 0.8955(26)(09) \text{ GeV} \qquad \alpha_M[\text{LO}] = -0.931(10)(02) \text{ GeV}^{-1} \quad (6.14)$$

$$M_N[\text{phys}] \;=\; 930(2)(1)\text{MeV}$$

At next-to-leading order, the nucleon mass has contribution from the pion-nucleon axial coupling g_A and the nucleon-delta $g_{N\Delta}$ coupling. We perform a χ^2 minimization similar to the one described above. The results are displayed in Table 6.4. The results after continuum extrapolation are given as,

$$M_0[\text{NLO}] \;=\; 0.766(27)(02) \text{ GeV} \qquad \alpha_M[\text{NLO}] = -2.43(27)(02) \text{ GeV}^{-1} \quad (6.15)$$

$$g_A \;=\; 1.28(27)(14) \qquad g_{N\Delta} = 0.0(0)(0)$$

The chiral extrapolation of nucleon mass gives us following result,

$$M_N[\text{phys}] = 840(17)(2)\text{MeV} \qquad\qquad (6.16)$$

We also perform a simple minded linear fit to the lattice data purely based on observation that the data describes a linear fit. The results of the analysis are presented in Table 6.5. The continuum extrapolated results are as follows,

$$M_0 = 0.8061(56)(09) \text{ GeV} \qquad \alpha_M = 0.988(24)(11) \qquad (6.17)$$

$$M_N[\text{phys}] = 940(5)(2)\text{MeV}$$

We now make several observations about our the analysis done so far,

1. The leading order fit to the nucleon mass while providing reasonable description of the data, as the χ^2 being close to unity, fails at chiral extrapolation of the nucleon mass. Hence this fit should not be trusted too well.

2. At NLO, the fits also describes the data well enough, but fails at several levels. While the continuum extrapolation reproduces the known phenomenological results for g_A, it completely fails to reproduce $g_{N\Delta}$. With explicitly inputting the phenomenological values of $g_{N\Delta}$, the results of such a fit fails at the chiral extrapolation of nucleon mass. Further comparing the results for α_M to that of LO fits, we see that there is a substantial change in the results that one cannot conclude that the results are converging in the sense of perturbation theory.

3. The results of the linear fits, based on pure observation, remarkably reproduces the correct chiral extrapolation of the nucleon mass. We repeat here that such a fit is based purely on observation.

6.3.2 Three Flavor Analysis

In the three flavor χPT , the baryons are represented in the adjoint and as such transform as an octet. The lattice computed results are shown in Table 6.2. We

Table 6.6: *Results from LO SU(3) χPT analysis of M_B*

Max	Coarse Ensembles				
m_l/m_s	M_0 [GeV]	α_M [GeV]$^{-1}$	β_M [GeV]$^{-1}$	σ_M [GeV]$^{-1}$	χ^2/dof
0.3	1.082(11)(02)	-0.4448(7)(2)	-0.4469(7)(2)	-0.054(11)(02)	9.7/4
0.2	1.093(10)(03)	-0.4460(7)(2)	-0.4494(7)(2)	-0.042(11)(03)	19.09/8
Max	Fine Ensembles				
m_l/m_s	M_0 [GeV]	α_M [GeV]$^{-1}$	β_M [GeV]$^{-1}$	σ_M [GeV]$^{-1}$	χ^2/dof
0.2	0.9482(43)(12)	-0.5567(32)(11)	-0.5580(31)(11)	-0.1179(68)(20)	48/14
0.4	0.9750(26)(10)	-0.5435(12)(05)	-0.4823(10)(05)	-0.1174(32)(11)	81/20

perfom a simultaneous *chi*^{2} minimization of the octet baryons as follows

$$\chi^2 = \sum_{SU(3)} \sum_{m_q} \left(\frac{M_B^{Latt}(m_q) - M_B^{SU(3)}[m_\pi^g(m_q), m_K^g(m_q), \alpha_M, \beta_M, \sigma_M]}{\sigma_B(m_q)} \right)^2 \quad (6.18)$$

where, $M_B^{Latt} = \{M_N, M_\Lambda, M_\Sigma, M_\Xi\}$ are the octet baryons computed on the lattice at the given quark mass. $M_B^{SU(3)}$ is the relevant chiral expression for the baryons. To determine the uncertainties in the extracted LEC's, we have generated gaussian distributed samples $\{m_\pi^g, m_K^g\}$ at the relevant quark mass m_q and use them in the χ^2 minimization. The results of analysis are presented in Tables 6.6 6.7 and 6.8. We now perform the continuum extrapolation of these results and then make observations from those results. The reader should find the results below and then the observations from those.

At leading order in SU(3) χPT , we have four LEC's $\{M_0, \alpha_M, \beta_M, \sigma_M\}$ which characterise the pion and kaon mass dependence of the octet. The continuum extrapolated results of the LEC's with the chiral extrapolation of nucleon mass are as follows,

$$M_0 = 0.799(17)(03) \qquad \alpha_M = -0.6828(30)(06) \qquad (6.19)$$

$$\beta_M = -0.6126(24)(11) \qquad \sigma_M = -0.2072(50)(20)$$

Table 6.7: *Results from NLO SU(3) χPT analysis of M_B - I*

Max	Coarse Ensembles				
m_l/m_s	M_0 [GeV]	α_M [GeV]$^{-1}$	β_M [GeV]$^{-1}$	σ_M [GeV]$^{-1}$	χ^2/dof
0.2	1.035(14)(03)	-0.416(29)(07)	-0.777(43)(14)	-0.307(32)(08)	16/8
0.3	0.989(10)(01)	-0.4915(91)(12)	-0.742(28)(04)	-0.297(24)(03)	28/12
Max	Fine Ensembles				
m_l/m_s	M_0 [GeV]	α_M [GeV]$^{-1}$	β_M [GeV]$^{-1}$	σ_M [GeV]$^{-1}$	χ^2/dof
0.2	0.921(30)(18)	-0.63(11)(07)	-0.57(11)(06)	-0.18(12)(05)	46/8
0.4	0.896(45)(41)	-0.73(17)(13)	-0.69(11)(12)	-0.25(11)(11)	48/12

Table 6.8: *Results from NLO SU(3) χPT analysis of M_B - II*

Max	Coarse Ensembles			
m_l/m_s	C	D	F	χ^2/dof
0.3	0.0(0)(0)	0.406(23)(07)	0.031(11)(03)	16/8
0.2	0.0(0)(0)	0.371(17)(03)	0.0533(34)(05)	28/12
Max	Fine Ensembles			
m_l/m_s	C	D	F	χ^2/dof
0.2	0.0(0)(0)	0.15(29)(12)	0.080(10)(05)	46/8
0.4	0.0(0)(0)	0.22(15)	0.108(80)(57)	48/12

$$M_N[\text{phys}] = 929(10)(2) \text{ MeV}$$

At NLO, the baryon masses have contribution from additional LEC's corresponding to the coupling to mesons and the delta resonance as $\{C, D, F\}$. The results of the fits have been split in Tables 6.7 & 6.8 for convenience. The results for the same after continuum extrapolations and chiral extrapolation of the nucleon mass are given

Table 6.9: *Results from NLO SU(3) χPT with $C = 1.5$, $D = 0.8$ and $F = 0.47$*

Max	Coarse Ensembles				
m_l/m_s	M_0 [GeV]	α_M [GeV]$^{-1}$	β_M [GeV]$^{-1}$	σ_M [GeV]$^{-1}$	χ^2/dof
0.4	0.566(38)(07)	-3.975(12)(08)	-3.6638(58)(08)	-1.452(30)(08)	1200/4
Max	Fine Ensembles				
m_l/m_s	M_0 [GeV]	α_M [GeV]$^{-1}$	β_M [GeV]$^{-1}$	σ_M [GeV]$^{-1}$	χ^2/dof
0.2	0.363(20)(04)	-3.566(11)(03)	-3.784(13)(04)	-1.731(33)(07)	200/14

as,

$$M_0 = 0.833(69)(41) \qquad \alpha_M = -0.80(25)(15) \qquad (6.20)$$

$$\beta_M = -0.34(25)(14) \qquad \sigma_M = -0.02(27)(11)$$

$$D = -0.12(69)(27) \qquad F = 0.114(23)(11)$$

$$M_N[\text{phys}] = 760(168)(61) \text{ MeV}$$

In addition to leading order and next-to-leading order fits, we also perform a hybrid NLO fit with the LEC's $\{C, D, F\}$ set to their phenomenological values. The results of this fit is presented in Table 6.9. We do not perform the continuum extrapolation as there is no meaningful information to be obtained from these results.

We now make several observations of the analysis done so far,

1. The leading order SU(3) χPT does not provide a reasonable description of the lattice data for baryon masses as the total $\chi^2 \sim 3$. The chiral extrapolation however yields a nucleon mass which agrees with experimental result. Hence this result should be trusted with caution.

2. The NLO SU(3) description does not provide a good description either and hence cannot be trusted at all. The continuum extrapolated fit results for the axial couplings fail to reproduce the known phenomenological results for $\{C,$

D, F}. The chiral extrapolation for nucleon mass although agreeing with the experimental result cannot be taken seriously due to size of the uncertainty. For the same reason, the results for the LEC although agreeing with the LO results have to discarded.

3. The NLO fit results with {$\mathcal{C}$, D, F} set to phenomenological values also fail to describe the data. Hence the results cannot be even considered to provide estimates of observables.

With the LO results, we now make estimates for the light and strange matrix elements of the baryon octet.

6.3.3 Estimates for the Light and Strange Matrix Elements

The light and strange matrix elements characterise the light and strange quark contribution to the octet baryons. In this section we present our results for the nucleon since that is phenomenologically more interesting. By the applying the Feynman-Hellman theorem to the nucleon mass, the matrix elements are defined as,

$$\sigma_q = m_q \, \frac{\partial}{\partial m_q} M_N \tag{6.21}$$

With isospin averaged up and down quark masses, the contribution of the pion sea to the nucleon mass is given as,

$$\sigma_\pi = m_\pi^2 \, \frac{\partial}{\partial m_\pi^2} M_N \tag{6.22}$$

In the two flavor case, the results for light sigma terms are,

$$\sigma_\pi = 34.6(4)(2)\text{MeV} \qquad \text{SU(2) LO Fit} \tag{6.23}$$

$$\sigma_\pi = 67(1)(0)\text{MeV} \qquad \text{SU(2) Linear Fit}$$

$$\sigma_\pi = 28.4(3)(1)\text{MeV} \qquad \text{SU(3) LO Fit}$$

As can be seen, the results for the two flavor and three flavor being on the same order disagree with the naive linear fit. This can be expected as in the two flavor case, the leading order results fail at chiral extrapolation. The results from the linear fit however do predict the nucleon mass correctly and the result for the σ_π also agrees with estimates from other lattice calculations.

The results for strange matrix elements is given as,

$$\begin{aligned}
\sigma_s &= m_s \frac{\partial}{\partial m_s} M_N \\
&= (2m_K^2 - m_\pi^2) \frac{\partial}{\partial m_K^2} M_N
\end{aligned} \qquad (6.24)$$

The results from our SU(3) analysis are,

$$\sigma_K = 97.6(6)(1)\text{MeV} \qquad \text{SU(3) LO Fit} \qquad (6.25)$$

We see again that the results are not in agreement with our previous estimate in Chapter 5. The result is also not in agreement with lattice average. This can be attributed to poor fit of SU(3) χPT to the lattice data.

6.4   Conclusions

In this chapter, we have analysed the baryon chiral perturbation theory from our lattice data. We have performed analysis with two and three flavor χPT at leading and next-to leading orders of chiral expansion. From our analysis, we find that the leading order description of two flavor χPT provides a good description of the data but fails at chiral extrapolation. With the inclusion of next-to-leading order terms in the analysis, the fit results fails to reproduce the known phenomenological axial couplings. This is an indication that upto this order χPT is not a good description of the data. Based on observation, we also perform a linear fit to our lattice data and find that it predicts correct nucleon mass at the physical point. The light sigma terms

corresponding to the linear fit are also in agreement with lattice calculations. We then analyse three flavor χPT . At the leading order, we find that due to relatively high χ^2, the SU(3) χPT doesn't describe the data well, although it predicts the correct nucleon mass at the physical point. At the next-to-leading order, the situation is not any better as the fits results again fail to reproduce the axial couplings $\{\mathcal{C}, D, F\}$. The SU(3) description upto this order also cannot be trusted which is further evident from the results of the light and strange sigma terms.

It is expected that in baryon χPT , since expansion parameters are $\mathcal{O}(m_{\pi,K}/\Lambda_\chi)$, the convergence is slower compared to the chiral description of mesons. A trustable chiral analysis will have to be performed at orders of NNLO and NNNLO. At these orders, the number of low energy are quite high and inturn demand a lot of more data than we have. Such an analysis cannot be performed at this time and hence we have to rely on empirical fits such as the linear fit to the data.

Chapter 7

Conclusions

In this thesis we have applied lattice techinques and effective field theory methods to present a first principle understanding of low energy QCD. In particular, we have attempted to understand the light quark mass dependence of low lying hadrons.

In chapter 3, we studied the quark mass dependence of pion mass and decay constant using two flavor low energy effective field theory to analyse the lattice results. It is found that mixed-action chiral perturbation theory correctly accounts for the unphysical effects and provides a reliable description of the lattice data. The results for $\bar{l}_3$ and $\bar{l}_4$ are found to be in agreement with the average determination of lattice calculations. For the range of quark masses used in this work, the chiral expansion for the pion mass seems to be very well converging from the next-to-leading to next-to-next-to-leading order. This is an indication that chiral perturbation theory can be reliably used to describe quark mass dependence of the pion mass.

In chapter 4, we studied the three flavor extension of chiral perturbation theory with the quark mass dependence of the pion and kaon masses and decay constants. The three flavor theory also allowed to study phenomenological interesting quantity f_K/f_π. We employed mixed-action theory upto next-to-leading order and found that the physical extrapolation of this quantity is an agreement with the experimental results indicating that the mixed action theory correctly accounts for the partial quenching and discretisation effects.

In chapter 5, we have performed a calculation of the scalar strange matrix element

of the nucleon. Currently, there is a great interest in the experimental community to know the $m_s \langle N | \bar{s}s | N \rangle$ and the heavy quark elements as they might couple to certain dark matter candidates. Our calculation, although suffering from the disadvantage of limited data, is in remarkable agreement with the lattice average.

Finally, in chapter 6, we attempt to use the methodology of effective field theory of baryons to our lattice computations. We perform a two flavor and three flavor analysis and find that to the order at which the analysis is performed, the results are not satisfactory. This is attributed to slow converging property of baryon chiral perturbation theory and hence should be regarded only as a guide for continuum extrapolations.

In conclusion, we find that the combined tools of lattice qcd and EFT provide an accurate description in the meson sector while the description for baryons remain untamed and remains to be solved in future.

LIST OF REFERENCES

[1] A. Bazavov *et al.*, "Full nonperturbative QCD simulations with 2+1 flavors of improved staggered quarks," *Rev. Mod. Phys.*, vol. 82, pp. 1349–1417, 2010.

[2] D. J. Gross and F. Wilczek, "Ultraviolet behavior of non-abelian gauge theories," *Phys. Rev. Lett.*, vol. 30, pp. 1343–1346, Jun 1973.

[3] H. D. Politzer, "Reliable perturbative results for strong interactions?," *Phys. Rev. Lett.*, vol. 30, pp. 1346–1349, Jun 1973.

[4] G. Hooft, "Renormalizable lagrangians for massive yang-mills fields," *Nuclear Physics B*, vol. 35, no. 1, pp. 167 – 188, 1971.

[5] J. Bjorken and E. A. Paschos, "Inelastic Electron Proton and gamma Proton Scattering, and the Structure of the Nucleon," *Phys.Rev.*, vol. 185, pp. 1975–1982, 1969.

[6] S. Weinberg, "Phenomenological Lagrangians," *Physica*, vol. A96, p. 327, 1979.

[7] J. Gasser and H. Leutwyler, "Chiral perturbation theory to one loop," *Ann. Phys.*, vol. 158, p. 142, 1984.

[8] J. Gasser and H. Leutwyler, "Chiral Perturbation Theory: Expansions in the Mass of the Strange Quark," *Nucl. Phys.*, vol. B250, p. 465, 1985.

[9] K. G. Wilson, "Confinement of Quarks," *Phys.Rev.*, vol. D10, pp. 2445–2459, 1974.

[10] S. Bethke, "Experimental tests of asymptotic freedom," *Progress in Particle and Nuclear Physics*, vol. 58, no. 2, pp. 351 – 386, 2007.

[11] J. B. Kogut and L. Susskind, "Hamiltonian Formulation of Wilson's Lattice Gauge Theories," *Phys.Rev.*, vol. D11, p. 395, 1975.

[12] D. B. Kaplan, "A Method for simulating chiral fermions on the lattice," *Phys. Lett.*, vol. B288, pp. 342–347, 1992.

[13] C. Vafa and E. Witten, "Restrictions on Symmetry Breaking in Vector-Like Gauge Theories," *Nucl.Phys.*, vol. B234, p. 173, 1984.

[14] S. R. Coleman, J. Wess, and B. Zumino, "Structure of phenomenological Lagrangians. 1.," *Phys.Rev.*, vol. 177, pp. 2239–2247, 1969.

[15] J. Callan, Curtis G., S. R. Coleman, J. Wess, and B. Zumino, "Structure of phenomenological Lagrangians. 2.," *Phys.Rev.*, vol. 177, pp. 2247–2250, 1969.

[16] E. E. Jenkins and A. V. Manohar, "Baryon chiral perturbation theory using a heavy fermion Lagrangian," *Phys.Lett.*, vol. B255, pp. 558–562, 1991.

[17] G. Colangelo and S. Durr, "The pion mass in finite volume," *Eur. Phys. J.*, vol. C33, pp. 543–553, 2004.

[18] G. Colangelo, S. Durr, and C. Haefeli, "Finite volume effects for meson masses and decay constants," *Nucl. Phys.*, vol. B721, pp. 136–174, 2005.

[19] S. R. Beane, "Nucleon masses and magnetic moments in a finite volume," *Phys.Rev.*, vol. D70, p. 034507, 2004.

[20] S. R. Beane, P. F. Bedaque, K. Orginos, and M. J. Savage, "I = 2 pi pi scattering from fully-dynamical mixed-action lattice QCD," *Phys. Rev.*, vol. D73, p. 054503, 2006.

[21] S. R. Beane, K. Orginos, and M. J. Savage, "The Gell-Mann - Okubo mass relation among baryons from fully-dynamical mixed-action lattice QCD," *Phys. Lett.*, vol. B654, pp. 20–26, 2007.

[22] S. R. Beane, K. Orginos, and M. J. Savage, "Strong-isospin violation in the neutron proton mass difference from fully-dynamical lattice QCD and PQQCD," *Nucl. Phys.*, vol. B768, pp. 38–50, 2007.

[23] S. R. Beane *et al.*, "Pi-K Scattering in Full QCD with Domain-Wall Valence Quarks," *Phys. Rev.*, vol. D74, p. 114503, 2006.

[24] S. R. Beane *et al.*, "Hyperon nucleon scattering from fully-dynamical lattice QCD," *Nucl. Phys.*, vol. A794, pp. 62–72, 2007.

[25] S. R. Beane *et al.*, "Precise Determination of the I=2 pipi Scattering Length from Mixed-Action Lattice QCD," *Phys. Rev.*, vol. D77, p. 014505, 2008.

[26] S. R. Beane *et al.*, "The K+K+ Scattering Length from Lattice QCD," *Phys. Rev.*, vol. D77, p. 094507, 2008.

[27] S. R. Beane *et al.*, "Multi-Pion Systems in Lattice QCD and the Three-Pion Interaction," *Phys. Rev. Lett.*, vol. 100, p. 082004, 2008.

[28] W. Detmold *et al.*, "Multi-Pion States in Lattice QCD and the Charged-Pion Condensate," *Phys. Rev.*, vol. D78, p. 014507, 2008.

[29] S. R. Beane, K. Orginos, and M. J. Savage, "Hadronic Interactions from Lattice QCD," *Int. J. Mod. Phys.*, vol. E17, pp. 1157–1218, 2008.

[30] W. Detmold, K. Orginos, M. J. Savage, and A. Walker-Loud, "Kaon Condensation with Lattice QCD," *Phys. Rev.*, vol. D78, p. 054514, 2008.

[31] W. Detmold and M. J. Savage, "Color Screening by Pions," *Phys. Rev. Lett.*, vol. 102, p. 032004, 2009.

[32] A. Torok *et al.*, "Meson-Baryon Scattering Lengths from Mixed-Action Lattice QCD," *Phys. Rev.*, vol. D81, p. 074506, 2010.

[33] D. B. Renner *et al.*, "Hadronic physics with domain-wall valence and improved staggered sea quarks," *Nucl. Phys. Proc. Suppl.*, vol. 140, pp. 255–260, 2005.

[34] R. G. Edwards *et al.*, "Hadron structure with light dynamical quarks," *PoS*, vol. LAT2005, p. 056, 2006.

[35] R. G. Edwards *et al.*, "The nucleon axial charge in full lattice QCD," *Phys. Rev. Lett.*, vol. 96, p. 052001, 2006.

[36] P. Hagler *et al.*, "Nucleon Generalized Parton Distributions from Full Lattice QCD," *Phys. Rev.*, vol. D77, p. 094502, 2008.

[37] A. Walker-Loud *et al.*, "Light hadron spectroscopy using domain wall valence quarks on an Asqtad sea," *Phys. Rev.*, vol. D79, p. 054502, 2009.

[38] J. D. Bratt *et al.*, "Nucleon structure from mixed action calculations using 2+1 flavors of asqtad sea and domain wall valence fermions," *Phys. Rev.*, vol. D82, p. 094502, 2010.

[39] J. Kogut and L. Susskind, "Hamiltonian formulation of wilson's lattice gauge theories," *Phys. Rev. D*, vol. 11, pp. 395–408, Jan 1975.

[40] C. W. Bernard *et al.*, "The QCD spectrum with three quark flavors," *Phys. Rev.*, vol. D64, p. 054506, 2001.

[41] Y. Shamir, "The Euclidean spectrum of Kaplan's lattice chiral fermions," *Phys. Lett.*, vol. B305, pp. 357–365, 1993.

[42] Y. Shamir, "Chiral fermions from lattice boundaries," *Nucl. Phys.*, vol. B406, pp. 90–106, 1993.

[43] Y. Shamir, "Reducing chiral symmetry violations in lattice QCD with domain-wall fermions," *Phys. Rev.*, vol. D59, p. 054506, 1999.

[44] V. Furman and Y. Shamir, "Axial symmetries in lattice QCD with Kaplan fermions," *Nucl. Phys.*, vol. B439, pp. 54–78, 1995.

[45] T. Blum *et al.*, "Quenched lattice QCD with domain wall fermions and the chiral limit," *Phys. Rev.*, vol. D69, p. 074502, 2004.

[46] O. Bar, G. Rupak, and N. Shoresh, "Simulations with different lattice Dirac operators for valence and sea quarks," *Phys. Rev.*, vol. D67, p. 114505, 2003.

[47] O. Bar, G. Rupak, and N. Shoresh, "Chiral perturbation theory at O(a**2) for lattice QCD," *Phys. Rev.*, vol. D70, p. 034508, 2004.

[48] O. Bar, C. Bernard, G. Rupak, and N. Shoresh, "Chiral perturbation theory for staggered sea quarks and Ginsparg-Wilson valence quarks," *Phys. Rev.*, vol. D72, p. 054502, 2005.

[49] M. Golterman, T. Izubuchi, and Y. Shamir, "The role of the double pole in lattice QCD with mixed actions," *Phys. Rev.*, vol. D71, p. 114508, 2005.

[50] B. C. Tiburzi, "Baryons with Ginsparg-Wilson quarks in a staggered sea," *Phys. Rev.*, vol. D72, p. 094501, 2005.

[51] J.-W. Chen, D. O'Connell, R. S. Van de Water, and A. Walker-Loud, "Ginsparg-Wilson pions scattering on a staggered sea," *Phys. Rev.*, vol. D73, p. 074510, 2006.

[52] S. Prelovsek, "Effects of staggered fermions and mixed actions on the scalar correlator," *Phys. Rev.*, vol. D73, p. 014506, 2006.

[53] C. Aubin, J. Laiho, and R. S. Van de Water, "The kaon B-parameter in mixed action chiral perturbation theory," *Phys. Rev.*, vol. D75, p. 034502, 2007.

[54] J.-W. Chen, D. O'Connell, and A. Walker-Loud, "Two meson systems with Ginsparg-Wilson valence quarks," *Phys. Rev.*, vol. D75, p. 054501, 2007.

[55] F.-J. Jiang, "Mixed action lattice spacing effects on the nucleon axial charge," 2007.

[56] K. Orginos and A. Walker-Loud, "Mixed meson masses with domain-wall valence and staggered sea fermions," *Phys. Rev.*, vol. D77, p. 094505, 2008.

[57] J.-W. Chen, D. O'Connell, and A. Walker-Loud, "Universality of Mixed Action Extrapolation Formulae," *JHEP*, vol. 04, p. 090, 2009.

[58] C. Aubin, J. Laiho, and R. S. Van de Water, "Discretization effects and the scalar meson correlator in mixed-action lattice simulations," *Phys. Rev.*, vol. D77, p. 114501, 2008.

[59] J.-W. Chen, M. Golterman, D. O'Connell, and A. Walker-Loud, "Mixed Action Effective Field Theory: an Addendum," *Phys. Rev.*, vol. D79, p. 117502, 2009.

[60] Y. Aoki *et al.*, "Continuum Limit Physics from 2+1 Flavor Domain Wall QCD," *Phys. Rev.*, vol. D83, p. 074508, 2011.

[61] T. Blum *et al.*, "Kaon Matrix Elements and CP-violation from Quenched Lattice QCD: (I) the 3-flavor case," *Phys. Rev.*, vol. D68, p. 114506, 2003.

[62] M. Golterman, Y. Shamir, and B. Svetitsky, "Localization properties of lattice fermions with plaquette and improved gauge actions," *Phys. Rev.*, vol. D72, p. 034501, 2005.

[63] S. R. Sharpe, "Future of Chiral Extrapolations with Domain Wall Fermions," 2007.

[64] S. R. Sharpe and J. Singleton, Robert L., "Spontaneous flavor and parity breaking with Wilson fermions," *Phys. Rev.*, vol. D58, p. 074501, 1998.

[65] G. Colangelo, J. Gasser, and H. Leutwyler, "pi pi scattering," *Nucl. Phys.*, vol. B603, pp. 125–179, 2001.

[66] K. Orginos and D. Toussaint, "Testing improved actions for dynamical Kogut-Susskind quarks," *Phys. Rev.*, vol. D59, p. 014501, 1999.

[67] J. Gasser and H. Leutwyler, "Light Quarks at Low Temperatures," *Phys. Lett.*, vol. B184, p. 83, 1987.

[68] W. J. Marciano, "Precise determination of —V(us)— from lattice calculations of pseudoscalar decay constants," *Phys.Rev.Lett.*, vol. 93, p. 231803, 2004.

[69] A. Bottino, F. Donato, N. Fornengo, and S. Scopel, "Implications for Relic Neutralinos of the Theoretical Uncertainties in the Neutralino Nucleon Cross-Section," *Astropart.Phys.*, vol. 13, pp. 215–225, 2000.

[70] E. E. Jenkins, "Chiral Lagrangian for Baryons in the $1/N_c$ Expansion," *Phys.Rev.*, vol. D53, pp. 2625–2644, 1996.

[71] R. Babich, R. C. Brower, M. A. Clark, G. T. Fleming, J. C. Osborn, *et al.*, "Exploring Strange Nucleon Form Factors on the Lattice," *Phys.Rev.*, vol. D85, p. 054510, 2012.

[72] K. Takeda *et al.*, "Nucleon Strange Quark Content from Two-Flavor Lattice QCD with Exact Chiral Symmetry," *Phys.Rev.*, vol. D83, p. 114506, 2011.

[73] G. S. Bali *et al.*, "The Strange and Light Quark Contributions to the Nucleon Mass from Lattice QCD," *Phys.Rev.*, vol. D85, p. 054502, 2012.

[74] S. Dinter *et al.*, "Sigma Terms and Strangeness Content of the Nucleon with $N_F = 2 + 1 + 1$ Twisted Mass Fermions," *JHEP*, vol. 1208, p. 037, 2012.

[75] M. Gong, A. Li, A. Alexandru, T. Draper, and K. Liu, "The Strangeness and Charmness of Nucleon from Overlap Fermions," *PoS*, vol. LATTICE2011, p. 156, 2011.

[76] H. Ohki *et al.*, "Nucleon Strange Quark Content from $N_F = 2 + 1$ Lattice QCD with Exact Chiral Symmetry," 2012.

[77] M. Engelhardt, "Strange Quark Contributions to Nucleon Mass and Spin from Lattice QCD," *Phys.Rev.*, vol. D86, p. 114510, 2012.

[78] R. Young and A. Thomas, "Octet Baryon Masses and Sigma Terms from an $SU(3)$ Chiral Extrapolation," *Phys.Rev.*, vol. D81, p. 014503, 2010.

[79] S. Durr, Z. Fodor, T. Hemmert, C. Hoelbling, J. Frison, *et al.*, "Sigma Term and Strangeness Content of Octet Baryons," *Phys.Rev.*, vol. D85, p. 014509, 2012.

[80] R. Horsley *et al.*, "Hyperon Sigma Terms for 2+1 Quark Flavours," *Phys.Rev.*, vol. D85, p. 034506, 2012.

[81] A. Semke and M. Lutz, "Strangeness in the Baryon Ground States," *Phys.Lett.*, vol. B717, pp. 242–247, 2012.

[82] P. Shanahan, A. Thomas, and R. Young, "Sigma Terms from an $SU(3)$ Chiral Extrapolation," *Phys.Rev.*, vol. D87, p. 074503, 2013.

[83] X.-L. Ren, L. Geng, J. M. Camalich, J. Meng, and H. Toki, "Octet Baryon Masses in Next-To-Next-To-Next-To-Leading Order Covariant Baryon Chiral Perturbation Theory," *J. High Energy Phys.*, vol. 12, p. 073, 2012.

[84] D. Toussaint and W. Freeman, "The Strange Quark Condensate in the Nucleon in 2+1 Flavor QCD," *Phys.Rev.Lett.*, vol. 103, p. 122002, 2009.

[85] W. Freeman and D. Toussaint, "The Intrinsic Strangeness and Charm of the Nucleon Using Improved Staggered Fermions," 2012.

[86] C. Aubin *et al.*, "First determination of the strange and light quark masses from full lattice QCD," *Phys. Rev.*, vol. D70, p. 031504, 2004.

[87] J.-W. Chen and M. J. Savage, "The Chiral Extrapolation of Strange Matrix Elements in the Nucleon," *Phys.Rev.*, vol. D66, p. 074509, 2002.

[88] H.-W. Lin, "Lattice Hadron Structure: Applications Within and Beyond QCD," *PoS*, vol. LATTICE2012, p. 013, 2012.

[89] A. Walker-Loud, "New Lessons from the Nucleon Mass, Lattice QCD and Heavy Baryon Chiral Perturbation Theory," *PoS*, vol. LATTICE2008, p. 005, 2008.

[90] M. A. Shifman, A. Vainshtein, and V. I. Zakharov, "Remarks on Higgs Boson Interactions with Nucleons," *Phys.Lett.*, vol. B78, p. 443, 1978.

[91] A. Kryjevski, "Heavy quark anti-q q matrix elements in the nucleon from perturbative QCD," *Phys.Rev.*, vol. D70, p. 094028, 2004.

[92] R. Young, "Strange quark content of the nucleon and dark matter searches," *PoS*, vol. LATTICE2012, p. 014, 2012.

[93] E. E. Jenkins, A. V. Manohar, J. W. Negele, and A. Walker-Loud, "A Lattice Test of $1/N_c$ Baryon Mass Relations," *Phys. Rev.*, vol. D81, p. 014502, 2010.

[94] K.-I. Ishikawa *et al.*, "$SU(2)$ and $SU(3)$ Chiral Perturbation Theory Analyses on Baryon Masses in 2+1 Flavor Lattice QCD," *Phys.Rev.*, vol. D80, p. 054502, 2009.

[95] A. Walker-Loud, "Evidence for Non-Analytic Light Quark Mass Dependence in the Baryon Spectrum," *Phys.Rev.*, vol. D86, p. 074509, 2012.

[96] J. Giedt, A. W. Thomas, and R. D. Young, "Dark Matter, the Cmssm and Lattice QCD," *Phys.Rev.Lett.*, vol. 103, p. 201802, 2009.

[97] J. R. Ellis, K. A. Olive, and C. Savage, "Hadronic Uncertainties in the Elastic Scattering of Supersymmetric Dark Matter," *Phys.Rev.*, vol. D77, p. 065026, 2008.

Appendix A

Effective Mass Plots

In this Appendix, we present the results of computations of lattice correlators in the form of the effective mass plots which have already been described in various chapters.

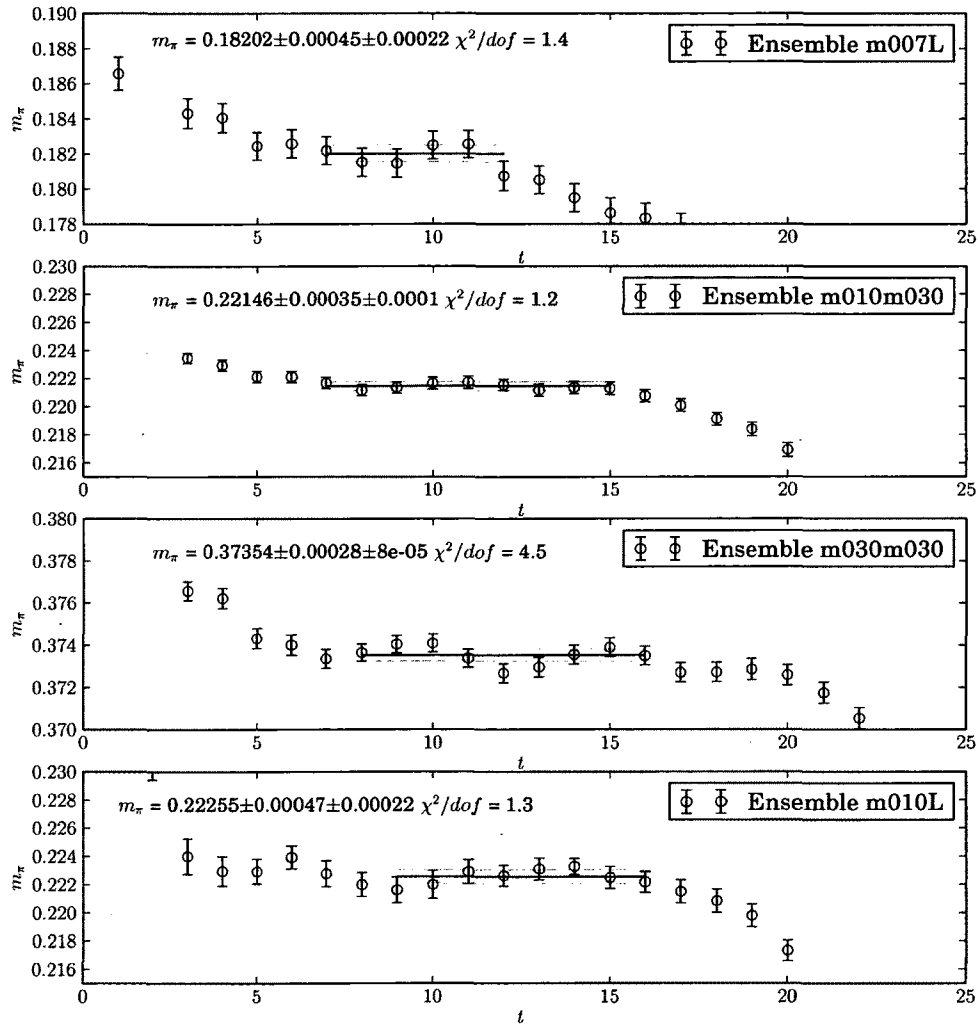Figure A-1: *Effective Mass Plots for Pions on $b \approx 0.125$ fm Ensembles*

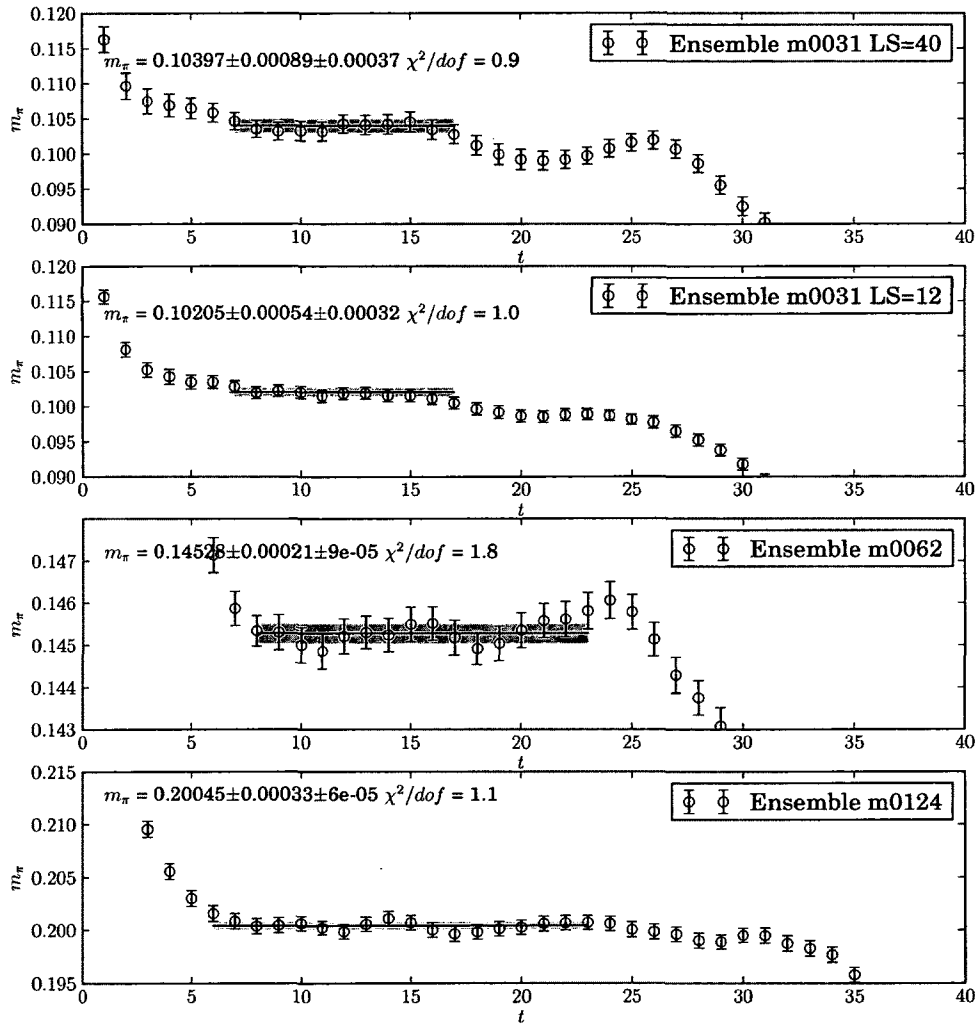Figure A-2: *Effective Mass Plots for Pions on* $b \approx 0.09$ *fm Ensembles*

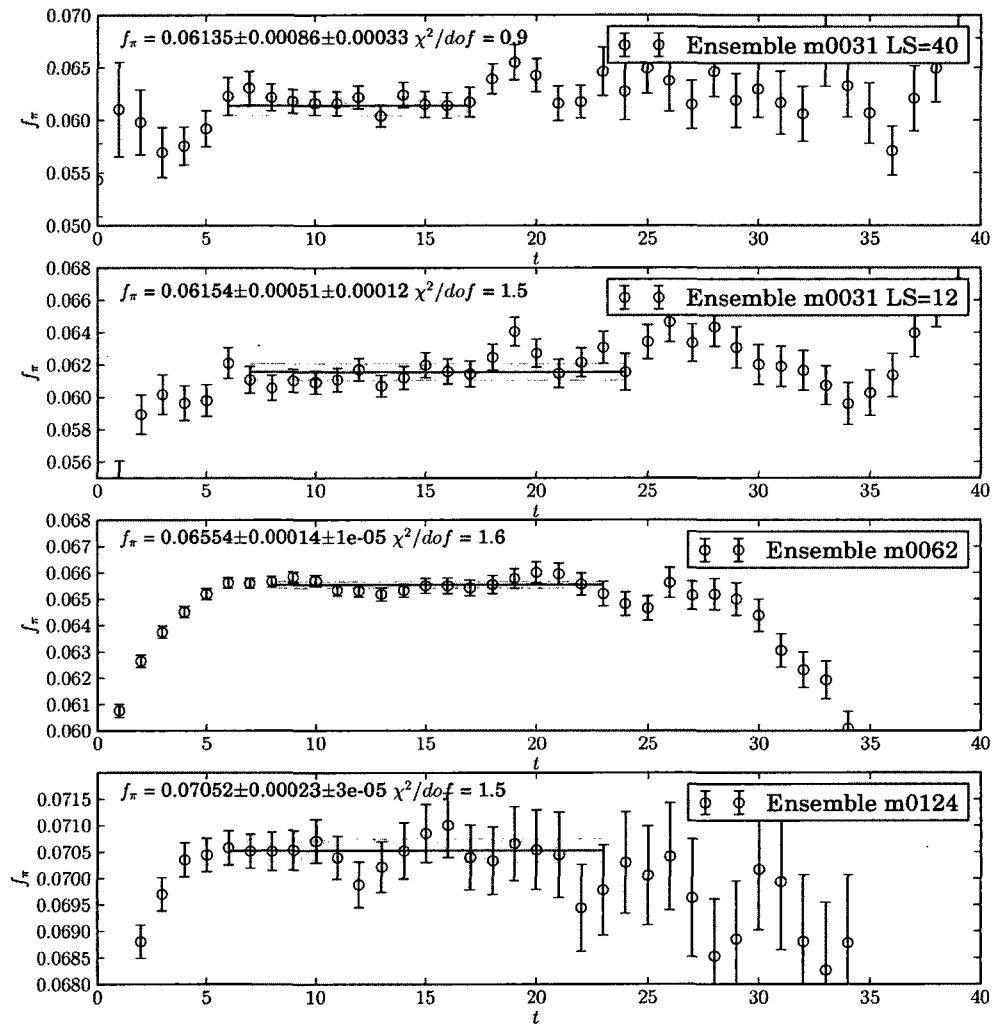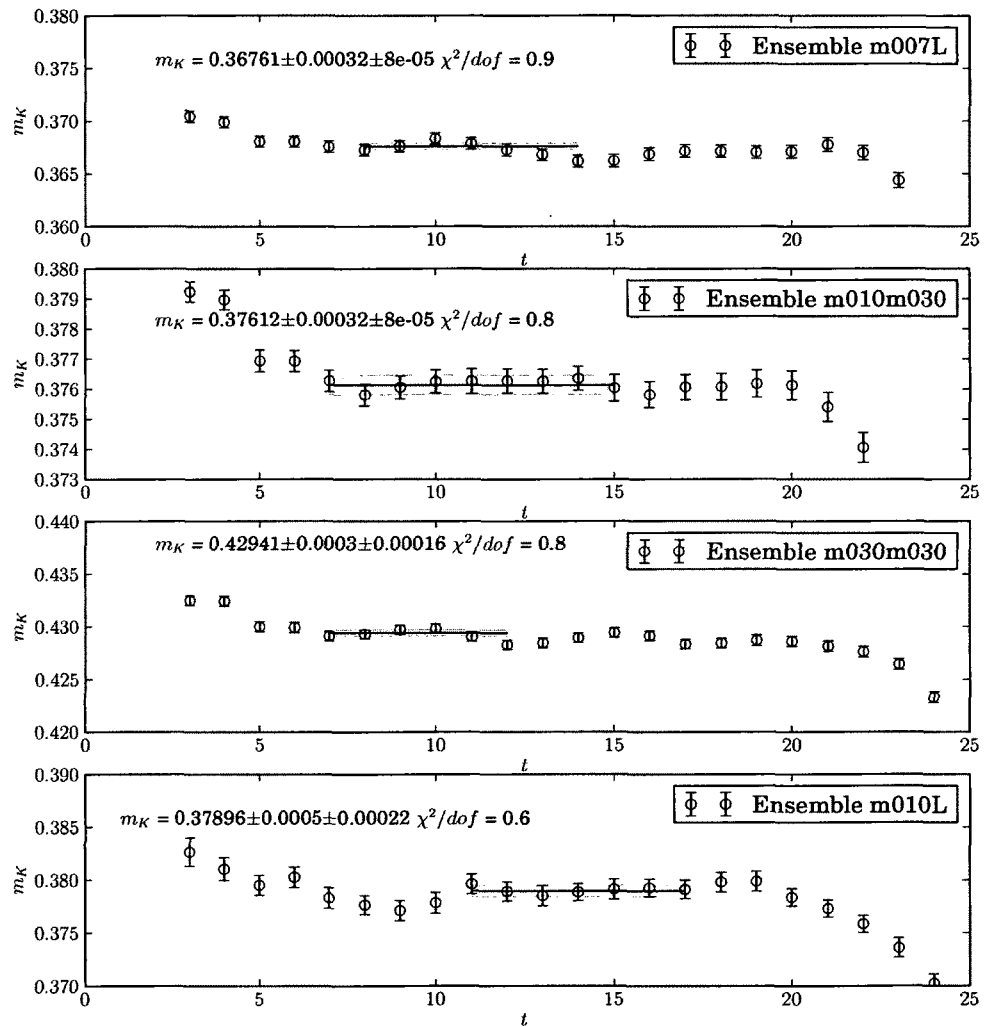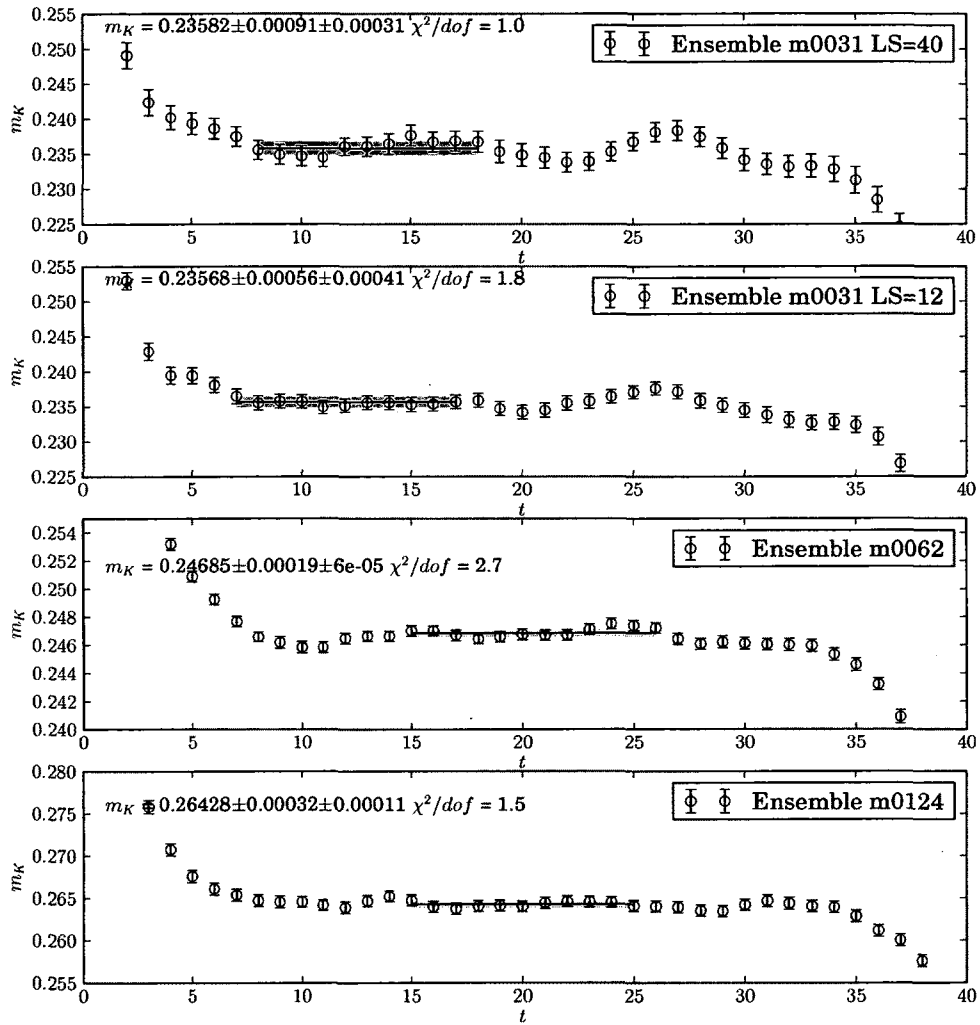Figure A-3: *Effective Mass Plots for Pion decay constant on $b \approx 0.09$ fm Ensembles*

Figure A-4: *Effective Mass Plots for kaons on b ≈ 0.125 fm Ensembles*

Figure A-5: *Effective Mass Plots for kaons on $b \approx 0.09$ fm Ensembles*

Figure A-6: *Effective Mass Plots for kaon decay constant on b $\approx$ 0.09 fm with Volume 40 $\times$ 96*
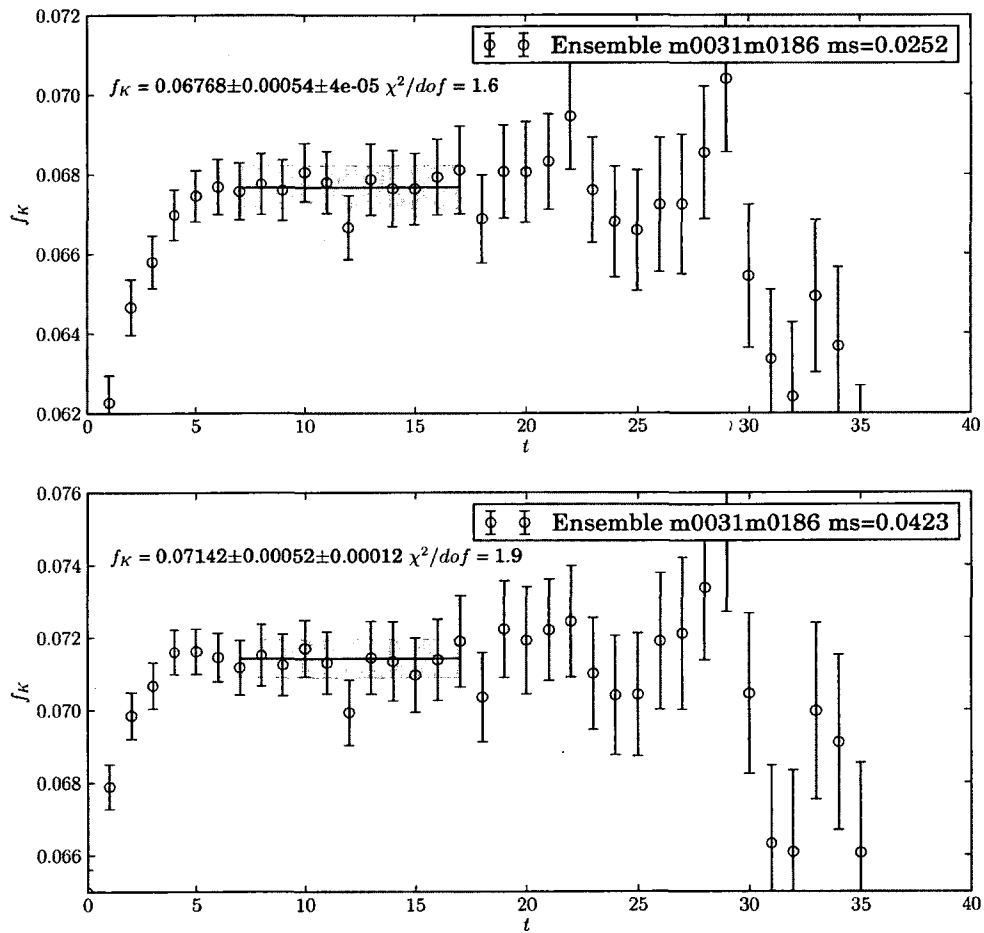
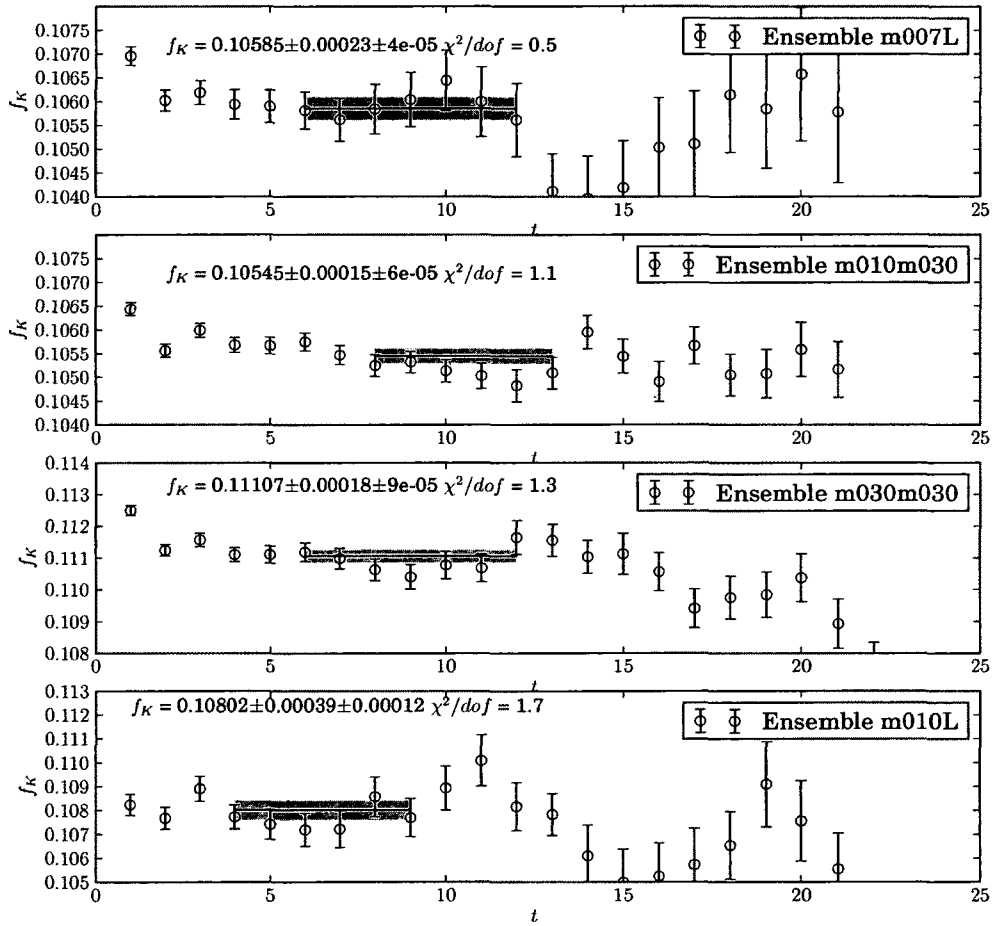Figure A-7: *Effective Mass Plots for kaon decay constant on b ≈ 0.125 fm Ensembles*

Figure A-8: *Effective Mass Plots for* f_K/f_π *on* $b \approx 0.125$ *fm Ensembles*
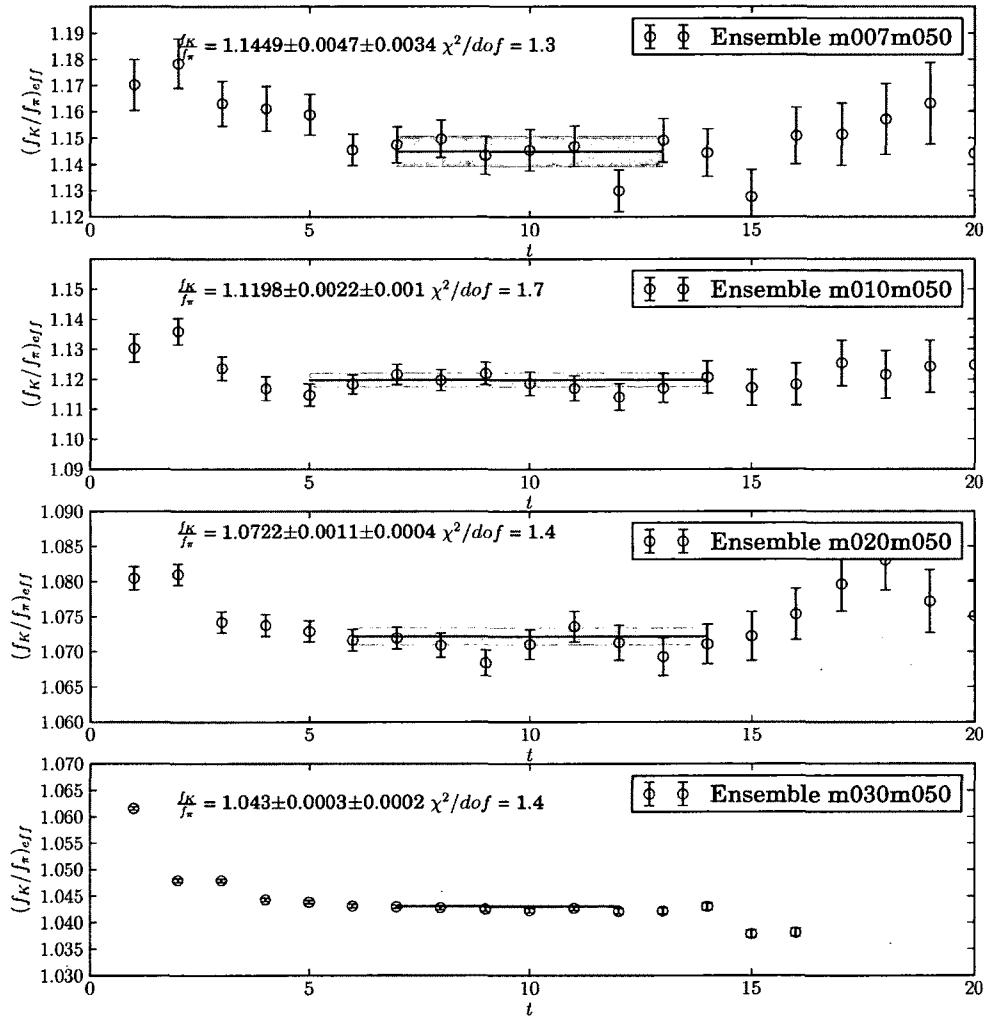
Figure A-9: *Effective Mass Plots for f_K/f_π on $b \approx 0.09$ fm Ensembles*